Acta Universitatis Sapientiae

Electrical and Mechanical Engineering

Volume 3, 2011

Sapientia Hungarian University of Transylvania
Scientia Publishing House

Contents

Acta Universitatis Sapientiae
Electrical and Mechanical Engineering, 3 (2011) 5-14

Action Descriptive Strings

Péter Megyesi[1], Sándor Molnár[2]

Department of Telecommunications and Media Informatics,
Faculty of Electrical Engineering and Informatics,
Budapest University of Technology and Economics, Budapest, Hungary
e-mail: megyo@fazekas.hu[1], molnar@tmit.bme.hu[2]

Manuscript received December 20, 2011; revised January 16, 2012.

Abstract: An outcome of a measurement frequently contains too many and redundant elements so extracting similar patterns can be a hard task. This paper presents an idea to convert time streaming measurement results into a special string format and to use existing motif finding methods for further analysis. We have created the Action Descriptive String (ADS) which is a projection of series of events. Although these strings are not an accurate description of the actual events they had been defined from, they are helpful in finding typical occurrences of short term events and comparing two series of events.

Following the presentation of the existing motif finding methods and the benefit of applying them for the Action Descriptive Strings, we give the idea of converting measurement results into ADS format. The method for finding frequently occurring patterns in the converted string format is also presented. We discuss the possibility of emulating long term events by a series of the extracted typical short term patterns. We have implemented an algorithm which is able to score the similarities between two Action Descriptive Strings. This algorithm is used for finding the most similar typical pattern for an arbitrarily given ADS. Since the scoring scheme of the algorithm is highly dependent on the measured phenomenon, we also present a process for adjusting the scoring values to a given measurement.

Keywords: String matching, motif finding, measurement analysis.

1. Introduction

Converting time serial measurement results into appropriate short string format can help us applying existing string based algorithms for further analyze.

This motivation led us to create a special string format (Action Descriptive Strings) from these raw measurement results.

Motif finding is widely used method in bioinformatics and has a deep literature that we can rely on. In bioinformatics the algorithms tend to find similarities in protein chains, typically in amino acid. These algorithms usually use a simple string input which contains the markings of the four proteins DNA is built from: A for Adenine, T for Thymine, G for Guanine and C for Cytosine. MEME suite is a comprehensive tool for discovering motifs in a group of related DNA or protein sequences [1].

Similar architectures are presented in [2], [3] and [4] for using string matching algorithms for signature generation in various network appliances. In these cases one byte represents a unit in the sequence therefore there are 256 different symbols.

The Action Descriptive Strings (ADS) can be used for representing any kind of time series measurement result. Using these strings and the algorithms presented in this paper the measurements can be further analyzed from a different point of view. We have implemented the ADS in a general way that can be suitable for various measurement types.

In the next section the general structure of the Action Descriptive Strings is presented. The idea of extracting typical patterns from converted measurements results is discussed in Section 3. Section 4 presents an algorithm which is able to suit a series of typical patterns for any given measurement result stream. The algorithm we implemented for scoring the similarities between two ADS is given in Section 5. Section 6 presents the idea of adjusting the scoring algorithm for unique measurement types. Finally, in Section 7 a summary of our work is found where we present a few possible utilizations for the Action Descriptive Strings.

2. Action Descriptive Strings

In an Action Descriptive String there are two types of characters: the action characters and the time delimiter characters. Although the time delimiter character can be chosen arbitrarily, we chose the “Z” characters for separating equal time intervals in an ADS. The other characters refer for one type of action. Thus an example an example for them looks like the following:

AZAZABZABZACZAZAZ

Since this example contains seven “Z” characters, this ADS represents a seven-time-unit-long scenario. This means that in this scenario an “A” type of

action occurred in every seven time unit, a “B” type of action happened in the third and the fourth, and a “C” type occurred in the fifth time unit.

During the conversation of measurement results the data must be separated to individual sources. Thus in case of an aggregated measurement the first step must be a discrimination of the sources (typically location based). In the next step every different action must be investigated for every time unit. If an action occurred in the given time unit we write its character into the ADS than we close the given time unit by the “Z” character.

The definition of the actions is a heuristic process which is highly dependent on the measurement itself. They can be simple event occurrences (for example if a motorcycle has crossed the road or a costumer has bought milk) or a limit for event occurrences (for example if the number of cars that crossed the road is greater than 100). Limit bands are also usable in event definition for detailed resolution but since the idea is to simplify the measurement results these bands should be minimized.

The choice of the used time resolution is also has to be adjusted for the given measurement type. Too short time units can result to an output where typical patterns are not extractable. On the other, hand using a too long time unit could hide the differences between distant inputs.

```
1223378304 ABZABZABZABZABZABZABZABZABZ
1223378306 HIZHIZHIZHIZHIZHIZHIZHIZHIZ
1223378809 FZFZFZFZFZFZFZFZFZ
```

Figure 1: The format of the input ADS file.

Taking these into account the format of the required input file is given in *Figure 1*. As the figure shows the input should also contain the UNIX timestamp of the beginning of the different sources’ action which will be used during the long term event emulation.

3. Extracting typical patterns

During the extract of typical patterns we tend to find substrings which are frequently occur in the input. In this procedure we search for fixed time length patterns between lower and a higher limit. The reason for the lower limit is that too short patterns are not describing stable event series. On the other hand, the longer a pattern the lesser it would occur in the input stream. Thus these limits have to be defined considering the time input’s time resolution.

As a first solution we have inspected bioinformatics problems. We have examined the possibility of applying the same architecture presented in [2] with

a different preprocessing method. In this paper the authors present a framework using Glam2 for signature generation. Glam2 is a software package for finding motifs in sequences, typically amino-acid or nucleotide sequences [5]. Glam2Scan is a part of the Glam2 software package which can find matches in a sequence database to a motif discovered by Glam2 [6]. Glam2Scan gives a score for each match indicating how well it fits the given motif so it also could be the base an approximately match algorithm during a long term event emulation.

However, after a long investigation process we have found that we can't use this technique for the general architecture of Action Descriptive Strings. The main reason behind this is that bioinformatics algorithm use alphabet where the roles of the characters are the same. In ADSs the time delimiter ("Z") character has completely different meaning than the others. Moreover, in our case we would like to have a method to define suitable replacements for certain event types therefore defining subclasses where the events are similar with each other and distant from the others.

Thus we implemented a unique algorithm which is able to extract typical patterns from the input. The key point in the algorithm is to split the Action Description Strings along the time delimiter ("Z") characters. That way we make sure that the individual time units' activities won't be corrupted. For preprocessing the algorithm does two things. First, it filters out the long idle periods (multiple consecutive "Z" characters) in the sources' activities thus the algorithm won't give back patterns in which the idle period is longer than the actual activity. Secondly, for symmetric ADS patterns (where the same characters occur in every time unit) the algorithm recalculates the real number occurrences. For example, in case of a 200 time-unit-long *"AZ"* run the occurrence for the five-time-unit-long *"AZAZAZAZAZ"* should be 40 not 196.

In the algorithm two limits have to be declared: a *hard limit* and *soft limit*. First, the tool counts the occurrences for every occurring ADS substring which has the given time length. Then the algorithm calculates the most similar ADS for every pattern below the *soft limit* using the scoring mechanism presented in Section 5 and increase the result's occurrence by one. After that, the ADS substrings occurring more than the *hard limit* are added into the typical patterns pool.

The choice of the limits is dependent on the result we would like to achieve. For example, setting the two limits to the same value will avoid the usage of the scoring mechanism and result in only the ADSs which occurrence is greater than then the given limit. On the other hand, setting the *soft limit* to 1 will give the most detailed result but it can significantly increase the run time of the algorithm.

4. Long term event emulation

The main idea behind the emulation of long term events is to substitute the entire stream of one source by a series of typical patterns. In order to do that, we have the input Action Descriptive String file and the database of the extracted typical patterns. The input ADS can be one line from the measurement result or can be generated artificially. The second method allows us to emulate arbitrary event type that would otherwise not occur in real measurements. In practice it means that we need an algorithm which is able to cover a source's entire Action Descriptive String with the extracted typical patterns' ADSs. Moreover, the algorithm must calculate the accurate timing information.

The first part of the implemented algorithm is a search for full-matching typical patterns in the input ADS. During this process two rules should be kept. First, we have to start the search with the longer patterns. During the emulation process we prefer the usage of longer term typical patterns since we consider their activity more stabile. With this action we make sure that we use the longer scenarios as much as possible. The second rule is that if we find a full-matching user pattern somewhere in the input ADS we have to switch that substring to only time delimiter ("Z") characters. That way we guarantee that the time units in the input stream will be covered by only one pattern. However, we have to leave the time delimiter characters in the ADS in order to properly calculate the timing information.

Since an arbitrary Action Description String can unlikely be covered by only typical patterns we have implemented an approximate matching part for the algorithm as well. During this procedure the algorithm uses a scoring scheme introduced in the next section which is able to find the most similar typical pattern for any given ADS.

After full-matching the remaining ADS may contain many consecutive time delimiter ("Z") characters. Since this "Z" runs means an inactive period or that it has been previously covered by a full-matching typical pattern, as a next step the algorithm splits the remaining string along three or more consecutive "Z" characters. The last step of the algorithm searches for the most similar typical pattern for every remaining substring after the split. These time period in the input stream will be emulated by the same action as the most similar typical pattern describes. If a reaming substring is longer than the higher time limit of the typical patterns the algorithm calculates the score for every prefix from the lower time limit to the higher. The one with the best result score will be emulated by the most similar pattern than the algorithm removes that ADS from the substring and repeats the approximate matching procedure.

5. The ADS scoring algorithm

When we were designing the ADS scoring algorithm the following rules were laid down:

1) If we compare an A sting to a B sting, the returned score must be less than or equal to score the algorithm returns comparing the A string with itself.
2) The equality must only stand if the same characters with the same amount are in both A and B.
3) The algorithm must inspect the time length of the ADSs and give lesser score if it differs.
4) We must have a way of setting unique values for which action types are suitable substitutions for each other and which are completely excluded.

Taking these considerations into account, we have defined a scoring matrix labeling its rows and columns with the defined types' characters. We also add the "X" character which will refer to no action. If we substitute an "A" character from the first string to a "B" character in the second string the score under the "A" row and "B" column will be added to the total score. Firstly, the algorithm concatenates "X" characters to the shorter string until both of them contain the same amount of characters. After this, a dynamic programming algorithm finds the best substitution solution for the characters calculating the maximal possible score [7], [8]. As the last step the algorithm modifies the given score with a divider if the time lengths of two strings differ.

In order to get the most ideal values of the scoring matrix and the length modifier we created a test database of Action Descriptive Strings. In contrast with the typical patterns this artificial database contains only ADSs in which the actions are the same in every minute. We integrated every variation of minimum four maximum ten minute long scenarios which contains maximum 4 type of action simultaneously. In the following section we will present a method for proper adjustment of the scoring values using the test database.

6. Adjusting scoring values

In this example we use Action Descriptive Stings which are made of four different characters: *"A"*, *"B"*, *"C"* and *"D"*. The initial scoring matrix is shown in *Table 1*. The scoring values were set up as following. "A" is the least significant action and we prefer to substitute it primarily to "B" and secondly to no action ("X"). Substitute "A" to "C" or "D" will decrease the score as their action is considered to be too distant. In case of the action marked by "B" the suitable substitutes are primarily "C" and secondly "A". For "C" we prefer "D"

and “B” while for “D” the suitable substitutions are “C” and “B”. If one action is replaced by itself five points are added to the final score.

All the values in the first row of *Table 1* are negative. This step is required for keeping the first rule since positive values would result in more score in case of adding more extra action. The values are different thus in case of an extra action the least significant actions will be preferred.

Table 1: An initial scoring matrix.

	X	A	B	C	D
X	0	-2	-3	-4	-5
A	2	5	3	-1	-2
B	0	2	5	3	1
C	-2	0	2	5	3
D	-5	-1	1	3	5

Table 2: Results for the initial scoring values.

Rank	Score	Relative score	Time unit	ADS
0	30	1	5	AZAZAZAZABZ
1	25	0.83	5	AZAZAZAZAZ
2	19	0.63	5	BZBZBZBZBZ
3	18	0.6	5	ABZABZABZABZABZ
4	12	0.4	5	ACZACZACZACZACZ
5	6	0.2	5	ADZADZADZADZADZ

Table 2 shows the five most similar ADS from the test database for the input *AZAZAZAZABZ*. This is a five-time-unit-long event which contains the action “A” in every time unit and the action “B” in the last one. The first row (rank 0) contains the result comparing the input string with itself. As it can be seen in *Table 2*, this result is 30 since there are six action characters in this ADS thus the final score is six times five.

Although the results show what can be previously expected, the actual rankings and the given points can be further investigated. For example, the second and the third result show that these scoring values prefer the substitution of an entire action to another than using both of them. An adjustment procedure for real measurement result can be inspected in many ways which are highly dependent on the phenomenon. For example, if the actions are fairly different from each other the scoring values for the preferred substitutions should be decreased significantly.

An example for this type of scoring matrix is presented in *Table 3*. The difference between this scoring matrix and the initial one is that the positive values for the substitutions are divided by ten. That way, substitute one character for a different one will result in lesser score. The results for the same input as in the previous test is given in *Table 4*. In this case the ADS where both "A" and "B" occurred in every time unit is the second most similar to input with the same score while the pattern containing only "B" got significantly less score. If this similarity is closer to the realty than the first one the modified scoring matrix should be used.

Table 3: Example for modified scoring matrix.

	X	A	B	C	D
X	0	-2	-3	-4	-5
A	0.2	5	0.3	-1	-2
B	0	0.2	5	0.3	0.1
C	-2	0	0.2	5	0.3
D	-5	-1	0.1	0.3	5

As a last example we let the algorithm to test Action Descriptive Strings which time length differs from the input. In these cases the calculated score from the scoring matrix is divided by a constant. The results using 1.2 as the length divider are presented in *Table 5*. As the results show the four and six time-unit-long variants of the previously best two results appeared in the array.

Table 4: Results for the modified scoring matrix.

Rank	Score	Relative score	Time unit	ADS
0	30	1	5	AZAZAZAZABZ
1	25	0.83	5	AZAZAZAZAZ
2	18	0.6	5	ABZABZABZABZABZ
3	9.3	0.31	5	ACZACZACZACZACZ
4	6.4	0.21	5	BZBZBZBZBZ
5	5.1	0.17	5	ADZADZADZADZADZ

Table 5: Results using different time lengths.

Rank	Score	Relative score	Time unit	ADS
0	30	1	5	AZAZAZAZABZ
1	25	0.83	5	AZAZAZAZAZ
2	21	0.7	6	AZAZAZAZAZAZ
3	18	0.6	5	ABZABZABZABZABZ
4	16.83	0.56	4	AZAZAZAZ
5	16.08	0.53	4	ABZABZABZABZ
6	10.83	0.36	6	ABZABZABZABZABZABZ

7. Conclusion

We have presented Action Descriptive Strings (ADS) which is a projection of real measurement results. By this conversation we are able to use existing motif finding methods for further analyzing a time stream measurement.

We have given methods for finding short term typical patterns in the input stream and use them for emulating long term activities. Both of these processes use an algorithm which can score the similarities between two Action Descriptive Strings. This paper contains an example for adjusting the scoring values of the ADS scoring algorithm using an artificially created pattern database.

An example for the application of the Action Descriptive Strings can be found in [7]. In [7] the author uses the same architecture for describe network traffic and determine the typical way of how users are using the Internet.

Acknowledgements

The authors would like to thank Géza Szabó, coworker of Ericsson Hungary Ltd. for providing support for this project.

References

[1] MEME suite: http://meme.sdsc.edu/meme/
[2] Szabó, G., Turányi, Z., Toka, L., Molnár, S., Santos, A.: "Automatic Protocol Signature Generation Framework for Deep Packet Inspection", *VALUETOOLS 2011, ENS, Cachan, France*, May 16-20, 2011.
[3] Ye, M., Xu, K., Wu, J., and Po, H.: "Autosig-automatically generating signatures for applications", in *CIT (2)- IEEE Computer Society*, 2009, pp. 104–109.
[4] Conrad, E., "Detecting Spam with Genetic Regular Expressions", http://www.sans.org/reading_room/whitepapers/email/detecting_spam_with_genetic_regular_expressions_2006.
[5] Glam2 manual: http://meme.sdsc.edu/meme/doc/glam2_man.html.
[6] Glam2Scan manual: http://meme.sdsc.edu/meme/doc/glam2scan_man.html.
[7] Megyesi, P., "Matching Algorithm for Network Traffic Descriptive Strings", *Scientific Students' Associations Conference, Faculty of Electrical Engineering and Informatics, Budapest University of Technology and Economics*, Nov 2011.
[8] "Dynamic Programming", http://www.cs.berkeley.edu/~vazirani/algorithms/chap6.pdf.

Acta Universitatis Sapientiae
Electrical and Mechanical Engineering, 3 (2011) 15-25

Photo Tagging in Urban Environments

Rezső HANDBAUER, Csaba SIMON, Markosz MALIOSZ

Department of Telecommunications and Media Informatics,
Budapest University of Technology and Economics, Budapest, Hungary
e-mail: {handbauer; simon; maliosz}@tmit.bme.hu

Manuscript received June 10, 2011; revised December 10, 2011.

Abstract: In this paper we investigate the applicability of the photo tagging to geo location in urban environments. We rely on photos taken at the location to be identified and not on the geographical coordinates. The difficulty of the proposal was to identify the building/landmark based on the photo provided on-line by the user. Our goal was to provide a working solution with a reasonably fast reaction time for urban environments. We have shown that the combination of division of the image and the color-based comparison with the original SIFT algorithm significantly improves the comparison process.

Keywords: Photo tagging, augmented reality, image comparison.

1. Introduction

Linking real and virtual worlds is vastly researched and experimented by the research community. The proposed solutions are based on the idea of providing a solution that maps the virtual world on the real one, extending the elements of the real world with useful information and/or properties. Several proposals targeted the urban environments, when different locations were associated with meta-information [1], [2], allowing the civil groups to interact and change the perception of others on the respective locations. By now we can state that the community agrees that there is a need for such solutions, the current research being focused on the proper technological solutions that satisfy the requirements of the various target applications.

Most of the solutions rely on *tag*s associated with real world locations and meta-information is indexed by these tags. The proposed solutions chiefly differ in the tagging system and the way these tags are obtained by real world characters. This research area is strongly related to the topic of location based services offered to mobile users [3]. Although GPS (Global Positioning System) is available in many devices, it is not always available in urban and indoor environments [4]. A different idea was to use mobile cell information to locate the device, but operators are reluctant to offer such data and the precision of this solution is not high enough [5]. Mobile tagging optimizes the barcodes to mobile environments, but it requires the dispatch of the tags on buildings and outdoor locations [6].

In this paper we investigate the applicability of the photo tagging to geo location in urban environments. We rely on photos taken at the location to be identified instead of geographical coordinates. The advantage of this solution is that the buildings or landmarks are already in place, and the loss of signal does not affect its operation. The difficulty of the proposal was to identify the building/landmark based on the photo provided on-line by the user. There were several proposals that deal with such problems, but the solutions are not public and have been publicized only through demonstration events. Our goal was to provide a working solution with a reasonably fast reaction time for urban environments. The use case of the proposed photo tagging solution is that an integrated system should be able to offer extra information on urban locations based on pictures taken and uploaded real time with smartphones.

In the next section we present the image processing issues relevant to our topic, and then we present the proposed solution. In section 4 we analyze the performance of our proposal and finally we conclude our paper.

2. Image processing aspects

As explained in the previous section, our proposal requires the image-based identification of buildings and landmarks. There have been proposed several solutions, but each of them had problems during operation. The most advanced and successful image comparison solutions have been developed in face recognition [7].

Compared to that area of image comparison, our case has several particularities. The pictures sent in by the users most probably will not be taken exactly from the same position as the reference ones, therefore the comparison of these types of images have some specific properties. The most important aspects that make the image comparison harder are the following ones.

- The pictures are not taken from the same angle.
- The pictures are taken from different distances from the building.

- There might be several distracting details on the picture taken by the user.
- Changing light conditions, depending on the time of the day, weather, etc.
- The quality of the picture taken by the user probably is different (typically worse).

In the urban environment most of the landmarks are buildings, which have distinctive edges. Research in computer imaging has widely studied the issue of edge detection [8], this one being the starting point of most solutions. Several interest points of an image can later be extracted from edges and these interest points are later used as inputs by other image comparison algorithms.

The most used technique in edge detection is based on the intensity gradient of the image. Canny's algorithm is still the most used one and is based on five, relatively simple, easy-to-implement steps [9], [10].

Edges are characteristic to a given image, but due to the issues enumerated above we need a much more robust solution. Several solutions have been proposed, which operate on a larger set of features, called keypoints. These solutions handle image translation, scaling, rotation, local geometric distortion and minor changes in illumination or color. The most known among these solutions is the Scale Invariant Feature Transform (SIFT) [11], and its enhancement, the Gradient Location-Orientation Histogram (GLOH) [12]. Relatively recent proposal is the Speeded Up Robust Feature (SURF) [13], partly inspired by the SIFT descriptor. SURF is faster than SIFT and is more robust to image transformation and noise. Nevertheless, the SIFT algorithm is better supported by programming libraries and for this reason we used it in our solution. As explained in the following section, we opted for a modular solution and therefore it can be replaced with newer/better algorithms.

The generic image recognition systems perform well if the objects on the images have been pictured under the same angle. Large angle-deviations result in false positives or no matches. In order to reduce the occurrence of such problems we pre-process the images. Using the algorithms presented in this section we proposed a framework that is able to recognize pictures, enabling a photo tagging application in urban environments.

3. The proposed image processing framework

Our solution is a combination of image processing mechanisms. We tried to speed up the comparison process by removing the irrelevant parts of the image or to use new information in order to exclude false positives.

A. Image pre-processing

The image pre-processing transforms the image into a canonic form. We expected that this step would improve the process by increasing its accuracy. As it will be presented later in section 4 this came with the cost of increased duration, therefore the feasibility of this step should be further studied.

We apply the Canny algorithm to detect the edges of the image. Even if this is an old solution, it is accurate, it has several implementations, its implementation is relatively simple and it is fast [14]. Then we apply a Hough transform [15] to the resulting image to extract the straight edges and lines from the image. In most of the cases in urban environment this yields the parallel edges of a building. An illustrative example of the above steps is presented in *Fig. 1*.

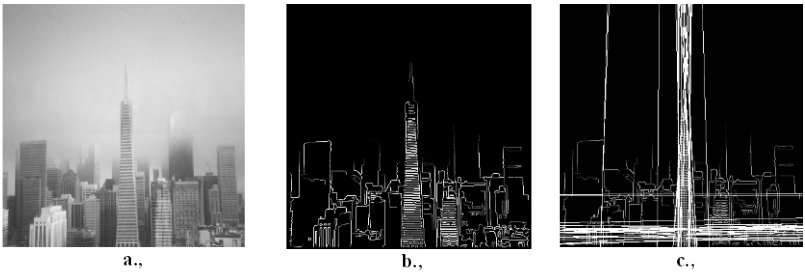

Figure 1: The picture a.) before any transformation, b.) after edge detection, c.) after Hough transform.

Finally we transform the image, which means the rotation of the object (building/landmark) on the picture. The reference points needed for this rotation are those obtained through the Hough transform, but the AffineTransform [16] process is applied to the original color image. Therefore we keep the extra information of the original image that was lost through the first two steps. An illustrative example of this transform is depicted in *Fig. 2.*, where a boat is rotated so that the top edge of the cabin becomes horizontal.

Figure 2: The picture a.) before rotation, b.) after rotation.

Note that these steps are useful only if we use a SIFT (or similar) algorithm to compare the images. E.g., if we use color based comparison, then the fill color would greatly bias the process.

B. Keypoint based comparison

The image comparison is primarily based on the SIFT algorithm, as already mentioned.

This process can be greatly improved if we have location information and the estimate of its accuracy. E.g., we might have a coordinate and then we can use the accuracy of this location information as the radius of a circle that probably contains the real location of the user. We can restrict the search, because in the case of a precision of 50 m probably we have 20-50 buildings or landmarks to run the search on.

We should compare our image against the images of the buildings closer to the coordinate: if the location information was accurate, then we do not waste time. Otherwise we still can increase the investigated area.

C. Color based identification

Our color based identification is built with the help of the Java Advanced Imaging (JAI) API [17]. This library allows us to get the color data of an image in several points of it, then builds a matrix that represents the image itself. Afterwards each image is represented by a matrix with the dimensions of 25×3. Based on our experiments the aggregation of the 15×15 pixel region of the image into one matrix element gives satisfactory results. Even if we use larger regions, the accuracy of the mechanism does not improve significantly, on the other hand its runtime is drastically increased. The aggregation of the pixel information is as follows: the RGB values of each pixel within a region are summed up, then the result is divided with the total number of pixels.

The size of the image does not influence the speed and quality of the process, because we resize every image to 300×200 pixel^2. Due to this and because the algorithm is much simpler than the SIFT, the comparison is much faster.

D. Speeding up the image comparison process

The image comparison methods and algorithms usually are computation intensive and require large amount of allocated memory. As a consequence a reliable algorithm takes a lot of time to complete, much more than it is acceptable for a real time photo tagging application. Specifically, the keypoint based algorithms to the likes of the SIFT are faster if the image depicts smaller objects, as there are fewer keypoints to compare. Starting from this observation we

experimented several practically feasible methods that are simple, do not affect significantly the precision of the algorithm, but still reduce its completion time.

The first solution is to ask the user, who takes the picture at the location to select a focus area on the picture. Anyway in the majority of the cases the photo of the user depicts a larger scene than the building itself. Therefore it is not a burden for her/him to select with a rectangle the exact building/landmark to be compared. This is illustrated in *Fig.3.a*, where the image contains the building of the Parliament and the river Danube, but the building in question occupies only half of the picture. The resulting picture uploaded by the user for comparison is shown in *Fig.3.*

A second solution is to further divide the image into zones, or areas and apply the comparison process zone-wise. These two solutions should be successively applied to the same picture, as illustrated in *Fig.3.b.*

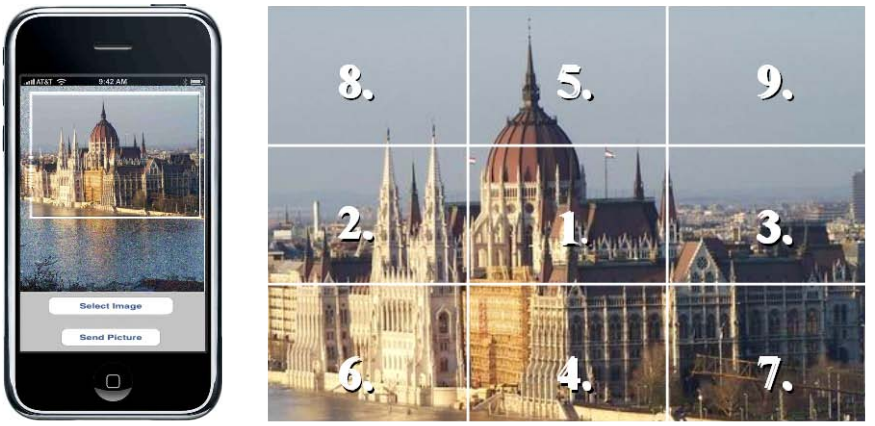

a.) ***b.)***

Figure 3: a.) Selecting the focus area within a picture b.) division of the picture into blocks.

Practically the users place the most important detail in the center of their photos. We ordered the areas of the image according to the order of processing and selected the central area of the image as the first one. In most of the photos the areas nr.8 and nr.9 are irrelevant (contain the sky), therefore those are placed at the end of the list. According to our experience the first three or four areas are enough to be processed in order to get an accurate result.

4. Performance evaluation

We tested our solution on a database of 88 images, and we compared each of them pair-wise. The images were taken in different conditions, as they would be in a real-life scenario (underexposed, overexposed, blurry). The pictures depict buildings from downtown Budapest taken from different angles and light conditions.

We have used an ASUS laptop with 1GB RAM, a 1.5GHz Intel Celeron processor and Microsoft Windows XP operating system to test our solutions. A dedicated server with faster processing units and larger memory can speed up the process. Further optimization alternative is to use a fast hard disk.

Nevertheless we considered that such a combination of database size and hardware gives a proper insight into the feasibility and performance of our proposal. In practice both the size of the database and the computational power of the server might be increased, resulting in a similar overall performance.

A. SIFT algorithm

Based on our experience the different lighting conditions, the blurred, noisy images do not significantly affect the reliability of the algorithm. On the other hand there are interfering objects in the fore- or background of the image, especially if the target object is masked (e.g., a truck or tree in front of a building).

An important issue is the angle of rotation, when the user takes his/her picture from a different angle than the reference image was registered. A similar problem is caused by the tight city street, where the optics of the mobile devices can not capture the whole front of a larger building. Even if the algorithm is scale free, these situations in practice result in lower number of captured keypoints, thus the algorithm becomes less accurate. In our case the algorithm could not recognize any building when the angle of rotation was 75° or larger.

In spite the above limitations the SIFT algorithm proves to be robust and reliable. We have found that downgraded resolution speeds up the process. We tested several solutions and we opted for a 0.5 megapixel size pictures, because the algorithm still is able to provide enough keypoints for stable operation.

We measured an 86% hit ratio and the duration of the comparison for an image was 19 seconds. We consider a successful comparison the case when the image provided by the user is compared against the images of the database and the image with largest matching keypoint pictures the same building indeed. The hit ratio expresses the ratio of successful comparisons among all the comparisons done. As a conclusion, the 86% hit ratio is an acceptable one, since in real life scenarios this can be used as the basis of a proper tagging.

The duration of a comparison is orders of magnitude larger than acceptable though. In the following we present several approaches that improved either the hit ratio or the duration of the comparison and finally we combined those that are acceptable in both terms.

B. Color based identification

The color based identification follows a different logic compared to the SIFT algorithm and its variants. This method is not a reliable one, therefore it is not used and it can not be used alone in our case. It still has a great advantage over the keypoint based solutions, since computationally it is orders of magnitude less demanding. Therefore it can be used to exclude those images that color-wise are "far" from the target image. It is also important to note that this approach is not sensible to those errors and noises that are hardly eliminated by the keypoint based algorithms. Practically the color based identification method complements the keypoint based ones.

First we applied the color based identification method in order to illustrate the above. The hit ratio has fallen to mere 56%, but the duration of a pair-wise comparison was less than 0.05 seconds. The low hit ratio confirms our expectation that this approach can not be applied alone. Due to the advantages of this approach we still did not abandon it, as shown later in this section.

C. The effect of the angle of rotation

The pictures taken from different angles decrease the accuracy of the comparison. We have found that in the case of large (i.e., above 30°) angles of rotation (the angle between the reference and the user-provided pictures) the SIFT algorithm could not take correct decisions. In order to alleviate this problem we transform the images to canonic form, and only then apply the SIFT algorithm. This method is not useful only in the case of the aforementioned large angles of rotation, since it increases the robustness of the SIFT algorithm in all cases.

We doubled the hit ratio with this method. Nevertheless this approach has several drawbacks. In the case of very large angles of rotation (above 50°) even if it increases the hit ratio, the result is still unacceptably low. Moreover, the rotation of the objects can be hardly realized in automatic manner, in most of the cases we had to adjust the automated results. Therefore further research is needed to find a solution for this transform to canonic form, which is feasible in real time environments. As a consequence in the following we do not use this transform in our tests, the presented results are obtained without this approach.

D. The effect of division of the image into areas

The main advantage of the division of the image into areas is that we can exclude those pictures right at the beginning whose low-ordered areas contain non-matching keypoints. We applied this method in combination with the SIFT algorithm and we achieved an improved hit ratio of 92%. In the same time the duration of the comparison was reduced to a mere 0.45 second for each pair-wise comparison. This value is orders of magnitude better than the 19 second achieved with SIFT alone.

E. Combination of the color based identification and the SIFT algorithm

The duration of a pair-wise comparison can be further reduced if we combine the color based identification presented earlier in this section with the SIFT algorithm.

We apply the color based identification after the approach presented in section 4.B. For each image the color based identification algorithm provides an aggregated color value. We ordered the images according to the Euclidean distances between their aggregated color values, and found that if we exclude the images from the lower half of the list we do not alter the hit ratio and at the same time we speed up the comparison process. Thus we apply the SIFT algorithm only on the half of the images compared to the method presented in section 4.B.

The effect of this approach on the duration of the comparison depends on the reliability of the color based identification method. Currently the method eliminated half of the images from further comparisons, thus the duration is approximately halved.

Theoretically this method also increases the accuracy of the comparison, since an image which significantly differs in colors from the target one is filtered out right at the beginning of the process. Nevertheless, we found that the ordered list provided by this approach in the 5% of the cases contained different buildings in the first part of the list, which lead to an increased ratio of false positives. These positive and negative effects neutralize the impact of the approach and the hit ratio is not increased. However the duration of the comparison was lowered to 0.25 seconds.

F. Summary of results

We have summarized in *Table 1* the results of our tests. Although the hit ratio of the original algorithm is already high, we could further increase it.

We can state that the processing time of a picture has been reduced by two orders of magnitude. This means that even if we compare this result against the faster SURF algorithm, the obtained gain is significant.

Table 1: Summary of the performance evaluations.

	Color based identification	*SIFT algorithm*	*SIFT algorithm + division of the image*	*SIFT algorithm + division of the image + color based filtering*
Hit ratio	56%	86%	92%	92%
Avg. processing time (per picture)	<0,05 s	19 s	0,45 s	0,25 s

If a photo tagging system is deployed in an urban environment and the location of the user is approximated as suggested in section 3.B, then the number of alternatives is around 100 pictures. Based on our tests the proposed solution keeps the response time within a single attention burst of a typical mobile user [18].

5. Conclusion

We have proposed an image identification framework solution that can support a photo tagging system. Such a photo tagging system may enable the implementation of a virtual community, social networks and related applications in urban environments.

The core of the photo tagging system is the image comparison. Our proposal builds on the widely known algorithm (SIFT) and we tried to fasten it up by finding those mechanisms that significantly reduce the per-picture processing time. Since the comparison is done at the server side, the computational resource was not a bottleneck.

We have tested our proposal on a test database. Although the transformation of the image to a canonic state significantly improves the accuracy of the process, it increases the duration of the process. A possible further research direction would be to apply this idea only in those cases when all the other mechanisms fail.

The combination of division of the image and of the color-based comparison with the original SIFT algorithm significantly improves the comparison process. At the same time it requires further research to improve the accuracy of the proposed method in the case of disturbances.

Acknowledgements

This work has been partially founded by Mobil Videó Konzorcium, Hungary. The authors would like to also thank the work of Zsolt Kosztovics and Norbert Érseki.

References

[1] Homepage of the BlueSpot project, http://bluespot.hu/.
[2] Robertson, D., Cipolla, R., "An image-based system for urban navigation" in *Proceedings of The 15th British Machine Vision Conference (BMVC'04), Kingston-upon-Thames, UK*, http://mi.eng.cam.ac.uk/reports/svr-ftp/cipolla_bmvc04.pdf, September 2004.
[3] Wang, S., Min, J., Yi, B. K., "Location Based Services for Mobiles: Technologies and Standards", *IEEE International Conference on Communication (ICC), Beijing, China*, 2008
[4] Global Positioning System, the homepage of the operator of the GPS system, http://www.gps.gov/.
[5] Varshavsky, A., et al., "Are GSM phones THE Solution for Localization?", in *Proceedings of 7th IEEE Workshop of Mobile Computing Systems and Applications (WMCSA), Semiahmoo Resort, Washington, USA*, April 2006.
[6] Mobile Codes Consortium – MC2: http://www.mobilecodes.org/.
[7] Sarfraz, S., Hellwich, O., "Head Pose Estimation in Face Recognition across Pose Scenarios", in. *Proc. of Int. conference on Computer Vision Theory and Applications, Madeira, Portugal*, pp.235-242, January 2008.
[8] Bebis, G., "Edge Detection", Department of Computer Science & Engineering, University of Nevada, USA, http://www.cse.unr.edu/~bebis/CS791E/Notes/EdgeDetection.pdf, 2003.
[9] Moeslund, T., "Canny Edge Detection", Laboratory of Computer Vision and Media Technology, Aalborg University, Denmark, http://www.cvmt.dk/education/teaching/f09/ VGIS8/ AIP/ canny_09gr820.pdf, March 2009.
[10] Kató, Z., Didactic material (in Hungarian), SZTE, Szeged, http://www.inf.u-szeged.hu/ ~kato/teaching/segmentation/03_edgedetection.pdf, July 2009.
[11] Meng, Y., Tiddeman, B., "Implementing the Scale Invariant Feature Transform (SIFT) Method", University report, University of St Andrews, St Andrews, UK, http://www.cs.st-andrews.ac.uk/~yumeng/yumeng-SIFTreport-5.18_bpt.pdf , May2006.
[12] Mikolajczyk, K., Schmid, C., "A performance evaluation of local descriptors", *IEEE Trans. on Pattern Analysis and Machine Intelligence*, Vol.10, No.27, pp.1615-1630, 2005.
[13] Bay, H., Ess, A., Tuytelaars, T., Van Gool, L., "SURF: Speeded Up Robust Features", *Computer Vision and Image Understanding (CVIU)*, Vol.110, No.3, pp.346-359, 2008.
[14] Gibara, T., "Implementation of the Canny algorithm", http://www.tomgibara.com/ computer-vision/ canny-edge-detector, 2009.
[15] Fisher, R., Perkins, S., Walker, A., Wolfart, E., "Image Processing Learning Resources", online book, http://homepages.inf.ed.ac.uk/rbf/HIPR2/hough.htm, 2004.
[16] Fisher, R., Perkins, S., Walker, A., Wolfart, E., "Affine Transformation", http://homepages. inf. ed.ac.uk/rbf/HIPR2/affine.htm, 2003.
[17] SUN Java Advanced Imaging, http://java.sun.com/javase/technologies/desktop/media/jai/.
[18] Oulasvirta, A., Tamminen, S., Roto, V., Kuorelahti, J., "Interaction in 4-second bursts: the fragmented nature of attentional resources in mobile HCI", in *Proceedings of the SIGCHI Conference on Human Factors in Computing Systems, Portland, Oregon, USA*, 2005.

Acta Universitatis Sapientiae
Electrical and Mechanical Engineering, 3 (2011) 26-38

Analysis of an Event Forecasting Method for Wireless Sensor Networks

András KALMÁR, Gergely ÖLLÖS, Rolland VIDA

High Speed Networks Laboratory (HSNLab),
Department of Telecommunications and Media Informatics,
Budapest University of Technology and Economics, Budapest, Hungary
e-mail: {kalmar; ollos; vida}@tmit.bme.hu

Manuscript received November 10, 2011; revised December 15, 2011.

Abstract: In this paper we introduce an event forecasting method for wireless sensor networks (WSNs), and its testing results in real world circumstances. The algorithm recognizes and differentiates the event sequences that turn up inside the sensor field, and then uses these recognized event sequences for event forecasting. The method uses the Fuzzy set theory and clustering methods. The events are represented with three different parameters (measurement data, sensor ID, and timestamp). According to the model of the algorithm, each sensor node periodically samples a predefined environmental parameter, and if the value of the measurement data is higher than a predefined threshold, the node stores this data as an event. A series of events is stored in the so called Time-Space fuzzy Signature (TSS). A TSS is a set of events, which are detected on a local node, or on its neighbors in its communication range. The algorithm performs hierarchical clustering on the TSSs to determine, which of them can represent the same event sequence, and as a result the same phenomenon. Then, on the results of the hierarchical clustering we perform a K-mean clustering, in order to filter out the noise events. The event forecasting feature of the WSN can be useful for target tracking or sleep scheduling protocols, among others. In this article, first we shortly introduce the theoretical background and definitions of the algorithm; then, we demonstrate the working.

Keywords: Wireless Sensor Network, event forecasting, fuzzy theory, clustering.

1. Introduction

A Wireless Sensor Network (WSN) consists of a large number of distributed nodes that organize themselves into a multi-hop wireless network. Each node has one or more sensors, embedded processors and a low-power radio. Typically, these nodes coordinate to perform a common task. The WSNs greatly extend our ability to monitor and control the physical environment from remote locations; furthermore, they can greatly improve the accuracy of information obtained via collaboration between sensor nodes. An interesting and useful feature of these networks is called event forecasting.

In [1], we suggested an event forecasting algorithm for WSNs, which builds up on a fuzzy framework. According to this method the sensor nodes try to forecast specific events from the changes of the environmental parameters, and from formerly registered measurements. This feature of the WSNs can be very useful in practice. The method is fully distributed and robust, and it does not require hard time synchronization or localization. In this article we would like to introduce an algorithm which is based on the same fuzzy framework, but tries to recognize and differentiate the event sequences that occur inside the area covered by the sensor network, and extract from them the "pure sequence(s)". (*A pure sequence is an event sequence that occurs inside the area monitored by the sensor network just because of a phenomenon and does not contain noise events.*) These pure sequences can be used then for event forecasting. The efficiency of the proposed method was tested in real circumstances as well, using a few Crossbow MicaZ sensor nodes that were placed next to different kinds of crossroads; the event-sequences recognized by the sensors model well the different trajectories of the passing cars.

In the next section we introduce the theoretical background, how the events are represented on the sensor nodes, and how the nodes store and sort the event sequences that appear in the network.

2. Definitions

In the following we provide a few definitions that are necessary to understand the context in which the forecasting model was developed and the measurements were done. These definitions and notations will be further detailed, and their usage will be explained in the following sections.

In [1] we defined a fuzzy set of events as follows:

$$E = \{(f, \mu_E(.), ID_f, t_f) \mid f \in F\} \tag{1}$$

where F is a certain feature space of the taken measurement. In Fuzzy terminology F is the universe of the features (f), where the events ($e \in E$) are defined. The parameter $\mu_E(.)$ is called fuzzy membership function. This function assigns to every f a number between 0 and 1, depending on the degree at which f belongs to the fuzzy set of events. ID_f means the *ID* of the sensor node where the event appeared, and t_f is the detection time of the event.

In the case when a node has more than one event to be managed, we store these events in the so called Time-Space fuzzy Signature (TSS)

$$\boldsymbol{TSS}_{\boldsymbol{ID},i} = \{e_{trg}, e_1, e_2, ..., e_n \mid e \in E\} \tag{2}$$

This is a set of events that occurred before the *i*-th target event (e_{trg}) being detected by the local sensor node (***ID***). The $e_1, e_2, ..., e_n$ events are either events detected by neighboring sensors, which alerted all the other nodes in their vicinity, or they are events detected by the local node itself, at a previous moment in time. These events are sorted in the TSS in descending order, by their time of occurrence (t_f).

3. Problem formulation

According to the model, each sensor node periodically samples a predefined environmental parameter, and in the case when the value of the membership function assigned to this environmental parameter is higher than a threshold limit, the node stores this data as an event. The shape of the membership function can be defined arbitrarily, according to a specific interval in the input space, based on what the user regards as an event. When a node detects an event, it sends a “limited broadcast” message to its neighboring nodes. Every sensor in radio range receives this message. All the sensors have a TSS database, which is filled up with their own events and the events detected by the neighboring nodes. A phenomenon passing through the monitored area creates event sequences (called *global event sequences*).

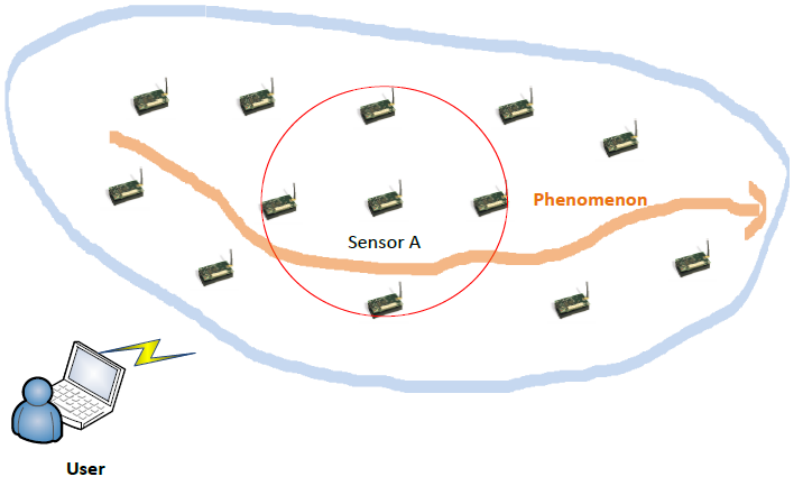

Figure 1: A local event sequence.

From this global event sequence a simple node senses only those events, which appeared in its communication range (called *local sequence*); in *Fig. 1* sensor node A sees only those events, which are logged in his communication range (red circle). There can be multiple phenomena in the sensor field at the same time, so the global sequences, and as a consequence the local sequences as well, can be overlapped with each other. In that case, the nodes can filter out from this mixed event set the pure local sequences, and then these pure local sequences can be used for event forecasting.

4. The TSS distance

As mentioned before, a phenomenon passing through the area monitored by the sensor network creates event sequences. Our aim is to estimate the number of the "pure sequences" that are mixed due to the overlapped sequences, i.e., how many different phenomena affected the sensor nodes. We have to find the similar event sequences, and assign them to the same cluster group. Then, we should extract from each cluster group the "pure event sequence", i.e., what phenomenon that group represents. To gain the ability to create clusters from the mixed event sequences, we must define a distance function between the different TSSs. But before doing so, in order to be able to compare the TSSs, that were created at different moments in time, we have to normalize the TSSs by time.

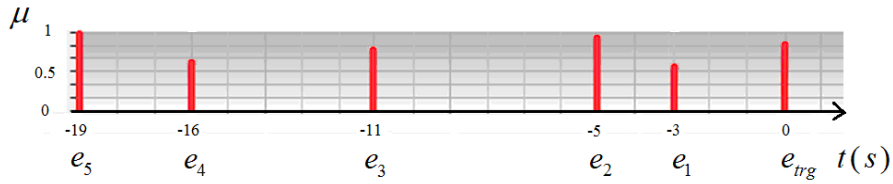

Figure 2: A normalized TSS.

Fig. 2 illustrates a TSS after normalization. As shown in the picture, normalization means that we shift the time parameter of the events so that the target event is at time 0, and all the other events, which occurred earlier in time than the target event, have negative time parameters. With this normalization we can transform all TSSs to a standard form.

The TSS distance function compares two normalized TSSs and assigns a number between 0 and 1 to them, in order to describe the similarity of the two TSSs. This is carried out in two steps. In the first step we try to order into pairs the events of the TSSs, while in the next step we try to quantify the differences between the pairs that we have found. One of the most important aspects in looking for event pairs is that we only search pairs in events which have the same sensor ID.

Fig. 3 illustrates a case, when two TSSs contain only events that are related to two different sensor IDs (sensorID = 1 and 2). In the figure we can see a possible pairing among events with sensorID = 1, but we also see that another pairing is possible too. Finding the best possible pairing is important, because we can filter out the noise events, as these events won't have pairs in the pairing. We can draw one important conclusion, that the time difference of the found pairs should be minimal.

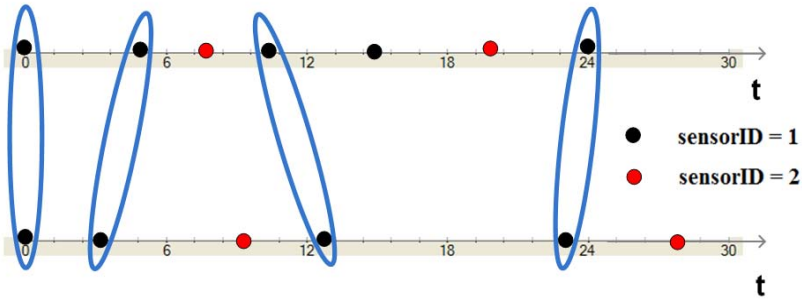

Figure 3: A possible event pairing.

Fig. 4 illustrates another case, where we can see that taking into account only the minimization of the time differences, as mentioned above, might not

lead to an optimal solution. The reason for it is that the event sequences of the two TSSs might be shifted a bit in time. This pair choosing method will thus not pair together those point pairs which really belong together.

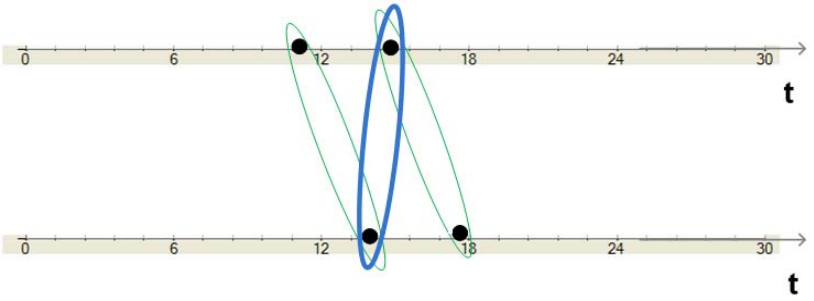

Figure 4: An example when the above greedy pair choosing algorithm does not get an optimal solution.

Thus, we have to redefine the conclusion above so that in the pairing the sum of the time differences should be minimal. This problem is equivalent with the assignment problem in graph theory, which consists in finding a maximum weight matching in a weighted bipartite graph. This assignment problem can be solved in polynomial time, for instance with the Hungarian method [3].

The weights of the edges are

$$w = \frac{1 - |\Delta\mu|}{\Delta t^2} \tag{3}$$

where, w is the weight of the edge, Δt is the time difference between two events, while $\Delta\mu$ is the μ difference between the two events. We can see that the weight of an edge between two events depends on the time and the membership function differences between the events. The weights should have a maximum and a minimum value. On one hand with the maximum value we can normalize the sum of the weights; on the other hand with the minimum value we can avoid the case when we should divide with zero according to the formula above.

At this point we have a weighted bipartite graph and we must search the maximum weight matching in the sub-graphs assigned to the different sensor IDs. Then, the distance between two TSSs is calculated as follows:

$$d = 1 - \frac{\sum w}{TSS_{length,\min} * w_{\max}} \tag{4}$$

where w denotes the weights of the different edges, while $TSS_{length,\ min}$ is the number of elements of the shorter TSS.

5. The event forecasting method

According to the model, each sensor node periodically samples a predefined environmental parameter, and if this sampled value is higher than the threshold limit, the node stores this data as an event. Every sensor has a TSS database, the purpose of the algorithm is thus to create cluster groups from the stored TSSs, and then to extract from these groups the pure event sequences. We used a hierarchical clustering solution, and the results are illustrated with a dendrogram, as shown in *Fig. 5*.

The root node of the dendrogram represents the whole TSS database, and each leaf node is regarded as a TSS. The intermediate nodes thus describe the extent to which the objects are similar to each other; while the height of the dendrogram expresses the distance between each pair of TSSs or clusters, or a TSS and a cluster.

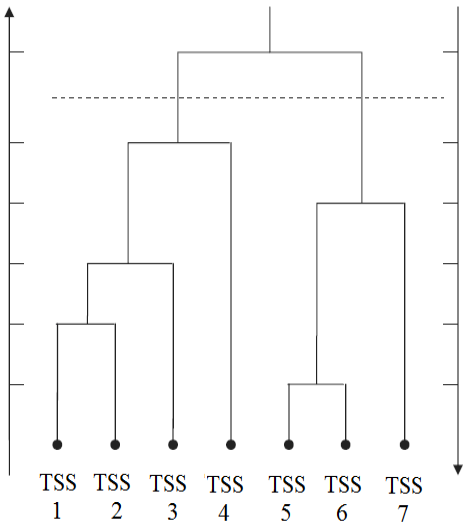

Figure 5: A dendrogram representing the result of the hierarchical clustering.

After the formation of the hierarchical cluster set from the TSS database, in order to attain the desired subsets the dendrogram should be cut at the proper levels. These subsets contain such TSSs, which represent the same event sequence mixed with noise events. After these subsets are available, the algorithm tries to extract the pure event sequences from them with the so called k-mean clustering.

K-mean clustering is one of the hard partitioning methods. It searches an optimal partition of the data by minimizing the sum-of-squared-error criterion (4) in an iterative optimization procedure [2].

$$J_s(\Gamma, M) = \sum_{i=1}^{K} \sum_{j=1}^{N} \gamma_{ij} \| x_j - m_i \|^2 \quad (4)$$

Let $\Gamma=\{\gamma\}_{ij}$ be the partition matrix, defined as follows:

$$\gamma_{i,j} = \begin{cases} 1, \textit{if } x_j \in C_i \\ 0, \textit{otherwise} \end{cases} \quad \text{and} \quad \sum_{i=1}^{K} \gamma_{ij} = 1, \forall j .$$

Let $M = [m_1, ...m_k]$ be the cluster centroid matrix, where $m_i = \frac{1}{N_i} \sum_{j=1}^{N} \gamma_{ij} x_j$ is the sample mean for the i^{th} cluster with N_i objects.

The steps of the *k*-mean clustering algorithm are then the following:

1. Initialize a *K* - partition randomly, or based on some prior knowledge. Calculate the cluster centroid matrix $M = [m_1, ...m_k]$
2. Assign each object in the data set to the nearest cluster C_a , i.e.,

$$x_j \in C_a \text{, if } \| x_j - m_a \| < \| x_j - m_b \|$$

$$j = 1, ..., N \text{ , } a \neq b \text{ , } a = 1, ..., K \text{ and } b = 1, ..., K$$

3. Recalculate the cluster centroid matrix based on the current partition,

$$m_a = \frac{1}{N_a} \sum_{x_j \in C_a} x_j$$

4. Repeat steps 2 and 3 until there is no change in any cluster.

In *Fig. 6* we can see the previously detailed steps for a two-dimensional case. The algorithm randomly assigns two cluster centroids to the input points. Each data point is assigned to a cluster centroid according to the predefined distance function. In the next step the centroids are recomputed. The clustering method executes these steps repeatedly, until there is no change in the centroid matrix. Returning to the forecast algorithm, as a result of cutting the dendrogram at the proper levels, the desired TSS subsets turn up. These subsets will contain TSSs which represent probably the same event sequence mixed with noise events. In that case, we divide the different events assigned to different sensor IDs in the subsets, and we group the three-dimensional (sensor

ID, timestamp, μ) event data structures into two-dimensional planes. These planes represent events which possess the same sensor ID. On those planes we use the formerly detailed k-mean algorithm, as follows: we start with one cluster group, and in each iteration we increase the number of the cluster groups. During an iteration we analyze two conditions: the variances of the groups, and the number of events in each group. If the variance of a group is less than a predefined parameter, it means that at this place in that plane (time stamp, μ) the events are placed densely, and these events can represent a pure event sequence. To verify this, we have to compare the number of events in this group with the number of the TSSs in the subset (dendrogram sub-tree).

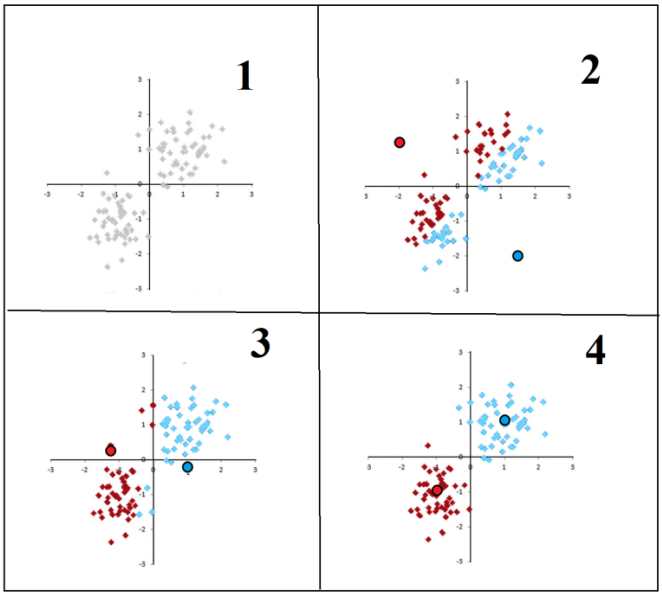

Figure 6: Steps of the K-mean clustering algorithm.

If their ratio is above a second predefined threshold, it means that we have found a pure event sequence, so we store the centroid (time stamp, μ) of the group with the sensor ID assigned to that plane. After that we continue the process on the next plane.

6. Performance analysis

The previously introduced event forecasting algorithm was tested in real circumstances as follows: we implemented a WSN with user interface from

Crossbow MicaZ sensor nodes, with the purpose to measure sound intensity in different kinds of crossroads. After the measurement, the measured data from each sensor node was uploaded to a WSN simulator that was running on a PC. The reasons why the testing of the algorithm was carried out in a simulator and not on the sensor nodes, are the relatively small program memory available on the nodes, the cumbersome nature of the debugging process on the real sensors, and the more clear and transparent supervision of the processes in a simulator. The main purpose of this experiment was to determine whether the event-sequences recognized by the sensors are modeling well the different trajectories of the passing cars.

One directional, straight road

Probably the simplest case is when the nodes are placed along a one directional, straight road. It is simple, because there is only one event sequence to be recognized. The potential difficulties in this case are the following. The different speeds of the cars along the road result in time shifts in the searched event sequences. The different sound intensities of the various cars cause offsets in the membership values of the events. In addition, the acceleration changes of the vehicles cause both of these problems. The setting of the nodes along the road can be seen in *Fig. 7*.

Figure 7: Setting of the nodes along the one directional straight road.

The red numbers mark the sensor IDs of each sensor. The distance between the nodes was approximately 20 meters. As we can see in the figure, the searched event sequence was the (3-2-1). The algorithm recognized this event sequence clearly, and in addition it recognized it in multiple forms, in the sense that in each form the order of the sensor IDs was the same, but the time differences between the events were different. On the whole it can be said that these event sequences (assigned to vehicles with different speeds) were differentiated.

Two directional, straight road

The second measurement was made along a two directional straight road. It was similar to the one directional case in the sense that all of the nodes were planted on the same side of the road in a line, the distance between the nodes being 20 meters. The setting of the nodes can be seen in *Fig. 8.*

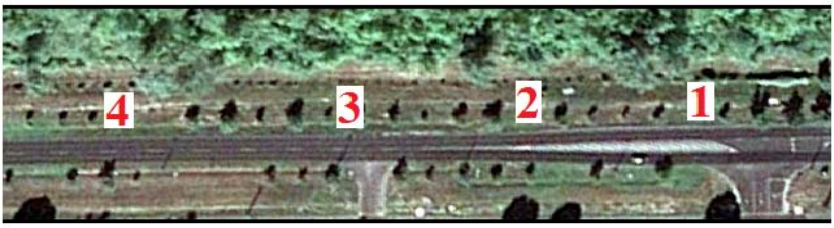

Figure 8: Setting of the nodes along the two directional straight road.

The difficulties to recognize the event sequences were the same as before (speed and acceleration changes), but in this case there were two event sequences to identify, caused by the cars moving on the two sides of the road. These event sequences overlapped with each other in most of the cases. The two event sequences were the (1-2-3-4) and the (4-3-2-1).

From the (1-2-3-4) event sequence the 4th sensor found the (2-3-4), the 3rd node the (2-3) and the 2nd sensor the (1-2) event sequences. There could be several explanations, why the nodes found only event "sub-sequences" from the complete sequence. The overlapping event sequences, the not ideal TSS length, or the noisy environment could all be the reasons for this.

From the (4-3-2-1) event sequence the nodes typically stored only their own sensed event, and that of the preceding sensor node. The recognized sequences were the following: (4-3), (3-2), and (2-1). Considering the fact that the nodes could sense the events of the distant lane less efficiently, and the events of the closer lane could fade them, it is most likely that the above mentioned possible error sources could have a greater impact on the results in this case.

Crossroad

After the straight road measurements, we analyzed a crossroad, which had an average traffic intensity. This case was the most difficult so far, as there were several event sequences to be recognized. If a vehicle tried to leave the horizontal main road for the vertical low priority road, it might have taken several seconds to carry out its task. This time interval depended on the actual

traffic conditions. This means that the time interval of the same event sequences could change. The topology of the measuring nodes can be seen in *Fig. 9.*

Figure 9: The placement of the nodes in the crossroad.

The recognized event sequences were the following: the 2nd node found the (4-3-2) sequence, and was able to mark the vehicles traveling horizontally from right to left on the main road. The 3rd sensor identified the (2-3), the 4th node found the (3-4), and the 5th node found the (4-5) sequences. The (2-3) and the (3-4) event sequences could mark the cars moving horizontally from left to right on the main road. The (4-5) sequence possibly marks vehicles, which turn down from the main road to the lower priority road. The 1st sensor node registered very few events and it didn't found any sequence as a result. The detected event sequences characterize the trajectories of the passing cars quite well.

To summarize the results it can be said that the recognized event sequences contain only two or three events. The density of the events and the small number of the nodes could cause this. In the case if the sensor nodes send these recognized local sequences to a base station, and this fits them together, than the desired global event sequences turn up.

6. Conclusion

In this paper we introduced an event forecasting method for wireless sensor networks and presented its testing results in real circumstances. With Crossbow MicaZ sensor nodes we measured the sound intensity of the vehicles next to various types of roads and in a crossroad. Our purpose was to ensure that the event-sequences recognized by the sensors model well the different trajectories of the passing cars. The experiments showed that in most of the cases the recognized event sequences contained only two or three events. This was probably caused by the small number of the used nodes and the density of the events. If a base station can communicate with all the nodes, then it has the ability to fit together these recognized event sequences and identify the global event sequences. These global sequences mark well the different phenomena appearing in the field of the WSN.

References

[1] Öllös, G., Vida, R., “Adaptive Event Forecasting in Wireless Sensor Networks”, in *IEEE Vehicular Technology Conference* (*IEEE VTC2011-Spring*), Budapest, Hungary, May 15-18, 2011.

[2] Xu, R., Wunsch, D. C., “Clustering”, John Wiley and Sons, New Jersey, 2009.

[3] Kuhn, H. W., “The Hungarian method for the assignment problem”, *Naval Research Logistics Quarterly*, Vol. 2, Issue 1-2, March 1955, pp. 83–97.

[4] Jang, J. -S. R., Sun, C. -T., Mizutani, E., “Neuro-Fuzzy and Soft Computing”, Prentice-Hall Inc., 1997.

[5] Akyildiz, I. F., Su, W., Sankarasubramaniam, Y., Cayirci, E., “Wireless Sensor Networks: a Survey”, *Computer Networks*, Vol. 38, pp. 393-422., 2002.

[6] L. A. Zadeh “Fuzzy sets”, *Information and Control*, Volume 8, Issue 3, June 1965, pp. 338-353.

Acta Universitatis Sapientiae
Electrical and Mechanical Engineering, 3 (2011) 39-50

Assistive Technologies for Visually Impaired People

Sándor Tihamér BRASSAI[1,2], László BAKÓ[2], Lajos LOSONCZI[2,3]

[1] Petru Maior University, Tg. Mureş,
[2] Department of Electrical Engineering,
Faculty of Technical and Human Sciences,
Sapientia Hungarian University of Transylvania, Tg. Mureş
[3] Lambda Communications Ltd., Romania
e-mail: tiha@ms.sapientia.ro

Manuscript received November 15, 2011; revised December 15, 2011.

Abstract: In this paper an overview of different types of assistive technologies is presented. Some of the most important aspects for the visually impaired are the solutions and assistance devices for the daily life. A simple categorization of this type of assistance devices is presented. Another important aspect for the visually impaired people is the indoor/outdoor navigation in dynamically changing environment. The technological advancement made possible the creation of different electronic equipments to help visually impaired/disabled persons in their navigation, such as different navigation systems, obstacle avoidance, object/obstacle localization, orientation assistance systems, in order to extend or change the basic support of guidance dogs and the white cane. In the paper a solution to integrate different assistive technologies is proposed, focusing on navigation and object detection, with the use of intelligent feedback by Human Computer Interfaces (HCI) with implication of Head-related transfer function HRTF functions. The paper is composed of three sections. In the first part a general description of the paper is presented. In the following section, entitled "Assistive technology", two main aspects are discussed: assistive technology for daily life and assistive technology for navigation and orientation of visually impaired. From the assistive systems for daily life, the following most important aspects/subjects are presented: personal care, timekeeping, alarms, food preparation and consumption, environmental control/household appliances, money, finance and shopping. Finally some conclusion is presented. The paper is a comprehensive overview of the literature and it does not contain implementation results.

Keywords: Assistive Technology, Navigation systems for visually impaired.

1. General information

The main objective is the presentation of a system for detection and avoidance of obstacles that assists visually impaired/disabled persons in their movement. In order to achieve the proposed results, the paper will focus on the presentation of different assistive technology solutions.

The concept is to integrate a multi-sensorial input system for distance measurement, and to determine from the measured signals if there are any obstacles in the path of the user. Artificial intelligence and neural networks have an important role in an adaptive learning of the dynamically changing known or unknown environment.

Although many scientists are preoccupied to obtain results regarding the improvement of the comfort of visually impaired persons, the research in this field remains an open subject, as there are many aspects of it that are unresolved.

In the detailed presentation of the paper the technologies used for assistance, monitoring and navigation electronic equipment are presented. Different methods and sensors are presented for the perception of the environment and the detection of objects, for the fusion of different sensors, navigation maps, decision modules and man-machine interfaces, in order to inform the user of the wrong direction of movement, appeared obstacles etc. Equipments and methods used by the person to transmit commands to the assistive system are also discussed.

An interesting section that is of great importance in the process of user localization, will be studied, with the implication of neural networks in environment modeling and decision making. The application of hardware implemented artificial neural networks for achieving an intelligent interface based on acoustical virtual reality for informing the person will also be presented.

2. Assistive technology

The motivation of the project is the interdisciplinary research of a very complex topic of assistance of orientation and navigation of visually impaired people, in a known or unknown indoor environment.

Although many researchers are concerned with obtaining results to improve the comfort of people with visual disabilities, the research topic still remains an open issue. With the advancement of technology concerning computer systems and of information technology, development of technologies to assist people with visual disabilities has also improved. Although such problems have been studied intensively, there are still many unsolved issues.

Assistive Technology is a generic term incorporating technology, equipment, devices, appliances, services, systems, processes and environmental change (Environmental Modifications) used by people with disabilities or older people to overcome social, infrastructural barriers, to actively participate in society and to perform activities easily and safely [22].

From the point of view of visually impaired people the perception of the surrounding environment is very important, even essential, in order to facilitate their mobility.

Assistive technologies for environmental perception and for navigation in the surrounding environment are advancing day by day. In the last decade a variety of portable navigation systems have been designed to assist people with visual disabilities during navigation in the indoor/outdoor known/unknown environments (STIPER [50], electronic cane for navigating in indoor environment [46], AudioMUD [49], SMART Vision [39], VONAVS[40], E-Glass [27], BLI - NAV [34], Tyflos).

Another important aspect concerning visually impaired people is the need for common information and its fulfillment by using modern assistive technologies: audio transcription of printed information, accessing documents and books, music software, communication and information access, computing, telecommunications, tactile access of information, speech, text and Braille conversion technology [1].

A. Assistive technology for daily life

Assistive technologies and development of tools for education, personal care, assistive technology in everyday life (cooking and eating, money, finance, shopping), systems for time management, entertainment (games, visiting museums) and recreation of visually impaired people also plays an important role in terms of research [1].

Assistive systems for daily life can be classified as follows:

- personal care,
- timekeeping, alarms and alerting,
- food preparation and consumption,
- environmental control/ household appliances,
- money, finance and shopping.

The personal care assistive technology refers to two main aspects: labeling and health care monitoring systems.

Concerning personal care, visually impaired people need assistance in identifying different elements of their clothing. Labeling can be grouped in the following types of systems: Tactile Labeling Systems (tactile labels using Braille, tactile labels using the Moon and Fishburne alphabets), Radio Frequency

Labeling Systems, Barcode Labeling Systems (BarTalk, ScanTell, Scanacan for Windows Deluxe, Scanacan Professional Deluxe, Scanacan Professional Elite.

Tactile labeling in general is based on different alphabets used for visually impaired like Braille, Moon or Fishburne alphabets.

The Radio Frequency Identification (RFID) is an automatic identification which retrieves data remotely using RFID tags or transponders. The tag contains silicon chips and antennas to enable to receive and respond to questions from a radio frequency transceiver RFID. Current induced in the antenna by the radio signals provides enough power for CMOS integrated circuit in the tag to send the response. The role of the antenna is to collect power from the input signal and to transmit information of the label.

The bar code readers include the following main components: bar code scanner, database application and voice synthesizer.

In order to assist visually impaired people in monitoring their general health, one can find a series of devices with audio and/or tactile output for measuring temperature, blood pressure, body weight, blood glucose level, devices for insulin measurement and delivery.

One can meet different types of time devices that exist for blind and visually impaired people. Many of these have speech output, but there are also timers with Braille or other tactile display.

From the alarms and alerting devices used by visually impaired people some can be mentioned: Talking Appliance Timer (count up and countdown timers), talking smoke and carbon monoxide detectors and alarms, freezer alarm.

Food preparation and consumption can be a real challenge for visually impaired and blind people. The solution for this problem can be a simple change in the design of common cookers, cutlery and kitchen tools in order to make them safe to use.

From the devices used in food preparation and consumption there can be mentioned: talking kitchen scale, talking measuring jug, liquid level indicator, talking microwave oven, talking kitchen and remote thermometers.

The control of the immediate home environment of the visually impaired people is a condition for their independent life. This means that they have to control a number of home devices and that they have a constant need for feedback from their environment, so that they can accommodate to changes. Light probe and color probe devices can be used to get information from the environment. In the category of environmental control and use of appliances there can be enumerated the following most important devices: talking and tactile thermometers and barometers, washing machine with special functions for visually impaired, talking vacuum cleaner.

Money (cash, debit and credit cards and cheques) is another important aspect of independent life. Accessing it by visually impaired people can be difficult

because of different currency systems. Traveling abroad means that blind or visually impaired people get into contact with different currencies, but most of the existing devices can recognize only one sort of currency. Thus the development of tools that can recognize more, or at least the most commonly used, currencies is an important aspect of assisting visually impaired people in gaining independence. Electronic money identifying devices have an important role in managing money by the visually impaired.

B. Assistive technology for navigation and orientation of visually impaired

Navigation of visually impaired people raises questions about orientation, the appropriate route selection, objects and obstacles detection and avoidance. The advancement of technology has allowed the implementation of various equipments helping visually impaired people in their navigation, such as different obstacle avoidance, localization of objects/obstacles, guidance support systems to extend the basic support provided by means of guide dogs and use of the white cane. Most existing systems do not replace the use of guide dogs and the white cane, but are helpful in taking decisions in navigating/orientation in unusual situations.

Electronic systems used in navigation can be grouped into three categories:

- electronic help for traveling (electronic travel aids, ETAs),
- electronic orientation aid (electronic orientation aids, EOAs),
- position location (position locator devices, PLDs) [48].

In recent years the traditional tools used by visually impaired people for navigation indoors and outdoors (white cane and guide dogs) have been extended/replaced by the use of electronic navigation aid systems. These systems, based on sensors and signal processing are able to improve mobility of persons with visual disabilities in unfamiliar or continually changing environment. By combining the ETA systems [3] [4] [7] and the Man Machine Interfaces based on virtual acoustic reality major successes were achieved in the navigation of visually impaired people.

ETA systems are complex tools to support navigation and are composed of several basic modules:

- obstacle detection system (obstacle detection systems inspired by biological systems) [5], [9],
- trajectory planning module,
- computer-man interface,
- monitoring system.

Monitoring systems follow the movement of persons to ensure that they are moving/progressing and are capable to reach their target. It is also important to know in every moment the current position of the subject, to help in case of a changing environment, or, more importantly, in case of emergencies. The path

planning module is responsible for generating the route to the intended target, combined with the avoidance of obstacles. Position of obstacles in front of subjects is determined through a 3D obstacle detection system.

The components specified must meet requirements similar to those encountered in the case of mobile robots for trajectory planning and detection of obstacles. The man-computer interface provides information extracted from the environment in a friendly manner and assists visually impaired people by navigating "hands free" in their work environment and everyday life.

As it results from the literature a system that integrates different technologies for the support of visually impaired people may have the structure presented in Fig. 1. The system is composed of two basic modules:

- a personal computer connected to the Internet (called service center),
- a portable equipment [5] [6] [7] [9].

Real-time communication between the two modules is achieved through a wireless communication module (GSM [3] [8] [18], GPRS [36], WIFI).

The personal computer serves as a support for various functions (technologies): navigation assistance, information, etc.

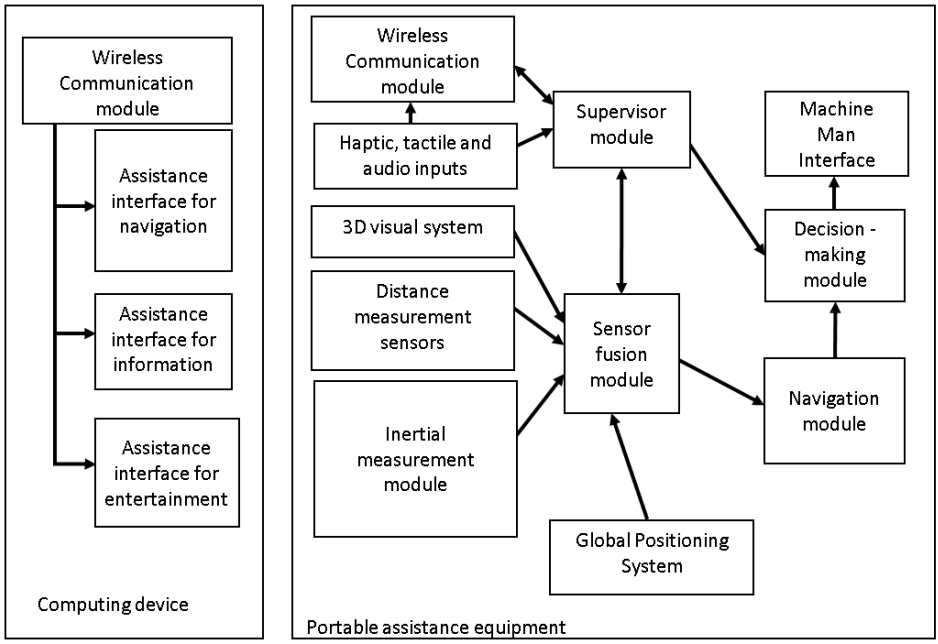

Figure 1: Block diagram of the proposed system.

It should always be checked (monitored) whether the person has reached the destination, has avoided being blocked in his/her movement because of changes

in the environment. This module stores the database of the environment (ex. GIS [42]), the defined trajectory and the current position of the person.

Through the information assistance interface, special information technologies can be accessed (reader of printed documents, access of documents and books, music software, communication, computer systems, telecommunications) [1].

The portable device serves several functions and involves the use of embedded systems of control and processing. Communication with the personal computer (connection type) is achieved by a real-time communication module (GPRS) [36], GSM [3] [8] [18], WiFi [37], RF, etc.).

The input interface has the role of introducing "specific commands". This unit can contain Braille keyboard, voice input unit, etc. Through this interface different commands can be addressed to the computer (examples: target specification, starting playing music, connection to a radio channel, different questions addressed to the system, voice communication interface [37], speech recognition [44], Braille reader).

For the visually impaired people the detection of objects and obstacles arising during route following is very important, but equally important is the location of the person and following his/her trajectory, because the location of the person must be correlated to the stored environment in the navigation environment's interface. Ultrasonic systems for distance measurement [21] [27] [41] [47] [37], visual systems (stereo vision systems [37]), infrared sensors, etc. can be used to detect obstacles.

For trajectory tracking, and orientation of the person, GPS tracking systems and tracking systems based on inertial movement sensors are used. A very important issue is the location of the person, because both GPS systems and inertial systems introduce significant measurement errors. GPS systems get the absolute position of the person but with errors of a few meters and a low sampling rate. GPS systems can be used only in outdoor navigation.

Inertial positioning systems based on accelerometers and gyroscopes introduce positioning error resulted from the integration of measurement and quantization noise By using magnetic compasses (with which absolute orientation can be obtained) as an extension of accelerometers and gyroscopes, superior results can be obtained. Research results related to positioning and navigation systems used in mobile robots can be used to locate people, detect obstacles.

By merging measurement data from several types of sensors, superior results can be obtained in the tracking of persons. Merging several types of sensors requires a very complex computation process. In order to solve these types of problems the Kalman Filter or the Extended Kalman Filter is used. The sensor fusion module is responsible for integrating different sensors.

Trajectory design is guided by detection or non-detection of obstacles. If there are no obstacles detected, the trajectory is dictated by the general

navigation system. In case of detected obstacles, the general navigation system is overwritten according to the position of obstacles. By the man-computer interface module orders (indices) are transmitted to the person.

There are several possibilities to implement the man-computer interface (Man Machine Interface, MMI) [5] [12] [4] [5] [6] [8]. In accordance with this principle, the proposed interface replaces the visual reality with the acoustic virtual reality.

The presence of various obstacles in the environment is indicated by a beeping sound based on the virtual position that suggests the real position of the obstacles. Various obstacles are differentiated by the different frequency of the sounds. The intensity and frequency of occurrence of the signal depends on the distance to the obstacles. A pilot signal of constant intensity and frequency indicates the direction of the route to follow. The module mentioned requires the implementation of a Head Related Transfer Function which differs depending on the frequency of the sound, head orientation and distance to the obstacle. Practical implementation of the AVR concept [3] requires knowledge of the Head Related Transfer Function for each point of the 3D space for each subject. Often, artificial neural networks are used for the implementation of HRTF functions [4] [5] [7] [13] [14] [28] [52] [54] (54 without RNA). A study on the use of Multi-layer Perceptron Networks for modeling HRTF functions is presented in [4].

Another example for the orientation of the person is the use of a voice processor which, by direct verbal commands directs and warns the person concerned [37]. Often the ultrasound module of object detection is combined with vibrators for informing the user [41] [47] (eg. vibro-tactile feedback for information, usually operating with two vibrators). There is also an interface with a simple keyboard and a voice synthesizer [42]. There are also systems in which the environment is described by spoken text [49], and navigation commands are transmitted by voice [34] to alert the user of the distance from the obstacles or from the destination [12]. There are also systems used for character recognition in real time in case of touching labels, restaurant menus and other printed materials. The network outputs are used to create a Braille matrix, driving the top of the fingers of blind persons, or converting into spoken text told by a regular Personal Digital Assistant (PDA) device [50].

A challenging problem for navigation support systems for visually impaired people is the instant and precise location of the user. Most of the proposed systems based on GPS sensors were found to be insufficient for usage for pedestrians and are limited to the external environment, with serious errors in urban areas.

The possibilities offered by neural networks as a tool to study spatial navigation in virtual worlds include methods to predict the next step for a

predefined path, obtaining basic spatial knowledge based on “landmarks” and configure a spatial “layout”. The question is how to develop a spatial representation of the virtual world, other than a cognitive map. The possibility of extending the methodology to study navigation in human-computer interaction (Human Computer Interaction, HCI), calculation methods of navigation, the potential usage of cognitive maps in the navigation process modeling, non-visual models for learning the special world by exploring the virtual world space and their applications are studied in the literature [2].

For the implementation of the sensorial interface, the related literature and the sensors used in case of mobile robots will be studied. The sensorial interface used for localization and object detection includes a sonar system, infrared sensors, inertial measurement unit, magnetic sensors, stereo vision system. For modeling of the environment (the position and orientation of detected obstacles) we propose to use of artificial neural networks. The surrounding space will be scanned and distances to the object will be recalculated/learned in real time in the neural network.

The decision making module, based on the results of the environment modeling, will take a decision regarding the orientation of objects and will inform the user by the man machine interface.

3. Conclusion

The assistive technologies used by visually impaired people are very complex. A wide range of different electronic assistive technologies exist and are used by visually impaired. Some of these tools are unreachable by most of the visually impaired persons.

The integration of different assistive solutions in a single assistive system is a great challenge.

Acknowledgements

This paper is a result of the project “Transnational Network for Integrated Management of Postdoctoral Research in Communicating Sciences. Institutional building (postdoctoral school) and fellowships program (CommScie)” - POSDRU/89/1.5/S/63663, financed under the Sectoral Operational Programme Human Resources Development 2007-2013.

References

[1] Keating, D., Parks, S., et.al, "Assistive technology for Visually Impaired and Blind People", Springer, 2008.

[2] Patel, K. K., Vij, S. K., "Spatial Navigation in Virtual word", *Advanced Knowledge based systems: Model, Application and research*, vol. 1 pp.101-125, 2010.

[3] Tiponuț, V., Ianchis, D., Haraszy, Z., "Assisted Movement of Visually Imaired in Outdoor Environments – Work Directions and New Results", *Proceedings of the 13-th WSEAS Conference on SYSTEMS*, by WSEAS Press, 2009, pp.386-391.

[4] Haraszy, Z., Cristea, D.G., Tiponuț, V., Slavici, T., "Improved Head Related Transfer Function Generation and Testing for Acoustic Virtual Reality Development", *Latest trends on Systems*, vol. II, pp 411-417, 2011.

[5] Tiponut, V., Ianchis, D., Bash, M., Haraszy, Z., "Work Directions and New Results in Electronic Travel Aids for Blind and Visually Impaired People", *Latest Trends on Systems*, vol. II, pp347-353, 2011.

[6] Haraszy, Z., Micut, S., Tiponut, V., Slavic, T., "Multi-Subject Head Related Transfer Function Generation using Artificial Neural Networks", *Latest Trends on Systems*, vol. I, pp. 399-405, 2011.

[7] Gavrilut, I., Tiponut, V., Gacsadi, A., Tepelea, L., "Wall-Following Method for an Autonomous Mobile Robot UsingTwo IR Sensors", *New Aspects of systems, Proc. of the 12th WSEAS International Conference on Systems*, Heraklion, Greece, 2008, pp. 205-208.

[8] Tiponut, V., Haraszy, Z., Ianchis, D., "Acoustic Virtual Reality Performing Man-Machine Interfacing of the Blind" *New Aspects of systems,, Proceedings of the 12th WSEAS International Conference on SYSTEMS*, Heraklion, Greece, 2008, pp. 345-350.

[9] Tiponut, V., Popescu, S., Bogdanov, I., Caleanu, C., "Obstacles Detection System for Visually Impaired Guidance", *New Aspects of system, Proceedings of the 12th WSEAS International Conference on SYSTEMS*, Heraklion, Greece, 2008, pp. 350-356.

[10] Gavrilut, I., Tiponut, V., Gacsadi, A.,"Mobile Robot Navigation Based on CNN Images Processing – an Experimental Setup", *Proceedings of the 13th WSEAS International Conference on SYSTEMS*, 2009, pp 220- 225.

[11] Bogdanov, I., Mirsu, R., Tiponut, V., "Matlab Model for Spiking Neural Networks", *Proceedings of the 13th WSEAS International Conference on SYSTEMS*, Rhodes, Rodos Island, Greece, 2009, pp. 533-538.

[12] Wada, C., "Basic Study on Presenting Distance Information to the Blind for Navigation", *Innovative Computing, Information and Control (ICICIC), 2009 Fourth International Conference on*, 2009, pp. 405 - 408.

[13] Hu, H. M., Zhou,Ma., H., and Wu, Z., "HRTF personalization based on artificial neural network in individual virtual auditory space", *Applied Acoustics*, vol. 69, issue 2, pp 163-172, Feb. 2008.

[14] Lemaire, V., Clerot, F., Busson, S.,Nicol, R., Choqueuse, V., "Individualized HRTFs From Few Measurements: a Statistical Learning Approach", *Proceedings of International Joint Conference on Neural Networks*, Montreal, Canada, 2005, vol. 4, pp. 2041-2046.

[15] Hollinger, K. J., "Orientation and Mobility Instruction Utilizing Web-Based Maps Association for Education and Rehabilitation of the Blind and Visually Impaired" *AER Report*, Vol. 26, No. 2 Summer, 2009.

[16] Hesch A. J., and Roumeliotis, S. I., "An Indoor Localization Aid for the Visually Impaired", *IEEE Internat. Conf. on Robotics and Automation*, Roma, Italy, 2007, pp. 3545 – 3551.

[17] Treuillet, S., Royer, E., Chateau, T., Dhome, M., Lavest, J. -M., "Body Mounted Vision System For Visually Impaired Outdoor and Indoor Wayfinding Assistance", *Conference & Workshop on Assistive Technologies for People with Vision & Hearing Impairments Assistive Technology for All Ages* CVHI 2007, M.A. Hersh (ed.), 2007. pp. 1-6.

[18] Helal, A., Moore, S. E., Ramachandran, B., "Drishti: An Integrated Navigation System for Visually Impaired and Disabled", *In Proceedings of ISWC'2001*. pp. 149-149, 2001.

[19] Jew, M., "Design and Implementation of an Integrated Navigation System on an FPGA-PhD thesis", New Mexico Inst. of Mining and Technology Socorro, New Mexico, 2010.

[20] Nordin, J., Ali, A. M., "Indoor Navigation and Localization for Visually impaired people Using Weighted Topological Map", *Journal of Computer Science*, Vol. 5, issue 11, 2009.

[21] Kish, D., "Sonic Echolocation: A Modern Review and Synthesis of the Literature", World Acces for the Blind, pp. 1-52, 2003.

[22] Hersh, M.A., "The Design and Evaluation of Assistive Technology Products and Devices Part 1: Desig", *International Encyclopedia of rehabilitation*, 2010.

[23] Horiuchi, T. K., "A Low-Power Visual-Horizon Estimation Chip", *IEEE Transactions on Circuits and Systems*, vol. 56, no. 8, Aug. 2009.

[24] Ouarda, H., "A Neural Network Based Navigation for Intelligent Autonomous Mobile Robots", *Internat. Journal of Math. Models and Methods in Appl. Sc.*, issue 3, Vol. 4, 2010.

[25] Laurent, B., Noupowou, T., Christian, A., "A sonar system modeled after spatial hearing and echolocating bats for blind mobility aid", *International Journal of Physical Sciences* vol. 2 (4), pp. 104-111, Apr. 2007.

[26] Horiuchi, T. K., "A Spike-Latency Model for Sonar-Based Navigation in Obstacle Fields", *IEEE Trans. On Circuits And Systems*, vol. 56, no. 11, Nov. 2009.

[27] Meridji, K., Al-Sarayreh, K. T., "Embedded System Using Ultrasonic Waves and Voice Biometric to Build an E-Glass for the Blinds", *Marsland Press Journal of American Science*, vol. 6, no. 4, pp. 34-42, 2010.

[28] Haraszy, Z., Ianchis, D., Tiponut, V.,"Generation of the Head Related Transfer Functions, Using Artificial Neural Networks", *Proc. of the 13th WSEAS International Conference on CIRCUITS*, 2009, pp. 114-118.

[29] Marx, W., "Addressing Today's Embedded Design Challenges with FPGAs", Embedded Platform Sales Mgr, North America September 29, 2007.

[30] Dinu, A., Cirstea, M.N., Cirstea, S. E., "Direct Neural-Network Hardware-Implementation Algorithm", *IEEE Trans. on Ind. Electr*., vol. 57, issue 5 pp. 1845 – 1848, 2010.

[31] Yang, Z., and Qian, J., "Hardware Implementation of RBF Neural Network on FPGA Coprocessor", *Information Computing and Applications, Communications in Computer and Information Science*, vol. 105, Part 7, pp. 415-422, 2011.

[32] Lin, C. -J., Lee, C. -Y., "FPGA Implementation of a Recurrent Neural Fuzzy Network with On-Chip Learning for Prediction and Identification Applications", *Journal of Information Science and Engineering*, pp. 575-589, 2009.

[33] Kumar N. V., "Integration Of Inertial Navigation System And Global Positioning System Using Kalman Filtering", Department Of Aerospace Engineering, Indian Institute Of Technology, Bombay, Jul. 2004.

[34] Santhosh, S.S., Sasiprabha, T., Jeberson, R., "BLI - NAV embedded navigation system for blind people", *Recent Advances in Space Technology Services and Climate Change (RSTSCC)*, 2010, pp. 277 – 282.

[35] Bourbakis, N, "Sensing Surrounding 3-D Space for Navigation of the Blind", *Engineering in Medicine and Biology Magazine*, IEEE, vol. 27 , issue 1, pp. 49 - 55, 2008.

[36] Chumkamon, S., Tuvaphanthaphiphat, P., Keeratiwintakorn, P., "A blind navigation system using RFID for indoor environments", *Electrical Engineering/Electronics, Computer, Telecommunications and Information Technology ECTI-CON 5th International Conference on*, 2008, vol. 2, pp. 765 – 768.

[37] Ran, L., Helal, S., Moore, S., "Drishti: an integrated indoor/outdoor blind navigation system and service", *PerCom 2004, Proceedings of the Second IEEE Annual Conference on*, 2004, pp. 23 – 30.
[38] Fernandes, H., Costa, P., Filipe, V., Hadjileontiadis, L., Barroso, J, "Stereo vision in blind navigation assistance", *World Automation Congress (WAC)*, 2010, pp. 1-6.
[39] Faria, J., Lopes, S., Fernandes, H., Martins, P., Barroso, J., "Electronic white cane for blind people navigation assistance", *World Automation Congress (WAC), 2010,* pp. 1 – 7.
[40] Punwilai, J., Noji, T., Kitamura, H., "The design of a voice navigation system for the blind in Negative Feelings Environment", *ISCIT 2009*, 2009, pp. 53-58.
[41] Bousbia-Salah, M., Redjati, A., Fezari, M., Bettayeb, M., "An Ultrasonic Navigation System for Blind People", *Signal Processing and Communications, 2007. ICSPC 2007. IEEE International Conference on*, 2007, pp. 1003 – 1006.
[42] Kaminski, L., Kowalik, R., Lubniewski, Z., Stepnowski, A., "VOICE MAPS" — portable, dedicated GIS for supporting the street navigation and self-dependent movement of the blind", *Information Technology (ICIT), 2010 2nd Internat. Conf. on*, 2010, *pp.* 153 – 156.
[43] Wong, S.M., Tang, C.E., Nik Zulkifli, N. H.,, "Efficient RFID tag placement framework for in building navigation system for the blind", *Information and Telecommunication Technologies (APSITT), 2010 8th Asia-Pacific Symposium on*, 2010, pp. 1 – 6.
[44] Kantawong, S, "Road traffic signs detection and classification for blind man navigation system", *Control, Automation and Systems, 2007. ICCAS '07. International Conference on,* 2007, pp. 847 – 852.
[45] Kantawong, S., Phanprasit, T., "Information signs compression and classification using vector quantization and neural network for blind man tourisms navigation system" *Electrical Engineering/Electronics, Computer, Telecommunications and Information Technology, 2008. ECTI-CON 2008. 5th International Conference on*, 2008, vol. 1, pp. 477 – 480.
[46] Ali, A.M., Nordin, M.J., "SIFT based monocular SLAM with multi-clouds features for indoor navigation", *TENCON 2010 - 2010 IEEE Region 10 Conference*, 2010, pp. 2326 – 2331.
[47] Hashino, S., Ghurchian, R., "A blind guidance system for street crossings based on ultrasonic sensors", *Information and Automation (ICIA), 2010 IEEE International Conference on*, 2010, pp. 476 – 481.
[48] Dakopoulos, D., Bourbakis, N.G., "Wearable Obstacle Avoidance Electronic Travel Aids for Blind: A Survey" *Systems, Man, and Cybernetics, Part C: Applications and Reviews, IEEE Transactions on,* vol. 40 , issue 1, pp. 25 – 35, 2010.
[49] Sanchez, J., Hassler, T., "AudioMUD: A Multiuser Virtual Environment for Blind People", *Neural Systems and Rehabilitation Engineering, IEEE Transactions on*, vol. 15 , issue 1, pp. 16 – 22 , 2007
[50] Ros, P. M., Pasero, E., "Artificial Neural Networks for Real Time Reader Devices", *Neural Networks, 2007. IJCNN 2007. International Joint Conference on*, 2007, pp. 2442 – 2447.
[51] Ros, P. M., Pasero, E., "A framework for developing Neural Networks based mobile appliances", *Neural Networks (IJCNN), The 2010 International Joint Conference on*, 2010, pp. 1 – 8.
[52] Seki, Y., Sato, T., "A Training System of Orientation and Mobility for Blind People Using Acoustic Virtual Reality", *Neural Systems and Rehabilitation Engineering, IEEE Transactions on*, vol. 19, issue. 1, pp. 95 – 104, 2011.
[53] Ivanov, R., "Indoor Navigation System for Visually Impaired", *International Conference on Computer Systems and Technologies - CompSysTech'10*, 2010, pp.143-149.
[54] Antonio Francisco Rodríguez-Hernández, A. F., Merino, C., et. al., "Sensory Substitution for Visually Disabled People: Computer Solutions", . *WSEAS Transactions On Biology And Biomedicine*, issue 1, vol. 7, Jan. 2010.

Acta Universitatis Sapientiae
Electrical and Mechanical Engineering, 3 (2011) 51-60

Adaptation of Energy Production to Forecast Values Using External Storage

Sándor KAZI

Department of Computer Science,
Faculty of Electrical Engineering and Informatics,
Budapest University of Technology and Economics, Budapest, Hungary
e-mail: kazi@cs.bme.hu

Manuscript received November 20, 2011; revised December 20, 2011.

Abstract: This paper introduces a real-world optimization task of electrical energy production. Electrical energy production and consumption relies in a large measure on forecasts, the main difference among countries and among sectors is in the person or organization who is supposed to make predictions. In some cases it is the responsibility of the consumer or of the energy producer, in other cases there are specialized companies for hire to make these forecasts (for ex. "*Regelzonenführer*"-s in Austria). This paper considers the problem when the forecast is already given by the producer and they have to predict almost the exact amount of electrical energy to be produced if they want to avoid penalties. The problem in question is from a sector and from a country (wind turbines, Hungary) where the forecast is made by the energy producer and large differences between the predicted and the actually produced values are penalized. The optimization problem is to use a storage facility effectively enough to increase the income of a wind farm by the later submission of previously overproduced electrical energy. This paper introduces this problem in details, and presents solutions for it. The steps to create a reinforcement learning solution for this kind of a stochastic problem are presented besides a simple and effective solution for this exact task. The reinforcement learning solution consists of a modeling and an algorithm application step, and also of the incremental steps to make the solution more effective by specialization.

Keywords: Wind energy, optimization, energy storage, reinforcement learning.

1. Detailed specification

In some countries energy producer companies are obligated to submit a forecast of their next production period. This is a reasonable expectation,

because the buyer (in most cases an electricity service provider) needs to know how much energy can they count on. Because of that, this schedule has to be as accurate as possible. Sometimes the companies are motivated by rewards or penalties according to the accuracy of their predictions. If they apply a storage facility they can balance the over- and underproduction by storing and retrieving energy. This paper is about the strategy of effectively using storage to enhance productivity and increase income by adaptation to the previous prediction and by not being penalized.

The available data of the era is from a wind farm (Mosonszolnok, Hungary; seven turbines), the owners of which have to submit predictions daily for each quarter hour. The data records are historical and consist of a timestamp (interval identifier), a forecast and the produced value.

The environment in question has law enforced buying prices for wind energy. If the difference between the prediction and the production is less than a previously specified threshold (currently that is fifty percent of the forecast), the buying price is approximately 0.1€ per kilowatt-hour. If the produced value is out of the margin the company has to pay a 0.04€ penalty per every kilowatt hour of the difference between the forecast and the production; the buying price remains the same.

Because of the structure of the data, we have to make a conversion from the real life control problem into a discrete time decision problem. To reduce the original optimization task into this kind of a mathematical form we should make assumptions and disregard some components of it.

We disregard the continuance of the quarter hour periods – we assume that decisions have to be made at the end of these periods where the forecast and the produced value are known. At the end of each period we can decide the submission rate of the production (how much should be stored and not submitted) – this is not a real life assumption but a reinforcement learning method designed to cope with this kind of problems can be a good approximation of a continuous time alternative.

We disregard the nature of the storage technology (dissipation and amortization) for this time, to test only the algorithms. There are three causes for this decision: the “continuity assumption” does not really support this kind of information (lifetime also depends on charging speed), this factor can also be considered later by altering the reward function, and the third cause is that it would be another stochastic factor added to the problem. It should be an independent parameter in the decision of whether it is reasonable or not to apply a storage facility, approximate costs can be calculated for these factors. The storage technology was considered only through its boundaries. Corresponding rated power and discharge time parameters belong to a storage which can be either an accumulator (NaS-accumulator for example) or pumped storage

facility (energy stored in the potential energy of water). These parameters are technology-dependent. In a step (quarter hour) the level of the storage can only be changed by the quarter of its rated capacity.

The algorithms consider the forecast to be fixed for each quarter hour and it is also considered out of scope: we assume that the prediction (which is based on meteorological data and personal expertise) is as close as possible. The aim of these algorithms is not to adjust the prediction but to develop a strategy to adjust to the forecasts using storage.

With these assumptions we have a discrete time environment, a decision is needed each step which defines the exact values to sell and to store into or to use up from the storage.

2. Reinforcement learning and modeling

Those who are not familiar with the concept of reinforcement learning can check the online[1] or printed version of an introduction book written by Richard S. Sutton and Andrew G. Barto [1]. This book clarifies the main ideas and methods of the area by the use of both mathematical reasoning and examples.

To apply a reinforcement learning method a Markov decision process is required. In most of the cases the aim of the algorithms is to discover the uncertain parts of the model or to develop a "valuable" strategy.

With the assumptions made in the previous section we have a discrete time stochastic environment which cannot be affected by our decisions, but has its own internal states and transitions among them. If we expand the "environment" with the current state of our storage it can be modeled with a discrete time Markov chain (the Markov-property is present). With actions taken into consideration it implies Markov decision processes (MDP for short) [1]. The "expanded environment" denomination mentioned above also has states, but they can be partly affected by our decisions.

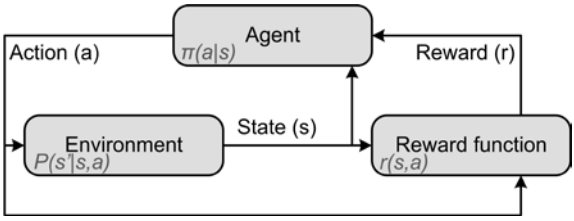

Figure 1: A common notation for a Markov decision process.

[1] An HTML version of the book can be found at the webpage of the author: http://webdocs.cs.ualberta.ca/~sutton/book/the-book.html

It was clarified above, that this problem can be modeled by a Markov decision process. The next step in the modeling phase is to specify the parameters describing the state, the action and the reward (or the reward function). It is clear that if these parameters are given the parts missing from the figure above are the transition probabilities (P) and the policy (π). The policy is driven by the algorithms so it is not a question of modeling, but the probabilities clearly depend on the definition of states and actions.

To specify the Markov decision process we have to assign meaning for the state and action parts. The reward function can be different for each algorithm; therefore it will be defined among the algorithms and in the evaluation section. The state can contain most of the information about the "expanded" environment like: previous and current production and forecast values, current storage level and also forecasts for the upcoming intervals. It is a matter of modeling what we choose to represent a state. In most of the following methods the state contains all the previously mentioned information: it has a backward window for forecasts and production, a forward window for forecasts and contains the actual values of the storage, forecast and produced energy.

It is clear that the action has to represent the choice we make. It can be specified in a few equivalent ways. I chose it to be the one of the most similar ones to the state description: the action is represented by the new storage level (caused by our choice).

After examination a person could notice that in this environment we have more information than in a general case. We can calculate the rewards for all actions that we did not choose – it can be a great deal of information for a learning algorithm and lead to faster convergence.

3. Algorithms

1. Algorithms "by the book" [1]

Algorithm planning can be an iterative process, as it was this time. There were a few less successful algorithms in coping with the above described problem, and a few which can be counted as a success. The first algorithm I used to test the applicability of reinforcement learning on the task was a well-known dynamic programming method [1]. This method had two flaws to fall back on: the accuracy of the transition probabilities, and the fact that it needs final (exit) states or an episodic MDP to calculate the reward backwards. After a conversional step to an episodic MDP (1 episode ~ one or a few days) the only uncertainty is the lack of information about transitions. This information can be gathered runtime, but the granularity (20000 different production values) and the quantity (9000 rows) of the data do not make it possible to gather enough

empirical information about the transition probabilities. Because of these factors I applied quantification in my dynamic programming method, which is compromise, because the margin is stiff, only a difference of 1kWh-s can make a difference.

I also applied an R-learning algorithm [1] on the model, which is an average reward maximization method. The flaw of the model is that it can be used effectively only if the forecast or the margin width is constant. The lack of information about transition probabilities is also present.

2. SARSA algorithms

The methods presented above had their flaws which made them ineffective. The algorithm class I applied next is the SARSA approach which is a different point of view among reinforcement learning methods. It considers state-action-reward-state-action tuples and operates by maintaining a value estimate for state-action pairs (instead of states). This algorithm in its basic form [1] still has the flaw that it needs a good estimate of transition probabilities. We still cannot provide these estimates to be accurate enough because of the quantity of the data. Yet again, quantification is an option, but it still makes the approximate values unreliable.

To improve the SARSA solution by the means of the learning process itself I transformed it into an algorithm using eligibility traces (SARSA(λ)). The eligibility traces are supposed to make the learning process faster by using the information from one step to update more than one value estimates. It is also important to shake off the problem of the unknown probabilities. It is easy to see, that close values represents similar states and actions. This fact calls for exploitation of generalization. Function approximation is a common technique for this kind of task, the linear, gradient-descent SARSA(λ) (for an algorithm using binary features, check [1]) suits these expectations. The effectiveness of linear, gradient-descent function approximation methods depends on the selection method of features.

The method which brought success is a linear, gradient-descent method using Gauss-functions as features. We need a method to select the appropriate feature which divides the state-action space by the features how they can best express the similarity among the state-action pairs. If we divide the space in every dimension for a grid-like Gauss-function placement, we will be stricken by the curse of dimensionality (for n attributes representing the state-action space, we need k^n features to set two values in each dimension). The number of the features is clearly a factor in the runtime of an algorithm, so it is recommended to keep the number of features lower. There are references on the effectiveness of random feature selection [2]. This method chooses a specified number of features randomly from the set of possible values. For the random

selection to be enough, the state and the action representations are also needed to be bounded in every dimension. Luckily, the building blocks of the state and the action representations are bounded variables or a realistic upper and lower bound can be selected. According to the dataset, the upper bound production value is approximately 25000 kWh, but it can be specified as 20000 kWh because with a probability of 0.98 it is also an upper bound. Disregarding very rare events in the feature selection can lead to a better model.

The pseudo-code for the first version of my SARSA(λ) algorithm can be seen on the figure below. The x_i-s are the Gauss functions used for the calculations of φ vectors, I_{acc} is an indicator distribution (equals to 1 in case of "accumulating traces" and to 0 in case of "replacing traces" mode [1]), $\langle \_, \_ \rangle$ is the scalar product of the two parameters. All other notations have the same meaning as in the original SARSA(λ) variant [1].

Linear, gradient-descent SARSA(λ) (Gauss features)

$n \leftarrow$ number of features
$\vec{\theta} \leftarrow$ any n-parameter gradient vector
$\vec{e} = 0$
for all $\forall i \in [1, n]$ **do**
  $x_i : \mathcal{S} \times \mathcal{A} \rightarrow \mathbb{R}_+$ (Gauss function) $\left(\vec{\phi}(s,a) = \left(x_1(s,a), x_2(s,a), \ldots, x_n(s,a)\right)^T \right)$
end for
$s \leftarrow s_0$
$a \leftarrow \arg\max_{a \in \mathcal{A}(s)} \left\langle \vec{\phi}^T(s,a), \vec{\theta} \right\rangle$
while s is not terminal **do**
  $\vec{e} \leftarrow I_{acc}\vec{e} + \vec{\phi}(s,a)$
  $a \rightarrow r,\ s'$
  $\delta \leftarrow r - \left\langle \vec{\phi}(s,a), \vec{\theta} \right\rangle$
  $a' \leftarrow \arg\max_{a \in \mathcal{A}(s')} \left\langle \vec{\phi}(s',a), \vec{\theta} \right\rangle$
  $\delta \leftarrow \delta + \gamma \left\langle \vec{\phi}(s',a'), \vec{\theta} \right\rangle$
  $\vec{\theta} \leftarrow \vec{\theta} + \alpha\delta\vec{e}$
  $\vec{e} \leftarrow \gamma\lambda\vec{e}$
  $s \leftarrow s'$
  $a \leftarrow a'$
end while

Figure 2: The pseudo-code of a linear, gradient descent SARSA(λ) solution with eligibility traces and Gauss features.

As already noted there is more information about the process itself than usually. We can calculate the rewards not only for the chosen action but for all of them. If we make the adjustment of eligibility traces according to all of the actions, not only to the chosen action, it can lead to a better approximation. This is a manipulation of the tenth line of the pseudo-code: instead of the addition of one specific (chosen action) φ vector, the added value is the average of all φ vectors for each eligible action.

The feature selection method can also be specialized. One method of specialization is that the distribution used for feature center generation is not a uniform distribution but the distribution of the data or a special distribution which is dense where we want to distinguish states more and sparse where we do not want to. There is another similar method to specialize: we can use taller (and narrower) Gaussian functions in the dimension where it is more important to distinguish states and lower ones otherwise. These two methods can lead to a better feature generation algorithm.

Another modification to upgrade the performance of the algorithm is to avoid penalties by narrowing the set of the actions for each state. If we avoid penalties every time we can, it is a greedy-like minimization of the penalty, and by that a greedy-like maximization of income. The action to choose is still not trivial, so the optimization problem will change, but henceforward needs a solution. This modification can be placed between the twelfth line and the thirteenth line (or we can adjust the model itself) as a step narrowing the set of actions eligible at the current state.

3. Decision tree

The above mentioned greedy-like method had been tested before the success of the SARSA variants. We can call this simple algorithm a decision tree method. Let there be a preferred storage level (c_{pref}), set the new storage level (action) to this level. Now we are going to fit it into the specification (if it is required) by moving it backwards in the direction of the previous storage level. Let the possible action set be the set of all actions possible in all states (from the minimum level, to the maximum). Narrow this action state to the reachable actions: the maximum difference between the actual and the next state of the storage is the quarter of the rated power parameter. Then choose the action from set which is the nearest to the preferred storage level.

4. Evaluation and conclusion

We have the forecasts and real produced values of three months which leaves us with 8736 records having 5506 different forecast and 1672 different production values from the interval between 0 and 24000. The modus of each is

0 (1513 and 1617 times), because of the predicted “windless” intervals and maintenance shutdowns.

Long zero sequences are not really useful for comparison: if we predicted zero we are penalized if we sell any of our production, if we produce zero, than we have to use energy from the storage to occasionally avoid penalty. Both ways, we can get stuck on a full or an empty storage while the zeros are still coming. On the other hand, if the prediction is rarely bad for a long interval (or commute between high and low) then the decision tree method would be absolutely enough to solve the problem.

It’s visible on the forecast and production comparison diagrams, that there is a positive correlation between the two parameters, so it is not impossible to develop a strategy, but it is also a warning of “commute” mentioned above.

The methods described above were tested using three different reward functions. The first type of reward was the exact income which could be negative in case of a large underproduction. The second type of reward was an indicator-like function: 1 if the there are no penalties, -1 otherwise. The third type was similar to the second, but it was multiplied by the forecast value.

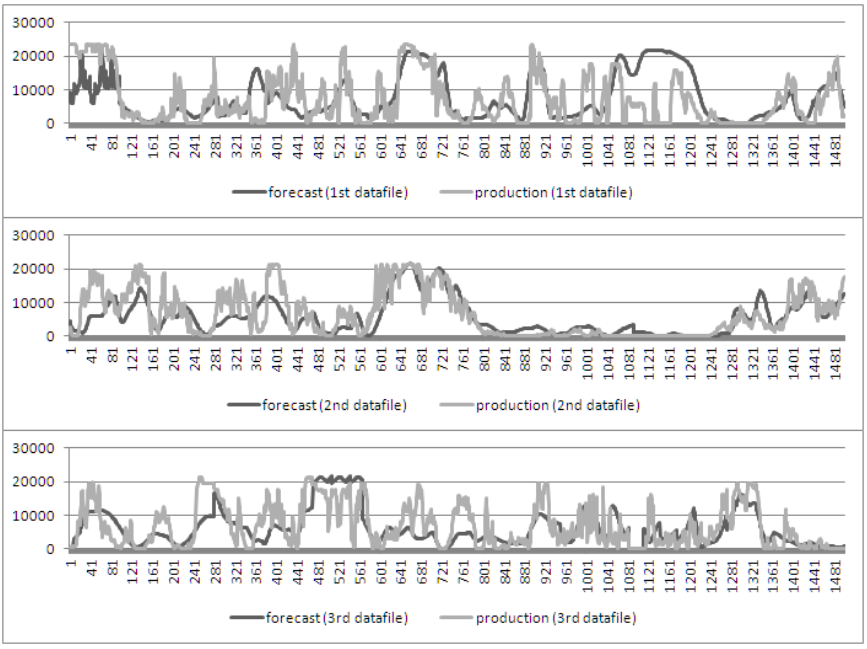

Figure 3: Forecast and production values compared to each other for each test set (horizontal axis represents the number of the interval, the vertical axis is the production or forecast value in kWhs).

But why do they represent the quality of the decision? The answer is trivial for the first one, because it is the income. The second one is not as obvious, and not always represents the real value of a decision, because a penalty can be associated with different values from a large interval. The third one represents the lost value by the penalty – it is twice as the margin size, so it is twice as the value which is sold or not sold on the highest price corresponding to the fact that we are penalized or not (if our prediction was 1000 and we sell 1500 we are not penalized, but if we sell another 500, then we get a penalty for the other 500 too, so we lose an amount directly proportional to the forecast).

More than one test is required to make assumptions, so I created three smaller histories (1500 rows each) and tested the SARSA and decision tree methods I created to cope with the problem. I also tested the "by the book" methods mentioned in the previous section, but the flaws already mentioned made them ineffective. R-learning performed better than dynamic programming (because of that, only R-learning is shown on the diagrams), but it still did not bring success. The biggest problem with them was the loss of accuracy because of the quantification.

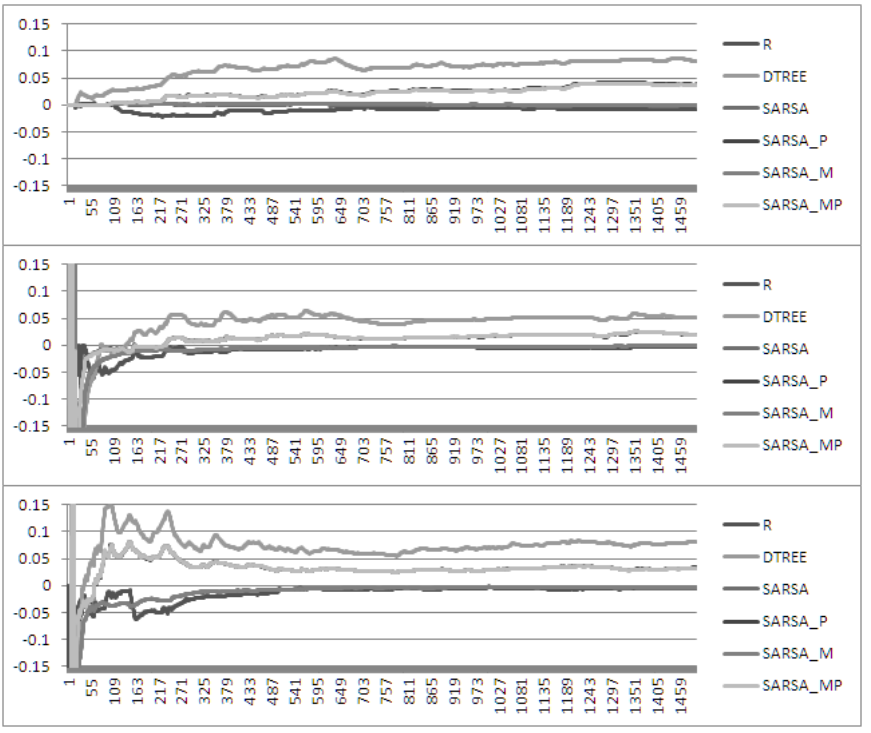

Figure 4: The sum of additional income over time divided by the original value (M stands for "multiple adjustments", P stands for "penalty avoidance").

There are higher values at the begging of two charts, the cause of these is the fact that one penalty avoidance step at the beginning can bring a huge additional income pro rata. All of the lines fall back after that, and stay on the displayed interval.

The best efficiency is presented by the decision tree algorithm, it brings from five to nine percent in addition, which is more than 8000€ for this less than 16 days long interval. Then it is not a surprise that penalty avoidance is also rewarding as a part of a SARSA algorithm: the two reinforcement learning algorithms using this bring approximately half of the success of the decision tree algorithm. The other tree algorithm types are slightly above (the other SARSA variants) or below (R-learning) 0.

Conclusion

The decision tree algorithm is simple, but effective. The SARSA algorithms with this upgrade can reach a reasonable additional income. It is clear that on these datasets the decision tree algorithm is better in this discrete time approach.

To make a real-world application the continuity assumption of the specification section has to be omitted. There are reinforcement learning methods to handle a continuous time problems ([3], [4]) and in these cases this model can be a good discrete model to start at.

References

[1] Sutton, R. S., Barto, A. G., “Reinforcement learning: An introduction”, MIT Press, Cambridge, MA, 1998.

[2] Szepesvári, Cs., “Reinforcement learning: dynamic programming”, University of Alberta, MLSS’08, Kioloa, 2008.

[3] Bradtke, S. J., Duff, M. O., “Reinforcement Learning In Continuous Time and Space”, *Advances in Neural Information Processing Systems, MIT Press*, pp. 393-400, 1994.

[4] Doya, K., “Reinforcement Learning In Continuous Time and Space”, *Neural Computation*, vol. 12, pp. 219-245, 2000.

Acta Universitatis Sapientiae
Electrical and Mechanical Engineering, 3 (2011) 61-81

Widely Configurable, DC Operated UPS for Small and Mid Sized Battery Backup Applications

László TUROS[1], Géza CSERNÁTH[2]

[1] Gautinfo Ltd., Tg. Mureş,
[2] Gautinfo Ltd., Department of Electrical Engineering,
Faculty of Technical and Human Sciences,
Sapientia Hungarian University of Transylvania, Tg. Mureş
e-mail: tlaci@gautinfo.ro, csgeza@gautinfo.ro

Manuscript received November 15, 2011; revised December 15, 2011.

Abstract: Today's desired power managing devices are smart, embeddable, highly energy efficient and with small form factor. The paper provides details concerning the design and implementation of a miniature uninterruptible power supply (UPS). The battery charging and balancing is analyzed and practical measurement results are presented. The performance can be raised with optimized control algorithms implemented on a powerful MCU platform capable of performing even multiple tasks in parallel. A good shaped charging and balancing algorithm can increase overall battery lifetime and performance when backing up critical systems that need to be up all the time, and doing all these at a relatively reduced cost. Fast reaction time of the system is critical so that the devices connected to the UPS output remain always powered. Several reconfigurable electrical and environmental parameters and different communication channels with this smart UPS ensure that it can be embedded in a wide range of electrical systems.

Keywords: UPS, battery charging, battery balancing, MCU, control algorithms, balancing algorithm, ADC, PWM, USB, I^2C, FLCS, embedded system.

1. Introduction

An UPS provides electrical power for a home automation system or server center when the main power fails, drawing stored energy from battery cells. With the fast growing number of intelligent electrical devices and computer systems that need to be powered 24h per day, 7 day per week the need arises for intelligent UPS solutions that are highly flexible and which can be easily integrated and embedded in existing solutions. In order to maintain the battery's capacity at maximum rate, the battery's cells need to be balanced periodically.

This means transferring energy from or to individual cells, until the state of charge (SOC) of each individual cell is equal to the battery's overall SOC.

In order to assure great flexibility the UPS should have wide input voltage range, digitally configurable output voltage range, should be able to charge multiple chemistry batteries and it should be able to balance multiple, serially connected cells used in a battery pack in order to maximize the overall capacity and lifetime of the battery.

The main goal of this paper is to present and prove all the methods used to fulfilling these requirements in a smart, embeddable UPS for small and mid size battery backup applications.

2. Levels of integration

Early in 2009 Microchip's engineers elaborated a quick classification guide [11] regarding the intelligent power supply topologies, defining four levels of integration: the lowest level was occupied by the On/Off control, the mid level was reserved for proportional control, at the third level stays the topology control, at the top level resides the full digital control. This classification somehow inspires our main UPS project, maintaining our goal to reach the highest possible level of integration. In order to determine a similar classification for UPS devices we are interested in, we try to reformulate the integration level constraints as follows.

Basic level of UPS integration: On/Off Control

The UPS's logical shell provides limited on/off control functions through a rudimentary, switch or jumpers based "user interface". Startup sequences, shutdown condition and battery fault detection can be set up for a standard analog design. On the basic level of integration the UPS has a deterministic response to system fault events.

Basic level integration does typically involve some monitoring and control functions, all functions coverable by tiny or small class microcontrollers with integrated voltage comparators and ADCs. These devices provide for the UPS a limited intelligence and integration capability by controlling the output sequencing and monitoring of input/output voltage, current and temperature.

Mid level of UPS integration: Proportional Control

This second integration level adds the digital control to the standard analog design. The basic level features remain, but it is possible to set up voltage and current thresholds, control output voltage, and even set up desired thermal limits. At the mid level, most of the operating parameters of the UPS can be digitally controlled and monitored. All these features allow better UPS

environment monitoring. ADC inputs are used to monitor the UPS inputs, batteries and outputs, comparators can also be used to ensure fast response to system events or faults. Digitally controlled PWM generators provide direct control of the analog PWM circuitry of the UPS. The MCU even dedicates communication channels (SPI, I2C, USB) to upper levels of user control. At this level of integration the reliability of the system is determined by the analog SMPS design with the absolute performance specifications determined by the MCU firmware performance.

High level of UPS Integration: Topology Control

At this level the standard analog design at the mid level of integration even the structure of the control loop can be reconfigured changing from a PWM control loop to a hysteretic [15] control loop at light loads. This allows for changing between continuous inductor current mode and discontinuous conduction mode, increasing system efficiency. The MCU runs more advanced control algorithms and also maintains communication channels (SPI, I2C, USB) to upper levels of user control.

Top level of UPS Integration: Digital Control

Full digital control replaces the standard analog UPS design and provides all of the UPS functions supported on lower integration levels. The SMPS-s (charger and main PSU) regulation functions are directly controlled by the digital circuits of the MCU (PWM generators, ADC-s) and by the control algorithm running on the MCU. This is how the full digital solution allows using techniques that are not possible employing only analog solutions. Some proprietary compensation algorithms can be used to maintain batteries at maximum performance level or to recover them if they become slightly damaged. The full digital solution enables customized response to power input change or load change events increasing the system efficiency. The MCU also dedicates communication channels to upper levels of user control offering a wide palette of settings and control parameters.

At this level the UPS can be easily embedded in any digital system, which can lower system cost and increase system efficiency.

3. Detailing the internal architecture

Our developed UPS solution is based on a combination between the High and Top integration levels to achieve optimal results. *Fig. 1* shows a highly flexible, 8 bit, RISC MCU based device with two separate, highly efficient buck-boost converters with digitally adjustable PWM control. Both the Output Buck/Boost block (which acts as the main PSU of the system) and the Charger

Buck/Boost block have their own digital potentiometer involved in their voltage feedback circuit, thus the MCU can directly control output voltage and charging voltage level through them. Low pass filters and external A/D converter are used to provide multi-channel, high resolution, filtered voltage measurements from batteries and input, output rails. A MOSFET based switching matrix is responsible for fast and efficient (with low losses) power path connections inside the system. The connected batteries and the main PCB temperatures are permanently monitored allowing an additional level of security to the system. The MCU also dedicates communication channels (USB and SMBUS) to upper levels of user control offering a wide palette of settings and control parameters to be changed in real time.

In order to minimize switching losses for different combinations of input and output voltages the switching frequency of the buck-boost converters can be set by a PWM signal generated from the MCU. This feature is one of the High level integration properties; the analog SMPS buck-boost outputs are digitally adjustable.

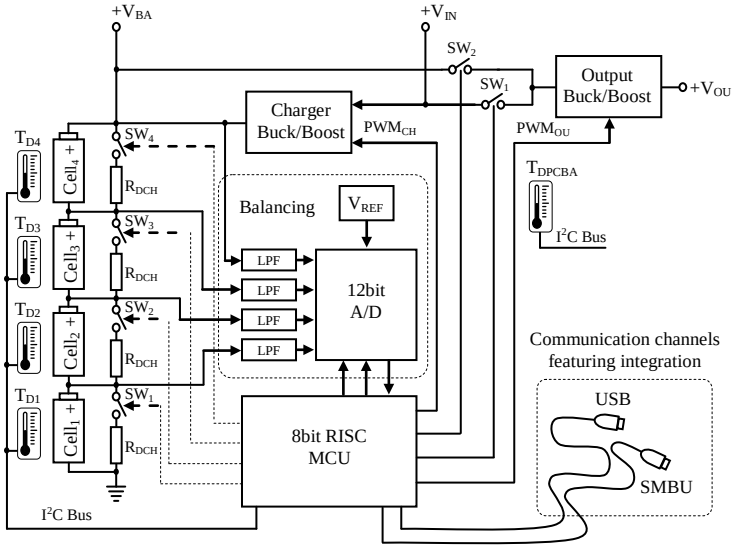

Figure 1: General schematic of the smart, micro-UPS, presenting the most important component blocks inside the device.

3.1. The charging circuit

The design also contains a highly flexible charger which has to work with several battery types and chemistries, therefore the charging voltage and current needs to be digitally fine-tuned on a wide scale. Because the required output charging voltage is often bigger than the maximum allowed voltage supported

by the digital potentiometers, they will be positioned in a low side configuration as it is shown in *Fig. 2*.

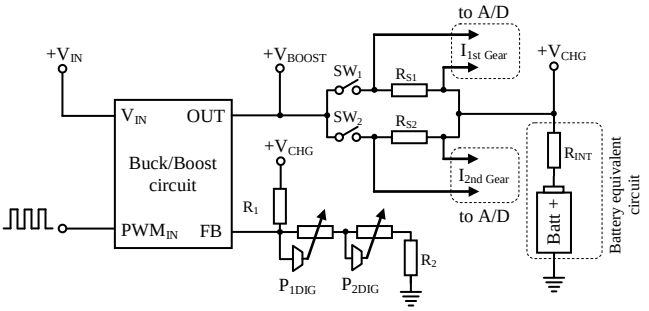

Figure 2: Schematic of the charging circuit.

Since the potentiometers are located on the low side of the voltage feedback circuit, the achieved voltage/current resolution is not linear, so to fulfill the voltage/current resolution requirements we opted for a design with two digital potentiometers with different resistance values and resolution (7bit and 8 bit) in series.

In order to increase the precision of constant current regulation the current steps needs to be small. The charging converter is operated in voltage control mode and the current through the charging resistor is determined by the converter output voltage. Thus, the resolution of the charging current depends on the resolution of the output voltage. In the design two current shunts were used for the possibility to limit high and low currents and for better current regulation and measurement at low charge currents. This helps determining possible end of charge conditions for different battery types. Each of these resistors is in series with a P channel MOSFET switch. The internal resistance of the switch also adds to the overall resistance of the charging circuit. The charging voltage is measured through a separate 12 bit A/D converter.

The charging buck-boost converter's output voltage is expressed by:

$$U_{BST} = U_{FB*}\left(1 + \frac{R_1}{R_{P1} + R_{P2} + R_2}\right) \quad (1)$$

Fig. 3 shows the simulation results about the relation between the digital potentiometer P2 settings and the charging buck-boost converter's output voltage at different P1 settings.

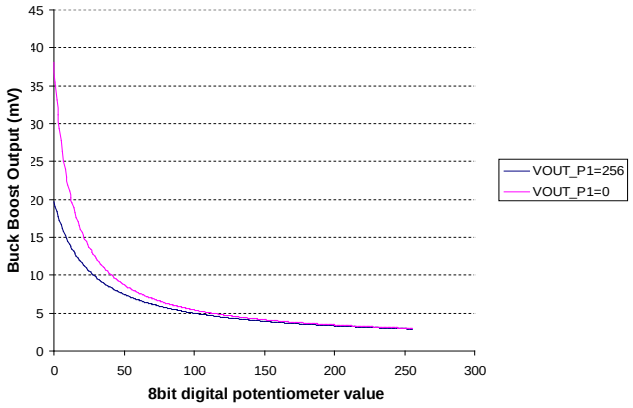

Figure 3: Rough tuning of the Charging Buck-Boost converter output voltage with digital potentiometer P2.

Fig. 4 shows the simulation results about the relation between the digital potentiometer P1 settings and the charging buck-boost converter's output voltage at different P2 settings.

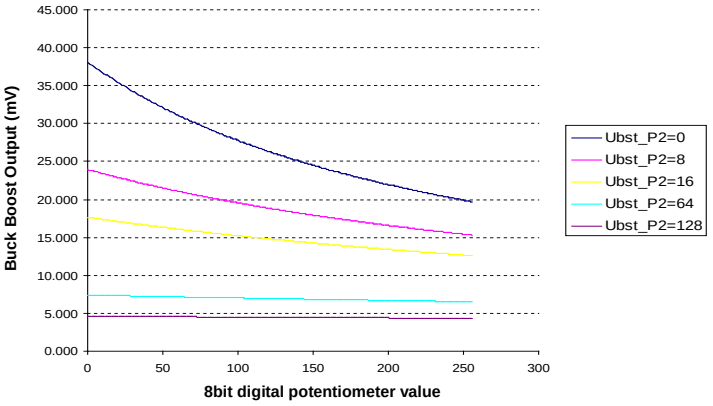

Figure 4: Fine tuning of the Charging Buck-Boost converter output voltage with digital potentiometer P1.

The voltage and current steps are defined by the following equations:

$$U_{step} = U_{BST} - U_{BAT} \tag{2}$$

$$I_{step} = \frac{U_{step}}{R_S + R_{DSon} + R_{INT}} \tag{3}$$

Fig. 5 shows the simulation results about the relation between the digital potentiometer P1 settings and the charging voltage steps at different P2 settings.

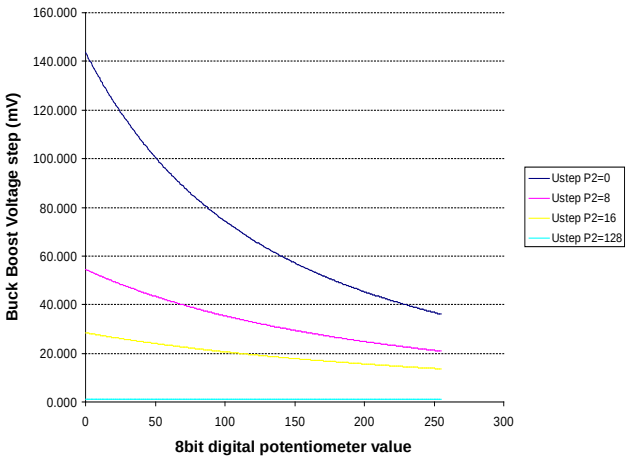

Figure 5: Charge voltage step.

Fig. 6 shows a simulation result about the relation between the control input of the digital potentiometer P1 settings and the charge current steps at different P2 settings.

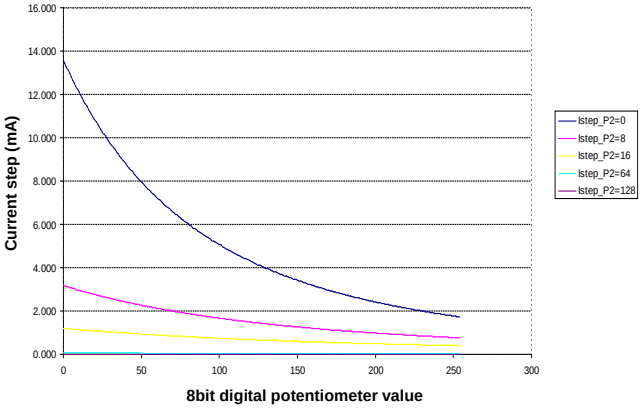

Figure 6: Charging current step variation for R_S=22mΩ, R_{INT}=10mΩ.

If the battery's internal resistance (R_{INT}) is not known or it is changing by battery aging, it can be identified and calculated using equation (4). The charger system applies two different charging voltage levels and measures the voltage on the battery and the charging current.

$$\begin{aligned} U_{CHG1} &= I_{CHG1} * R_{INT} + U_{BAT} \\ U_{CHG2} &= I_{CHG2} * R_{INT} + U_{BAT} \end{aligned} \tag{4}$$

where:

U_{BAT}: is the voltage measured on the battery when the charging current is 0

U_{CHGn}: is the voltage measured on the battery when charging

U_{BST}: is the output voltage of the buck-boost converter

We can quickly find the two unknown values from this equation i.e. the internal resistance and the actual battery voltage. For better results several measurements are made and the arithmetic mean is used for further processing. A simplified technique used in practice is to measure the battery voltage in open circuit (at $I_{CHG1}=0$) which results in the case $U_{CHG1}=U_{BAT}$.

For the battery voltage range from 5V to 30V knowing the internal resistance of the battery helps the charging system to estimate the effect of a voltage step applied to the battery. It has a direct impact on the current step applied to the battery and by knowing this information the precision of the constant current regulation can be greatly improved.

3.2. The charging algorithm

The applied charging algorithm consists of five main steps as follows.

Step 1: Check the battery state – temperature and voltage. If there is no over-voltage or over-temperature the charging process can be started.

Step 2: Pre-charge stage – Switch to low current charging stage by selecting the higher value shunt resistor (R_{S1}). Ramp up fast the charging voltage, until a small amount of charge current is sensed. Limit the current to a small predefined level and keep on charging until the battery voltage exceeds a pre-charge voltage threshold. Proceed forward to Step 3.

Step 3: Constant current stage – Switch to high current charging stage by selecting the lower value shunt resistor (R_{S2}). Ramp up the charge current and limit the current by regulating it to the predefined value. If the battery voltage exceeds the maximum allowed bulk voltage than proceed forward to Step 4.

Step 4: Constant Voltage stage – Apply the bulk voltage to the battery until the charge current drops to a predefined small value than proceed forward to Step 5.

Step 5: Depending on the battery chemistry float charge is applied.

During all stages the charge current is also regulated depending on the temperature of the battery cells and of the PCB. If during charging the battery temperature is above the normal limits the charge current is gradually lowered. If the battery temperature exceeds the maximum allowed threshold the charging is immediately stopped.

The measurements results when charging 3x3400mAh LiFePO4 cells connected in series are presented in *Fig. 7*.

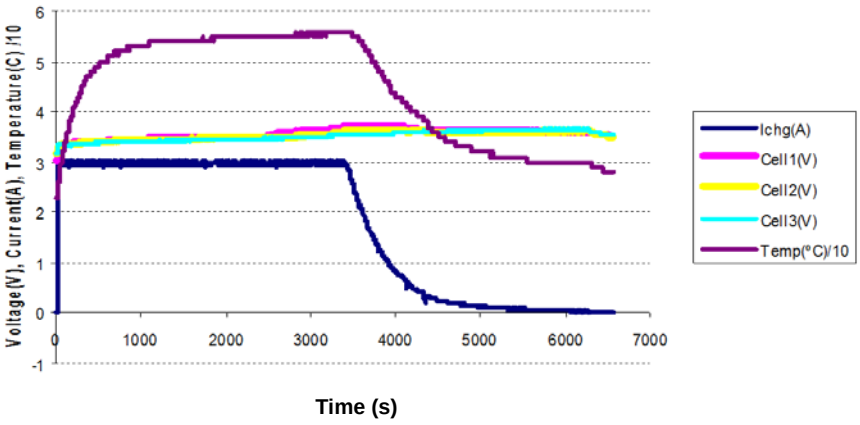

Figure 7: Constant current, constant voltage charging diagram scaled with the temperature response of the board.

3.3. Fuzzy charging control

The proposed Fuzzy Logic Control algorithm is used mainly because robust control is needed, with more than one control rules. If there is an error in one of the measurements the impact of the decision is not fatal. The digital potentiometer used is a cheap one because of economical constrains, but it has also poor precision (20% only) so using a lookup table for possible charge voltages is not possible.

The Fuzzy Logic Control System (FLCS) is presented in *Fig. 8*.

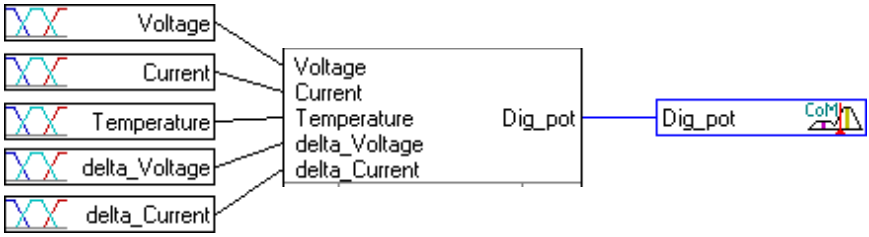

Figure 8: The Fuzzy Logic Control System.

The input variables are defined as: Voltage [5-30V], Current [0-3A], delta_Voltage (difference between the desired battery voltage and current battery voltage), delta_Current (difference between the desired charge current and current charge current), Temperature (battery temperature). The output variable is defined as: Dig_pot (the digital potentiometer value). The charging voltage range is between 0-30V, the desired set voltage is 14.4V. *Fig 9.* shows the charging voltage is not at the desired voltage. Changing the digital potentiometer resistance has a nonlinear, nearly exponential effect on the charging voltage in the upper range of the desired voltage. This had to be accounted for by selecting the Fuzzy membership functions accordingly. *Fig. 10* shows the delta_Voltage, currently at -0.3V.

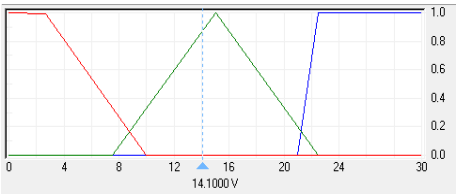

Figure 9: Membership function of the charging voltage input.

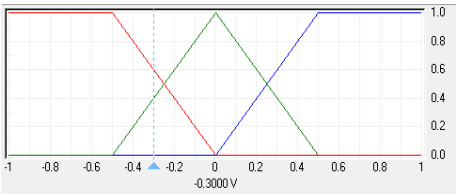

Figure 10: Membership function of the charging voltage error input.

The charging current can vary between 0-3A, the desired current in the presented example is 2A. The charge current information is correlated with the battery temperature to provide the necessary rules for the Fuzzy Knowledge base (*Fig. 11*). The delta_Current is the difference/error between the required charge current and the actual charge current, currently at +0.2A (*Fig. 12*).

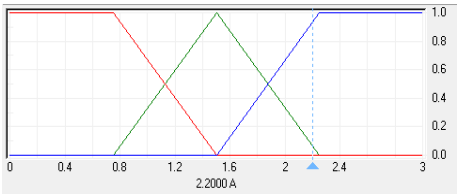

Figure 11. Membership function of the charging current input.

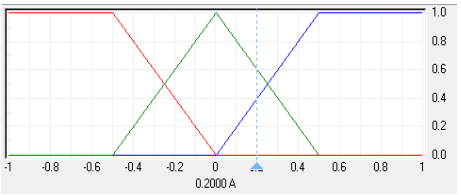

Figure 12. Membership function of the charging current error input.

The Temperature input to the system is the measured battery temperature. Currently 28°C (*Fig. 13*). Finally the membership function of the output variable of the FLCS referring to the digital potentiometer's value is represented in *Fig. 14*.

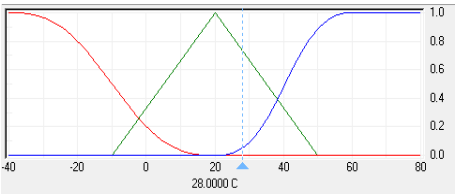

Figure 13: Membership function of the temperature input.

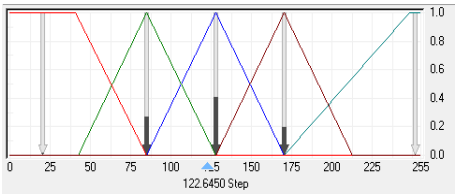

Figure 14: Membership functions of the digital potentiometer output.

We choose to use the Mamdani inference method used for it's simplicity in implementing on an 8 bit microcontroller. The knowledge base was designed using all our experience gained in the field of charging batteries with different chemistries. For defuzzification we chose the Center Of Mass method because it offers more precise calculation of the control signal output at the cost of additional computing power which we were able to deliver to the system by optimizing some other, non time critical algorithm parts, running on the same MCU.

3.4. Running on batteries

When the system is running on battery the cells are carefully monitored and the system enters low power consumption mode when an under-voltage condition is sensed. In order that the UPS enters the low power consumption mode, one of these two conditions must be fulfilled: either the voltage measured on one of the battery cells is less than a predefined threshold or the coulomb

counter is below a predefined value. Both parameters are configurable for flexibility (*Fig. 15*).

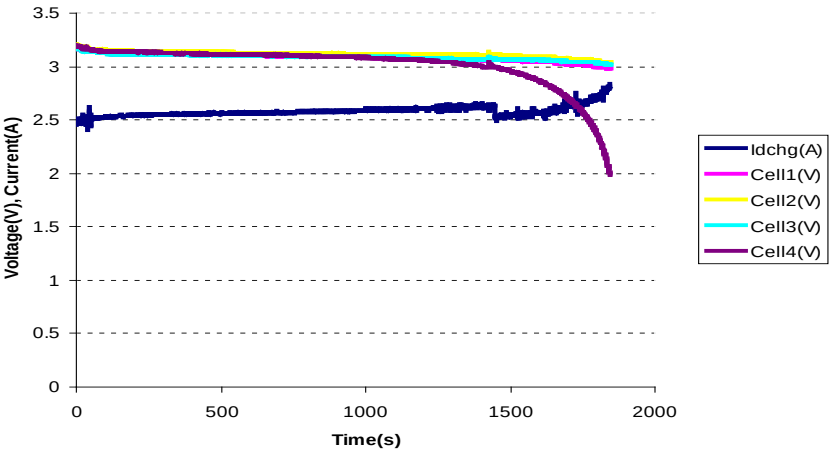

Figure 15: Battery discharge featuring under-voltage protection at 2V/cell.

3.5. The UPS switching technique

In order to keep the system running we need very fast switching between the DC input and the battery sources [16]. For this reason we used a voltage comparator located in the microcontroller. In case the input voltage drops below a predefined threshold the comparator trips, triggering an interrupt in the microcontroller. The interrupt service routine is the highest priority one from all the interrupts used in the system.

The threshold to which the falling voltage is compared is digitally configurable which gives higher flexibility to the system when used in a wide range of input voltage. The switches are composed by P-MOS transistors in back to back configuration for proper blocking [16]. The gate drivers of the switches are designed with active pull-up/pull-down stages to accomplish high speed switching. See the principle of operation presented below in *Fig. 16*.

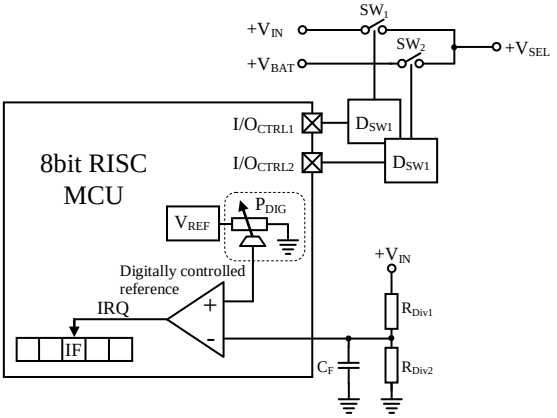

Figure 16: Schematic of the UPS switching technique used.

The delay between the input voltage fall event and the event of switching the current path to the battery is given by the following equation:

$$T_{DELAY} = T_{LPF} + T_{COMP} + T_{IR} + T_{MOS\_close} + T_{MOS\_open} \quad (5)$$

where:

T_{LPF} = Low pass filter to filter out high frequency noise;

T_{COMP} = the response time of the comparator;

T_{IR} = time spent in the interrupt routine;

$T_{MOS\_close=}$ turn off time of the MOSFET connected to the DC voltage input;

T_{MOS_open}= turn on time of the MOSFET connected to the battery.

The longest delay is introduced in this equation by the T_{IR} component. For best results this part of the microcontroller code was optimized for speed by writing this part of the code in assembly language and making this interrupt the highest priority. The measured delay is below 35us, which is sufficient for maintaining the output near close to the reference voltage providing the necessary power to the output.

The high efficiency LTC3780 synchronous buck-boost controller is selected as analog output module because of its very good line transient characteristics. The resulting line transient characteristics of the UPS can be observed in *Fig. 17.*

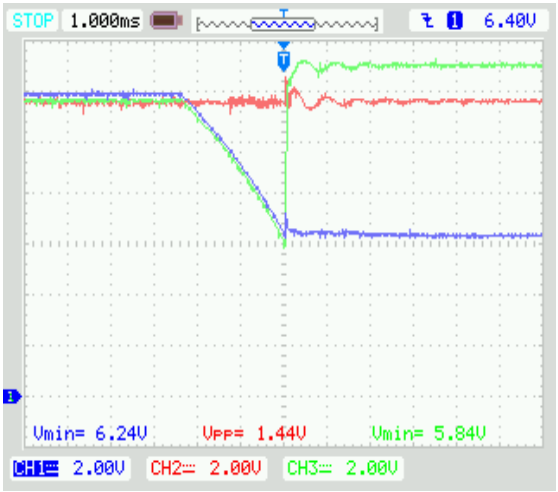

Figure 17: The line transient effect on 1ms time base.

Channel 1 is the main input voltage (V_{IN}), channel 2 is the main output voltage (V_{OUT}) and channel 3 is the voltage in the common point (V_{SEL}) of the two switches SW1 and SW2, which is also the input voltage in the output buck-boost controller.

The output of the UPS was connected to an electronic load previously set to sink 4A constant current. The UPS is configured to switch on battery if the input voltage falls below 6.2V. The battery configuration used in this setup was made by four of 3.2V LiFePO4 cells connected in series. We can distinguish three different stages from the oscilloscope image.

In the first stage the system is running on the main input, the output voltage is generated from the main input. In the second stage at some point the input voltage falls with dv/dt=3V/ms. As soon as the input voltage drops below the predefined threshold the UPS switches to the battery by connecting it to the buck-boost controller's input.

In the third stage we can see that the output remains stable with damped oscillation around 12V. The ripple voltage amplitude is well below 10% of the +12V nominal voltage, which is defined by the ATX standard validating our system.

3.6. Battery Balancing

As stated in the referenced document [1], in order to accurately balance battery cells, high precision and high resolution measurements of the cells'

voltage are needed. The system is able to measure battery voltages up to 30V with less than 10mV resolution. Most of the mid range microcontrollers have only a 10bit resolution A/D converter on board which was not enough for this purpose. Therefore a stand alone, 12bit, I2C A/D converter has to be chosen [6]. The main idea is presented back in *Fig. 1*. The MCU commands the on board PSU and discharge switches, communicating with the A/D converter via I2C lines. Since the voltage variation on a battery cell is a relatively slow phenomenon low pass filters are used on the analog inputs.

Balancing [2] can be done by passive or active methods. Passive balancing means drawing energy from the most charged cell through discharge resistors. This energy is wasted as heat. Active balancing draws energy from the most charged cell and transfers it to the least charged one. This method presumes less wasted energy, but involves DC-DC converters for each cell and it can be more costly than the previous method. Since the solution presented has to be cheap and the space is constrained, using active balancing is not appropriate.

The faster the balancing the more heat is produced, more space is needed on the PCB since higher power resistors are bigger [10]. On the other hand over-heating the board is not allowed, temperature can also influence the measurements' stability. However temperature compensation is possible since temperature is measured on the board. Balancing 12V/Cell (SLA) batteries versus 3V/Cell (LiFePO4) implies more dissipated heat if using the same discharge resistor [8]. In order to dissipate the same amount of power, PWM controlled balancing is used for each cell of the 12V cells batteries as shown in *Fig. 18a* and *Fig. 18b*.

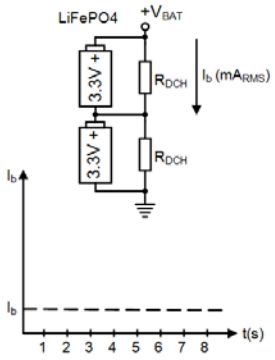

Figure 18a: Direct discharging LiFePO4 Cells.

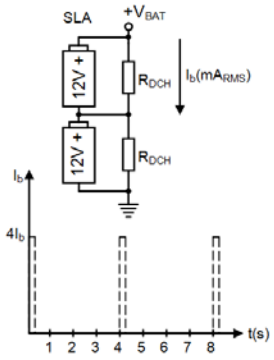

Figure 18b: Slow-PWM discharging SLA Cells.

The balancing algorithm finds the weakest cell, then for each cell calculates the difference between its own voltage and the voltage of the weakest cell (minimum). In case if the cell voltage is less than the discharge limit voltage, discharging is stopped for that cell. This is extremely important to prevent deep discharging [3] of the battery cells [9]. If the difference found is bigger than a preset start value the cell will be discharged. If the difference is less than the differential start value it will be further checked against a preset stop value. If it is less than the stop value the discharging will be stopped for this cell. This algorithm introduces a hysteresis in the balancing procedure. In order to obtain the balancing logic with hysteresis working well, the start voltage parameter needs to be bigger than the stop voltage parameter. The internal impedance of the battery cells can also affect the voltage based balancing if it is done when charging with high current. The best results are achieved if balancing is done near to the end of the charging cycle, when the charging current decreases. The balancing results for six LiFePO4 3.2V/3400mAh cells are shown in *Fig. 19*. The achieved accuracy is self explanatory, presenting a variation between balanced cells comparable to the A/D converter resolution of 8mV/LSB.

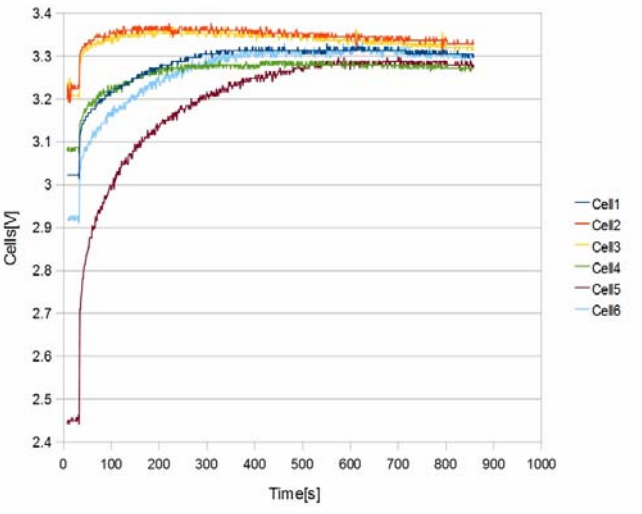

Figure 19: Charge balancing graph of six LiFePO4 cells.

4. Integration of the micro sized UPS

For fulfilling the project's main goal to create an intelligent UPS module, rated near the Top Level of Integration, besides the internal control techniques

and methods an important aspect remains still uncovered in earlier explanations: embedding. Embedding power electronics has some drawbacks regarding the size, wiring, heat dissipation, and communication layers.

4.1. Some physical aspects

In order to facilitate the size related integration aspect in already existing systems the physical dimensions and connection layout of the device were carefully optimized. *Fig. 20* shows the UPS device on the top of a 12V SLA battery for size comparison. It is designed with components on a two sided, multilayer PCB with power components placed on the top, facilitating heat dissipation even in case of passive cooling methods. The digital and analog signal components were placed on the bottom of the PCB, shielded by a GND layer for noise reduction. The three main power component groups, (the charger buck-boost, the output buck-boost and the power switches for current path selecting (marked with red rectangles) were compacted and placed following an optimal topology for high current throughputs. All the wire inputs and outputs were placed in strategically optimal positions to allow short wire harnesses to be used.

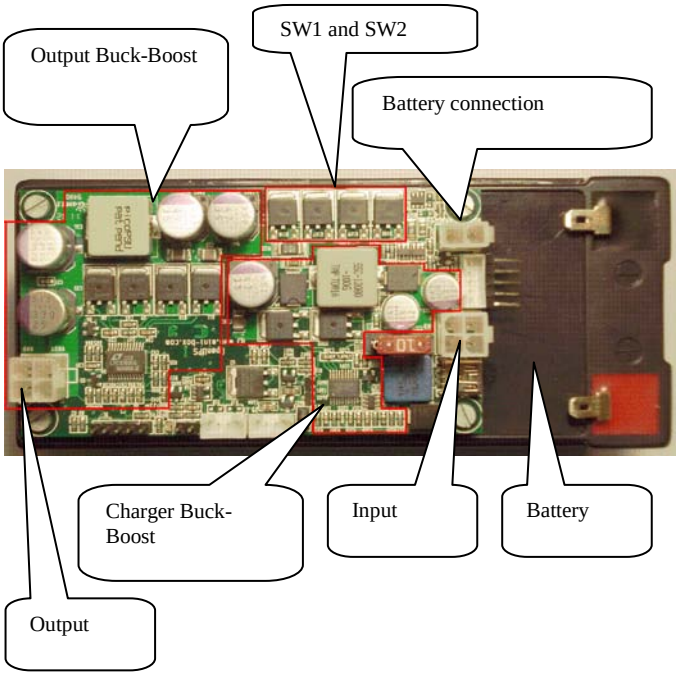

Figure 20: The UPS device, with delimited main functional groups.

4.2. Logical level aspects

On the logical level the UPS can handle two types of integration methods:

- Combined with the battery pack and presented as a SBP (Smart Battery Package) over the SMBUS communication line;
- Like a system level device, usable under various operating systems trough USB line and corresponding low- and user-level drivers.

Both profiles (SMBUS and USB) were integrated in the interfacing algorithm allowing lots of required and even specific (custom) parameters to be set to meet the requirements of the main system.

On the PC side the UPS driver and application software has three main levels upon the lovest hardware level [12]: on the top level is placed the application software presenting a GUI, the lower level consists of the user mode driver and at the bottom of the structure is the HID-USB low level driver (as shown on the right side of *Fig. 21*).

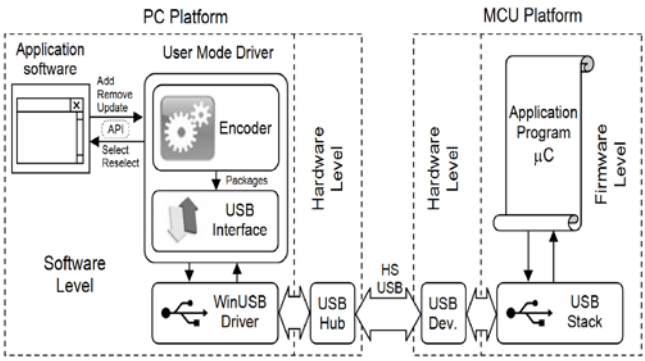

Figure 21: Schematic of the HS USB integration layers.

In the background of the GUI's task another parallel task communicates with the user mode driver via API functions. The user mode driver is also built on level structure [11] as follows:

- the Encoder is responsible for composing the messages and feeding the USB interface. The outcoming messages are packed accordingly to the requests of the communication protocol.
- the USB interface handles the message flow (up and down) between the low level HID-USB driver and the user mode driver.

The universal WinUSB driver is an add-on feature of MS Windows type operating systems since SP2. This low level driver can handle full speed USB

links with a bandwith rated at 40Mb/s, wide enough for handling such applicatons.

On the MCU side an event driven, direct USB Stack has been built over the hardware layer, handling the opened up- and down-pipes of the USB channel (as shown in the left side of *Fig. 21*). The application program runs an advanced parser algorithm to maintain the communication flow as the internal parameter matrix changes over the time. The system is able to send ON/OFF pulse signals to the motherboard based on the Coulomb counter and/or based on the battery voltage level, or based on input voltage level or when starting. Even more, once connected to a PC, the device installs itself as a smart battery in Windows operating system, using the Windows HID-USB driver without the need of any additional driver installation, and becomes immediately visible as a battery icon in the tray bar. Features include both UPS and LAPTOP mode.

4.3. Special and proprietary features

Many of today's UPS applications are situated in a price sensitive field where the possibilities of integration, and feature palette are both often minimized or even non existent to preserve a low price range. As stated before the UPS developed by us tries to overcome these limitations with a wide palette of special and proprietary features. First it can handle different types of batteries; many types of UPS are limited to a predefined battery type. It also has a Battery Wizard application aiding the user in setting some entry level parameters to the device selecting between only a few predefined battery profiles. The user resumes selecting the battery type and capacity, the nominal battery voltage and the number of battery cells to use. In addition individual or global measuring points are defined with graphical representation on the right side of the GUI, aiding the user to properly connect the individual measuring points to the battery poles. Then the wizard generates the charging voltages, charging currents, as well as initial voltage based remaining capacity estimation (fuel gauge) thresholds, under-voltage shutdown threshold and other useful parameters (*Fig. 22*). Besides of the wizard application the user also has the ability to manually change each of the generated parameters to further customization.

Another feature consists in an increased flexibility for fuel gauge estimation, where the voltage based thresholds are also configurable. There are six estimated parameters, each of them setting a threshold for 0%, 10%, 25%, 50%, 75%, 100% fuel gauge, used by the MCU firmware to determinate the initial, remaining battery run-time.

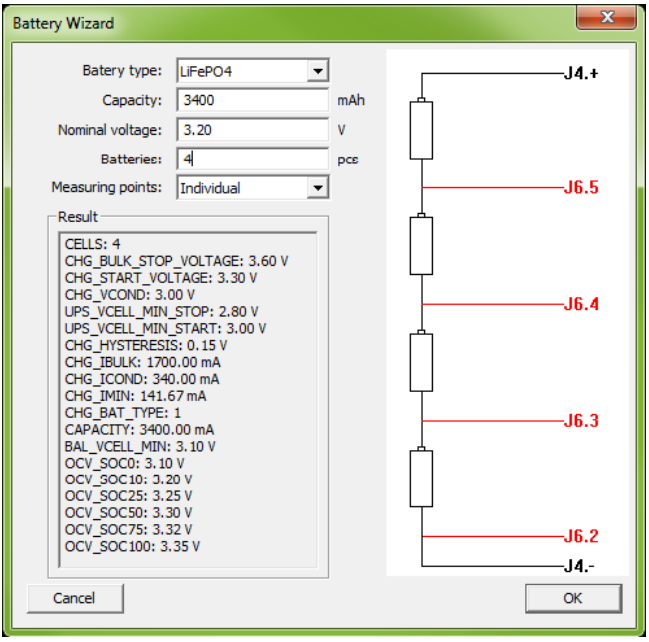

Figure 22: Screenshot of the Battery Wizard GUI.

When the system is running on battery and its voltage falls below the predefined under-voltage threshold or the coulomb counter is down to a minimal value the UPS takes care to shut down the OS and PC nicely, preventing OS damages. After the system has shut down, the device achieves ultra low power consumption (below 50uA) to preserve battery. This feature is achieved with a proprietary MCU power supervisor circuit disconnecting the 3.3V rail which also powers the MCU and other digital logic ICs. In case of a discharged battery the UPS can be waked up only if the input voltage appears in which case the battery re-charging is started immediately. In case of a partially charged battery the UPS can be woken up also by pressing its start button.

5. Conclusion

More time spent on this project means being more involved in low level optimization of the control algorithms. The system was designed to provide user specified regulated voltage output over a wide range of input voltages, battery backup, multi-chemistry charging and cell balancing by means of a single PCB at a noticeable level of efficiency (over 80%), all controlled by a single mid-range MCU.

Any input, output and charge voltage between 5-30V can be used in any possible combination. This allows the system to be easily embedded in many existing electrical systems. Features also include USB and SMBUS interface, programmable parameters and thresholds, multiple battery chemistry, battery balancing up to 6 cells, Coulomb counting.

At the end of this paper it can be concluded that the main goals can be considered fulfilled at a relatively low cost, where the optimum between price, system integration skills and power efficiency have been achieved for a relatively wide application palette for these types of devices.

References

[1] Turos, L., Csernáth, G., Csenteri, B., "Balancing Multiple Chemistry Batteries in a DC voltage Operated UPS", in *Proceedings of the 3rd International Symposium MACRo 2011, Sapientia University of Tirgu Mures*, 2011, pp. 231-238

[2] DelRossi, R, "Cell Balancing Design Guidelines", Application Note Nr. 231, Microchip Technology Inc., 2002.

[3] "Discharge methods, Battery University", Cadex Electronics Inc., http://batteryuniversity.com/learn/, 2003.

[4] Martinez, C., Sorlien, D., Goodrich, R., Chandler, L., Magnuson, D., "Cell Balancing Maximizes The Capacity of Multi-Cell Li-Ion Battery Packs", Intersil Inc., 2008

[5] Wen, S., "Cell balancing buys extra run time and battery life", Texas Instruments Inc., 2008.

[6] Yun, R., "Calibration of Pipelined AD-Converters- MSC Thesis", Stockholm, June 2006.

[7] Delic-Ibukic, A., "Continuous digital calibration of pipeline A/D converters- MSC Thesis", University of Maine, Orono, 2004.

[8] Altemose, G., "Achieving cell balancing for lithium-ion batteries", Aeroflex Plainview Inc., http://www.aeroflex.com/ams/pagesproduct/articles/BEUElectronicProductsArticle.pdf, 2008.

[9] "Li-Ion, NiMH Battery Measuring, Charge Balancing and Power-supply Circuit", Atmel, http://www.atmel.com/dyn/resources/prod_documents/doc9116.pdf, 2010.

[10] Barsukov, Y., "Battery Cell Balancing – What to Balance and How", Texas Instruments Inc., http://focus.ti.com/download/trng/docs/seminar/Topic 2 -Battery Cell Balancing – What to Balance and How.pdf, 2008, pp. 2-5

[11] "Intelligent power supply integration levels", http://www.microchip.com/en_US/technology/intelligentpower/integration/.

[12] Csernáth, G., Csenteri, B., Asztalos, A., Brassai, S. T., Székely, I., "Driving QVGA and WQVGA LCD panels with 30fps live video stream using HS USB", *Proceedings of the 14th International Symposium for Design and Technology of Electronic Packages SIITME '08 – Transilvania University of Brasov*, 2008, pp. 276-280

[13] Nazri, G. -A., Pistoia, G., "Lithium Batteries, Science and Technology", Springer Science+Business Media, LLC 2003.

[14] Rashid, M., "Power Electronics Handbook", Academic Press, 2001.

[15] Song, C., "Optimizing Accuracy of Hysteretic Control", Power Electronics Technology, www.powerelectronics.com, February 2006.

[16] Balogh, L., "Design And Application Guide For High Speed MOSFET Gate Drive Circuits", http://www.ti.com/lit/ml /slup169/slup169.pdf., pp. 11-14

Acta Universitatis Sapientiae
Electrical and Mechanical Engineering, 3 (2011) 82-92

Theoretical Study of the Gradient Method to Find the Optimal Control for the Reactive Sputtering Process

Katalin GYÖRGY, András KELEMEN,
Sándor PAPP, László JAKAB-FARKAS

Department of Electrical Engineering, Faculty of Technical and Human Sciences,
Sapientia Hungarian University of Transylvania, Tg. Mureș,
e-mail: {kgyorgy; kandras; spapp; jflaci}@ms.sapientia.ro

Manuscript received September 15, 2011; revised December 15, 2011.

Abstract: One of the main tasks in the optimal control theory is to find a controller that provides the best possible performance with respect to some given measure of performance (optimality criterion). For linear plant dynamics and quadratic performance criteria it is possible to obtain the optimal control law by numerically integrating a Riccati type matrix differential equation. In general, for nonlinear plants the variational approach leads to a nonlinear two-point boundary value problem, which can be solved by iterative numerical methods, for example by the steepest descent (gradient) method.

A model of the reactive sputtering process can be determined from the dynamic equilibrium between the quantity of reactive gas inside the chamber and the quantity of sputtered metal atoms which form the compound with the reactive gas atoms on the surface of the substrate. The analytically obtained dynamical model is a system with nonlinear differential equations which can result in a hysteresis-type input/output nonlinearity. The present paper proposes a theoretical study of the steepest descent gradient method to obtain the optimal control signal and trajectory for this nonlinear reactive magnetron sputtering process.

Keywords: Optimal control, nonlinear systems, Hamilton-Iacobi equations, reactive sputtering process, gradient method**,** hysteresis loop, cost function, boundary conditions.

1. Introduction

Mathematical models may be developed along two methods. One method is the analytical modeling, which does not necessarily involve any experimentation on the actual system. The other method is known as system

identification and this is directly based on experimentation. The analytically obtained dynamical model generally is a system with nonlinear differential equations. In general optimal control theory the objective is to find a controller that provides the best possible performance with respect to some given measure of an optimality criterion (cost function). If the plant dynamics is linear and the cost function is a quadratic performance criterion than it is possible to obtain the optimal control law by numerically integrating a Riccati type matrix differential equation. When faced with an engineering problem of a nonlinear system, the first approach usually is the linearization; in other words, trying to avoid the nonlinear aspects of the problem. After linearization we obtain a linearized model, which is valid just in a small region around the selected operating point. In general for nonlinear plants the variational approach leads to a nonlinear two-point boundary value problem, which can be solved by iterative numerical methods, for example by the steepest descent (gradient) method.

The reactive sputtering processes frequently exhibit stability problems. The analytically obtained dynamical model is a system with nonlinear differential equations. The present paper proposes a theoretical study of the steepest descent gradient method to obtain the optimal control signal and trajectory for this nonlinear reactive magnetron sputtering process.

2. Analytical modeling and numerical simulation of the reactive sputtering process

A. Analytical modeling

A very sensitive aspect of the reactive sputtering process is the dynamic equilibrium between the reactive gas inside the chamber and the sputtered metal atoms which form the compound with the reactive gas atoms on the surface of the substrate. The components of this rather complex balance are schematically shown in *Fig. 1*. The phenomena on both the surfaces of the target and of the substrate include sputtering of the metal and gettering of the reactive gas atoms. The larger the surface of elemental nonreacted metal, the stronger the flux of sputtered metal atoms which further reduces the reactive gas concentration by forming compound on the surface of the substrate. The reactive gas consumption increases when the fractional coverage with compound is smaller. It results that the reactive sputtering process is strongly nonlinear. The main type of nonlinearity is hysteresis, which can be observed both from theoretical results (obtained by simulation using the mathematical model), and from practical measurements.

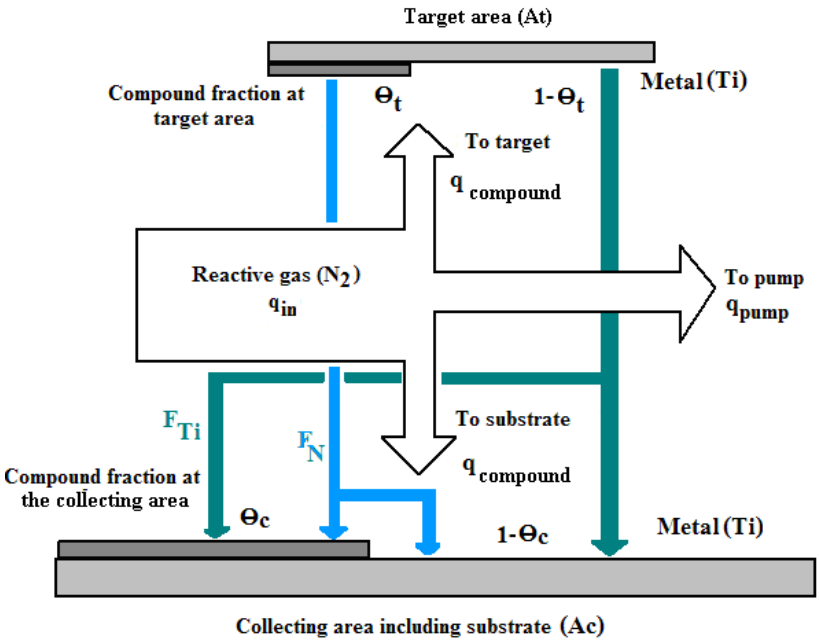

Figure 1: Schematic representation of the reactive gas balance and of the main particle fluxes on the target and substrate surfaces.

The mathematical model developed is based on the hypotheses and formulation used by S. Berg [1] [2] as follows: the partial pressure of the reactive gas has uniform distribution in the processing chamber; the secondary electron emission due to the ionic bombardment of the target surface is uniform and independent of the surface fraction covered by compound; the glow discharge takes place in a mixture of inert gas and reactive gas (ex. Ar and 2…3% of N_2); the contribution of the reactive gas ions to the bombarding ion flux is negligible due to the small concentration of the reactive gas; no reactive gas is consumed at the fraction of the target surface that is already covered by compound; homogenous sputtering rate is assumed on the whole surface of the target [3][4]. These hypotheses are based on widely accepted research results in the field of PVD by reactive magnetron sputtering; respectively provide a reasonably correct description of the process by a model which is simple enough to be considered for stability analysis and process controller design [5].

The dynamic model of the reactive magnetron sputtering process is defined by the system of equations (1):

$$\begin{aligned}
\frac{dp_N}{dt} &= k_1 \cdot (q_{in} - q_p - (\alpha_{tM} \cdot F_N \cdot (1-\theta_t) \cdot A_t + \alpha_{cM} \cdot F_N \cdot (1-\theta_c) \cdot A_c) \\
\frac{d\theta_t}{dt} &= \frac{1}{N_{Ti}} (2 \cdot \alpha_{tM} \cdot F_N \cdot (1-\theta_t) - J \cdot \eta_N \cdot \theta_t) \\
\frac{d\theta_c}{dt} &= \frac{1}{N_{Ti}} (J \cdot \eta_N \cdot \theta_t \cdot \left(\frac{A_t}{A_c}\right) \cdot (1-\theta_c) + 2 \cdot \alpha_{cM} \cdot F_N \cdot (1-\theta_c) - J \cdot \eta_M \cdot (1-\theta_t) \cdot \left(\frac{A_t}{A_c}\right) \cdot \theta_c)
\end{aligned} \tag{1}$$

In this mathematical model the following notation has been used:

p_N- the partial pressure of reactive gas (nitrogen) in the sputtering chamber;
θ_t, θ_c - the surface fraction of the target and of the condensation area covered by compound molecules;
F_N- the flux of reactive gas molecules (N_2) on the target or on the substrate;
q_{in}, q_p- the input reactive gas flow and the gas flow evacuated by the vacuum pump;
A_t, A_c- the target area and the condensation (substrate and chamber) area;
m_N, m_{Ti} - mass of the reactive gas molecule (m_N=28 a.u.) and of the metal (m_{Ti}=47.9 a.u.);
η_M, η_N - sputtering yield of the elemental metal (titanium) and of the compound (titanium nitride);
α_{tM}, α_{cM} - sticking coefficients for the nitrogen molecule (to the titanium target or to the covered part);
N_{Ti}- the superficial density of the Ti atoms on the surface of the metallic target;
J- the particle density of argon ions on the surface of the target, which is proportional to the discharge current intensity (I_d);
k_1- coefficient, calculated in function of temperature and chamber volume.

This mathematical model in state space representation (1) has three state variables (p_N, θ_t and θ_c), two input signals (q_{in} and I_d) and we can choose the surface fraction of the target covered by compound molecules (θ_t) or the sputtering rate (R_p) as the output signal.

B. Numerical simulation

The reactive sputtering process was simulated employing a Runge-Kutta algorithm, where the sampling time was set to 0.01 sec. The parameters used for simulation are: η_M=1.5, η_N=0.3, N_{Ti} =140e-12 m^{-2}, A_t=0.0084 m^2, A_c=0.22 m^2 and α_{tM}=α_{cM}=1, k_1=1.18e6 $J/(kg.m^3)$.The steady-state analysis of the process yields very nonlinear characteristics defining the steady-state relationship between the input reactive gas quantity and the state variables from equations (1). For simulation we considered the reactive gas flow as input. Different time

variations of the input signal used in simulations and experiments are presented in *Fig. 2. a*. The fractional coverage of the target (Θ_t) in function of the input quantity (q_{in}) is shown in *Fig. 2. b.*, where the particle density of argon ions (J) is calculated for a constant discharge current value (I_d=1.125 A). These results obtained by simulation using the dynamic model (1) put in evidence the hysteresis loop described in the plane defined by Θ_t and q_{in} for different variation speeds of the input reactive gas flow in accordance with *Fig. 2.a.*

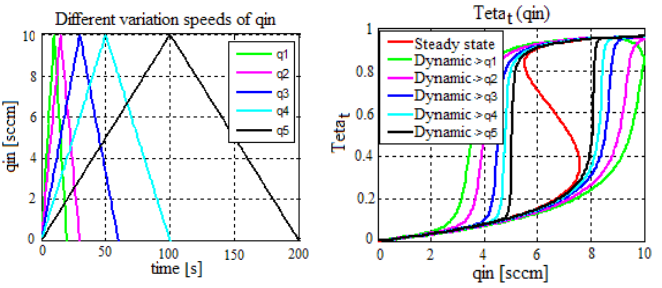

a) *b*

Figure 2: Variation in time of the reactive gas flow for different variation speeds (a), the steady-state and dynamic relationship between the fractional surface coverage of the target and the input reactive gas flow (b).

3. Application of the gradient method to find the optimal control

The nonlinear plant model in general state space representation is defined by the following equation:

$$\frac{\mathrm{d}}{\mathrm{dt}}\underline{x}(t) = \underline{f}(\underline{x}(t), \underline{u}(t), t) \tag{2}$$

where $\underline{x}(t)$ is the state vector and $\underline{u}(t)$ is the input vector.

The cost function is defined as:

$$J(\underline{u}) = \lambda(\underline{x}(t_f)) + \int_{to}^{tf} L(\underline{x}(t), \underline{u}(t), t)dt \tag{3}$$

where t_0 and t_f are the initial and the final time, $\lambda()$ and $L()$ are scalar functions.

For the system defined by the relation (2) we search the optimal control law that minimizes the cost function (3). To solve this problem we define the Hamilton function as:

$$H(\underline{x}(t), \underline{u}(t), \underline{p}(t), t) = L(\underline{x}(t), \underline{u}(t), t) + \underline{p}^T(t) \cdot \underline{f}(\underline{x}(t), \underline{u}(t), t), \tag{4}$$

where $\underline{p}(t)$ is the costate vector. The required conditions for optimality are:

$$\frac{d}{dt}\underline{x}(t)=\frac{\partial H}{\partial \underline{p}}\left(\underline{x}(t),\underline{u}(t),\underline{p}(t),t\right) \tag{5}$$

$$\frac{d}{dt}\underline{p}(t)=-\frac{\partial H}{\partial \underline{x}}\left(\underline{x}(t),\underline{u}(t),\underline{p}(t),t\right) \tag{6}$$

$$\frac{\partial H}{\partial \underline{u}}\left(\underline{x}(t),\underline{u}(t),\underline{p}(t),t\right)=0 \tag{7}$$

and the boundary conditions are:

$$\underline{x}(t_0)=\underline{x}_0;\quad \underline{p}(t_f)=\frac{\partial \lambda\left[\underline{x}(t_f)\right]}{\partial \underline{x}} \tag{8}$$

The resulting nonlinear two-point boundary-value problem cannot be solved analytically, so we will use an iterative numerical technique, the steepest descent gradient method, to determine the optimal control.

The formal algorithm of this method is [6], [7]:

0. Select a discrete approximation to the control signal $\underline{u}(t)^{<0>}$, $t\in[\,t_0, t_f]$, and fix the iteration index k at 0.

1. Using this control signal $\underline{u}(t)^{<k>}$ integrate the state equation (5) from t_0 to t_f with initial conditions $\underline{x}(t_0)$.

2. Integrate the costate equation (6) from t_f to t_0 with „initial condition" $\underline{p}(t_f)$.

3. Evaluate the $\frac{\partial H}{\partial \underline{u}}$ expression. We can calculate its norm as follows:

$$\left\|\frac{\partial H}{\partial \underline{u}}\right\|=\int_{to}^{tf}\left[\frac{\partial H}{\partial \underline{u}}\right]^T\cdot\left[\frac{\partial H}{\partial \underline{u}}\right]dt\cdot \tag{9}$$

Terminate the iterative procedure (the outputs of the algorithm are the external state vector $\underline{x}(t)^{<k>}$ and the control signal $\underline{u}(t)^{<k>}$), if

$$\left\|\frac{\partial H}{\partial \underline{u}}\right\|\le\varepsilon \tag{10}$$

where the ε is a preselected small positive constant. If the stopping criterion (10) is not satisfied we generate a new control function given by (11) and return to step 1

$$\underline{u}(t)^{<k+1>}=\underline{u}(t)^{<k>}-\gamma\cdot\frac{\partial H}{\partial \underline{u}}\cdot \tag{11}$$

In (11), γ is the constant step size for the gradient method.

4. Numerical simulation of the gradient algorithm for the optimal control of the reactive sputtering process

A. Determination of the Hamilton-Iacobi equations

The nonlinear mathematical model (1) for the reactive sputtering process can be written in the general state space form (2), where the state vector is $\underline{x}(t)=[x_1(t)\ x_2(t)\ x_3(t)]^T=\left[p_N(t)\ \theta_t(t)\ \theta_c(t)\right]^T$, and the control input vector is $\underline{u}(t)=[u_1(t)\ u_2(t)]^T=[q_{in}(t)\ I_d(t)]^T$. We select a linear quadratic cost function

$$J(\underline{u})=\tfrac{1}{2}\underline{x}_e(t_f)^T\cdot F\cdot\underline{x}_e(t_f)+\tfrac{1}{2}\int_{to}^{tf}\left(\underline{x}_e(t)^T\cdot Q\cdot\underline{x}_e(t)+\underline{u}_e(t)^T\cdot R\cdot\underline{u}_e(t)\right)dt \qquad (12)$$

where R, Q, F are positive defined diagonal matrices, $\underline{x}_e(t)=\underline{x}(t)-\underline{x}_p(t)$ and $\underline{u}_e(t)=\underline{u}(t)-\underline{u}_p(t)$, where the $\underline{x}_p(t)$ is the prescribed state vector and $\underline{u}_p(t)$ is the value of control input which is necessary to keep the states at their prescribed stationary values. The required conditions for optimality are characterized by the following differential equations for states:

$$\frac{\partial H}{\partial p_i}=\dot{x}_i(t)=f_i(\underline{x}(t),\underline{u}(t))\quad i=1,2,3 \qquad (13)$$

and the following differential equations for costates:

$$\frac{\partial H}{\partial x_i}=-\dot{p}_i(t)=Q_i\cdot(x_i(t)-x_{p_i}(t))+p_1(t)\cdot\frac{\partial f_1}{\partial x_i}+p_2(t)\cdot\frac{\partial f_2}{\partial x_i}+p_3(t)\cdot\frac{\partial f_3}{\partial x_i}\quad i=1,2,3 \qquad (14)$$

The expressions of the derivate of the Hamilton function versus the control signals are:

$$\frac{\partial H}{\partial u_i}=R_i\cdot(u_i(t)-u_{p_i}(t))+p_1(t)\cdot\frac{\partial f_1}{\partial u_i}+p_2(t)\cdot\frac{\partial f_2}{\partial u_i}+p_3(t)\cdot\frac{\partial f_3}{\partial u_i}\quad i=1,2 \qquad (15)$$

For updating the control signal we can use the relationship:

$$u_i(t)^{<k+1>}=u_i(t)^{<k>}-\gamma_i\cdot\frac{\partial H(t)}{\partial u_i(t)}\quad i=1,2 \qquad (16)$$

Using these relations the algorithm has been implemented in Matlab environment in order to obtain the optimal control for the reactive sputtering process.

B. Results of the numerical simulation

For numerical integration of the differential equations (13) and (14) there was used a Runge-Kutta method [8], [9]. The initial points and the prescribed

points were selected from the steady state simulation of the reactive sputtering process. There were simulated the following control versions:

V1: control with input reactive gas flow (q_{in});

V2: control by means of the discharge current intensity (I_d);

V3: control with both input signals (q_{in} and I_d).

The results of simulation are influenced by the step sizes (γ_1 and γ_2) of the gradient methods, the selected initial control trajectory ($u_1(t)^{<0>}$ and $u_2(t)^{<0>}$), the maximum number of iterations (N_{max}), the values of weighting matrices (R_1, R_2 respectively Q_1, Q_2 and Q_3) and the position of prescribed state vector in comparison with the initial state vector. The simulation time interval and the sampling time are fixed for each version: $t \in [0, 1]$ sec and T_s=0.01 sec. The other simulation parameters are presented in Table 1.

Table 1: Simulation parameters for the three types of control

Control type	γ_1	γ_2	R_1	R_2	Q	N_{max}
V1	10^{-16}	0	10^{-4}	0	10 I_3	100
V2	0	0.1	0	10^{-5}	10 I_3	100
V3	10^{-17}	0.01	10^{-3}	10^{-3}	10 I_3	800

Diagrams from *Fig.3* to *Fig.8* are presented for the visualization of some simulation results of this control algorithm. At first we considered that the system is controlled just by the input reactive gas flow (q_{in}). In *Fig. 3.a* there is presented the cumulative error (corresponding to relation (9)), and in *Fig. 3.b* there is presented the evolution in time of the control signal. The controlled quantities are presented in *Fig.4*, along with the prescribed constant state values. Similarly, when we considered as control input signal the discharge current (I_d), the corresponding simulation results are presented in *Fig.5* and *Fig. 6*.

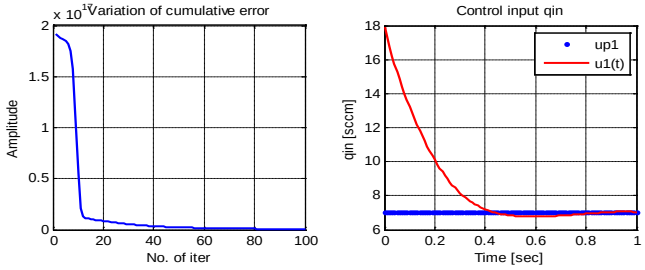

a) *b)*

Figure 3: Variation of the cumulative error (a) and variation in time of the control signal input (b) – version V_1.

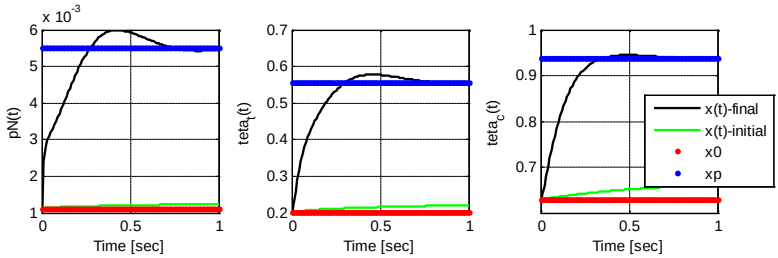

Figure 4: Variation in time of the controlled states obtained for the initial and the final control signals – version V_1.

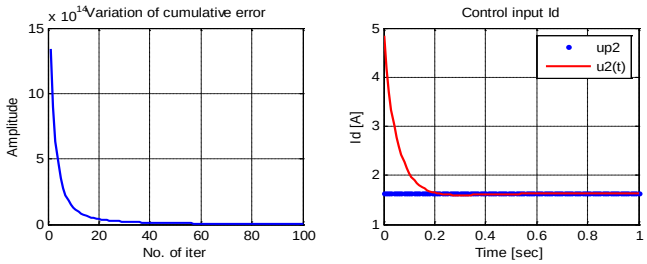

a) *b)*

Figure 5: Variation of the cumulative error (a) and variation in time of the control signal input (b) – version V_2.

Finally we realize simulation for the case when the plant is controlled simultaneously by both inputs (q_{in} and I_d). The results are shown in *Fig. 6* and *Fig. 7*. We present the evolution in time of the control signals: the input reactive gas flow (*Fig. 6.a*) and the discharge current variation (*Fig. 6.b*). On the other hand there are presented in *Fig. 7* the controlled quantities (the partial pressure of the reactive gas (p_N), the fractional surface coverage of the target (θ_t) and the fractional surface coverage of condensation area (θ_c)) versus the input reactive gas flow (q_{in}). The dashed curves represent the characteristics obtained using the steady state model. These put in evidence the initial values and the prescribed final values of the states.

The prescribed final operating point is situated on the negative slope of the steady state characteristic. This is an unstable operating point for the plant. From the simulation it results that first the control by means of the reactive gas flow has a bigger emphasis than the control by means of the discharge current. When the reactive gas flow is close to its value corresponding to the prescribed states (u_{p1}) than the second control quantity (I_d) is gaining more importance. The efficiency of the algorithm is determined by the initial conditions and the maximum number of iterations because the determination of the control signals

needs time. In this algorithm the restrictions of the control signals can be realized just by the proper choice of the weight matrices (*R* and *Q*).

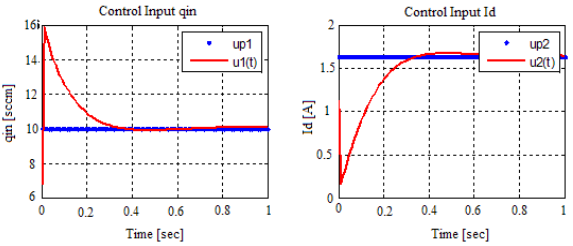

a) *b)*

Figure 6: Evolution in time of the control signals: input reactive gas flow (a) and discharge current intensity (b)–version V_3..

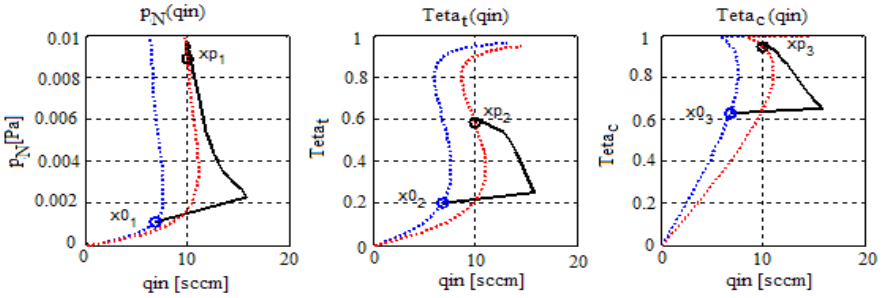

Figure 7: Variation of the three controlled quantities (p_N , θ_t and θ_t) versus the input reactive gas flow (qin) - version V_3..

3. Conclusion

The present investigation shows that the dynamical modeling of the reactive sputtering process is characterized by nonlinear differential equations and the optimal control of this plant is a very complex problem. In case of most of the modern control theories it is needed to know the linear model of the controlled process. In this paper there was presented a theoretical study about the application of the optimal control algorithm, where the results are obtained by numerical iterative techniques. The nonlinear optimal control problem is solved using the gradient method applied directly to the highly nonlinear model and was simulated for the nonlinear reactive sputtering process. Both the input reactive gas flow and the discharge current have been considered as control variables and the results of simulation have shown that this method is can be

used only if we have some proper preliminary information for the algorithm: initial input sequences of the control inputs, values of weight matrices, etc.

References

[1] Berg, S., Blom, H. -O., Larsson T. and Nender, C., "Modeling of reactive sputtering of compound materials", J.Vac. Sci. Technol. A5(2), pp.202- 207, 1987.

[2] Berg, S., Nyberg, T., "Fundamental understanding and modeling of reactive sputtering processes", *Science direct, Thin Solid films*, pp. 215-230, 2005.

[3] Mateescu, Gh., "Tehnologii avansate. Straturi subțiri depuse în vid", *Ed. Dorotea, Bucureşti*, 1998.

[4] Nyberg, T, Berg, S., "Method for reactive sputtering deposition", *United States Patent*, (*US 7.465.378 B2*), 2008.

[5] Biro, D., David, L. and Haller, P., "Dynamic control of reactive magnetron d.c. sputtering process for tribological coatings development", *COST 516 Tribology Symposium, Espoo, Finland*, 14-15 May, 1998, pp. 325-336.

[6] Kirk, D., "Optimal Control Theory", *Dover Publications Inc. Mineola New-York*, 1998.

[7] Dávid, L., "Tehnici de optimizare", *Ed. Univ. "Petru Maior" Tg. Mureş*, 1997.

[8] György, K. and Chindriş, M., "Different methods for theoretical modeling and simulation of reactive sputtering process", *Acta Electrotehnica, MPS 2010, Cluj-Napoca*, pp. 158-156, 2010.

[9] Malkomes, N., Vergohl, M., "Dynamic simulation of process control of the reactive sputter process and experimental results", *Journal of Applied Physics, American Insititute of Physics*, pp. 732-739, 2011.

Acta Universitatis Sapientiae
Electrical and Mechanical Engineering, 3 (2011) 93-104

Study of the Edge Profile Variation Caused by the Re-sharpening by Profiled Milling Heads with Cutting Inserts

Márton MÁTÉ, Dénes HOLLANDA

Department of Mechanical Engineering, Faculty of Technical and Human Sciences,
Sapientia Hungarian University of Transylvania, Tg. Mureş
e-mail: mmate@ms.sapientia.ro, hollanda@ms.sapientia.ro

Manuscript received October 04, 2011; revised December 18, 2011.

Abstract: The paper presents the calculus of the cut profile and the variation of this caused by the re-sharpening, that appears by a special profiled milling head construction, that uses cutting inserts. The advantage of the proposed milling head versus the classical concave profiled milling disk is evident, if considering the repartition of the cutting speed vector and the chip forming and exhausting conditions. The cutting insert's rake face is plain. Its relief face is a part of a common thorus realized by grinding. The insert occupies two distinct positions in the body of the tool: one for cutting and the other one for re-sharpening. Indexed positions are ensured through conical holes and corresponding slotted head sets. The re-sharpening can be done on the rake face or on the relief face. In both cases a minor profile error occurs but the profile is kept in the limits of the tolerance. This paper discusses the definition of the profile error and its dependence on the angular setting parameters and the number of the re-sharpening. The final conclusion is that the classical concave profiled milling disk can be replaced with the proposed variant.

Keywords: Profile milling, profiled milling head profile error, inserts, geometry.

1. The assembly of the profiled milling head

Profiled milling, especially in cases of convex profiles, is a difficult operation. The classical concave profiled disk mills present low rigidity on the teeth base [2, 3, 4, 5] and as a consequence, the cutting speed and feed cannot be set to high values. The productivity of operation is low and the surface roughness, due to the small rake angle values in most of the cases results just on the limit. Profiled disc mills are rather expensive due to the relieving operation.

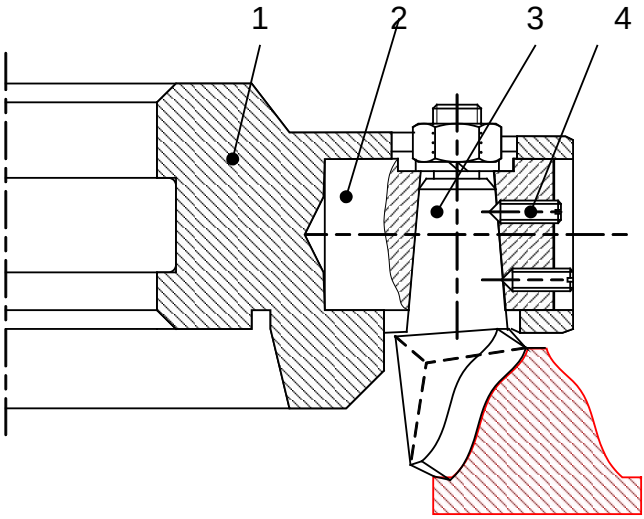

Figure 1: The profiled milling head.

An alternative to the profiled milling disks can be realized with a milling head that includes profiled cutting inserts (*Fig.1)*. The body (1) of the milling head contains 6-8 radially disposed holders (2), where the holder's axes intersect the rotation axis of the body. The holder contains the profiled cutting insert (3).

Holders and inserts can be set at certain angular positions due to the positioning slotted head sets (4). The insert and the holder can be set in two certain positions: the first for profiling and /or re-sharpening, and the second for cutting. When cutting, the holder is turned away with the angle α_T for ensuring the top relief angle, and the insert in the holder is also rotated with α_s in order to realize the side relief angle as shown in *Fig. 2*. The relief faces of the inserts are subsets of a common revolved surface, where the axis of revolution coincides with the axis of the milling head.

Paper [1] presents two calculus procedures for determining the profile of the grinding disk that realizes the relief faces of the inserts. Starting from the parametric equations of the workpiece profile, first the cutting edge in work position is calculated. Rotating the insert and its holder to the profiling /re-sharpening position, the profile of the grinding tool is calculated.

The re-sharpening of the insert can be done in two ways:

a. on the rake face, analogously to the re-sharpening of profiled turning disks, separately for each insert;
b. on the relief face, by profile grinding, simultaneously for all inserts.

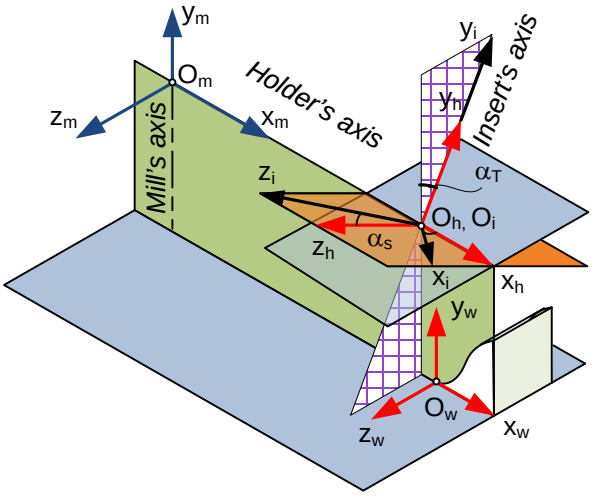

Figure 2: The geometrical model of the milling head – the attached coordinate-systems.

However, the new cutting edge moves in a new position, correlated to the insert's axis. When the insert and the holder are turned back in the cutting position, the cutting edge generates a revolved surface with a different axial section, despite the fact, that its shape remains invariant. In conclusion, profile error occurs.

In the following, the evolution of the profile error in the case of re-sharpening on the rake face will be analyzed.

2. The mathematical model of the cutting edge

Let's consider the geometric model of the milling head, with the coordinate-systems attached to the rigid body and to the mobile components as shown in *Fig. 2*. System $\mathbf{S}_m\{O_m x_m y_m z_m\}$ attached to the body, is used to define the equations of the cutting edge, the grinding wheel profile and the cut profile. System $\mathbf{S}_h\{O_h x_h y_h z_h\}$ of the holder is turned about axis x_h with angle α_T, while the system $\mathbf{S}_i\{O_i x_i y_i z_i\}$ of the insert is rotated about axis y_h with angle α_s. When the insert and the holder occupy the re-sharpening position, all axes are parallel with the corresponding axes of $\mathbf{S}_m$. Starting from the parametric coordinates $(\varphi(u),\psi(u),0)$ of the workpiece profile given in the workpiece

system $\mathbf{S}_w\{O_w x_w y_w z_w\}$ and applying the necessary coordinate transformations as shown in [1], there result the equations of the cutting edge. Omitting the calculus, the edge's equations in the $\mathbf{S}_m$ system are

$$\begin{cases} x_m^{(e)}(u) = (\varphi(u) + R_0 + \Delta)\cos\theta(u) \\ y_m^{(e)}(u) = \psi(u) \\ z_m^{(e)}(u) = (\varphi(u) + R_0 + \Delta)\sin\theta(u) \end{cases} \tag{1}$$

where the function $\theta(u)$ is obtained from the equations of the revolved generating surface of the milling head and the rake face, positioned for cutting (α_T and α_s are set to their cutting values):

$$\theta(u) = \arcsin\frac{R_0\tan(\gamma_0 - \alpha_s) - (\psi(u) - H)\sin\alpha_T}{(\varphi(u) + R_0 + \Delta)\cos\alpha_T} - \arctan\left(\frac{\tan(\gamma_0 - \alpha_s)}{\cos\alpha_T}\right) \tag{2}$$

With this, the new cutting edge is completely determined.

Now it is necessary to model how the cutting edge position and/or shape will change after the re-sharpening process.

3. The profile variation by re-sharpening on the rake face

The re-sharpening on the rake face consists in the renewal of the rake plane, conserving the shape of the cutting edge. This procedure is executed when the insert and the holder are turned in the re-sharpening position characterized by the zero value of α_T and α_s. The rake face in the re-sharpening position is parallel with the mill's axis of rotation. After the re-sharpening it will occupy a new position that is rotated away from the first position with angle λ as shown in *Fig. 3.*

First the equations of the edge have to be rewritten in the insert's system. Denoting with $\mathbf{r}_i^{(e)}$ the homogeneous coordinates of the cutting edge in the insert's system, and $\mathbf{r}_m^{(e)}$ the same coordinates in the mill's system, it can be written that

$$\mathbf{r}_i^{(e)} = \mathbf{M}_{im}\mathbf{r}_m^{(e)} = \begin{pmatrix} \cos\alpha_s & \sin\alpha_T\sin\alpha_s & \cos\alpha_T\sin\alpha_s & -R_0\cos\alpha_s \\ 0 & \cos\alpha_T & -\sin\alpha_T & 0 \\ -\sin\alpha_s & \sin\alpha_T\cos\alpha_s & \cos\alpha_T\cos\alpha_s & R_0\sin\alpha_s \\ 0 & 0 & 0 & 1 \end{pmatrix}\mathbf{r}_m^{(e)}. \tag{3}$$

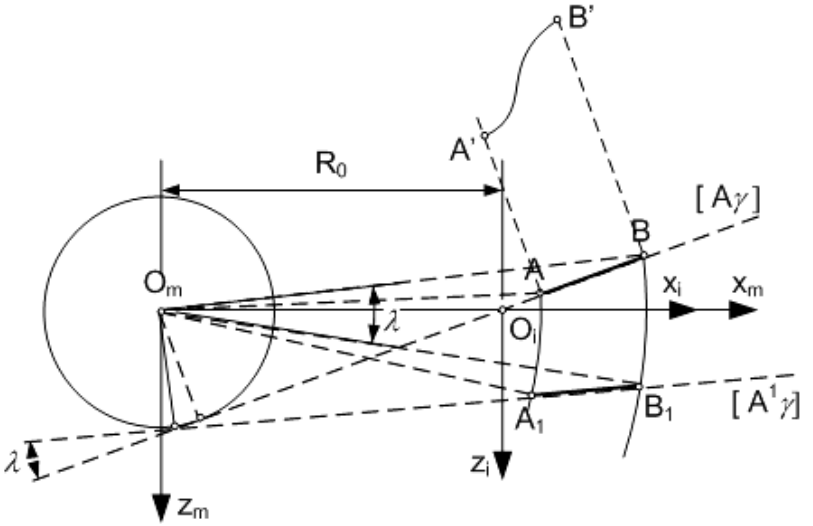

Figure 3: The rake face before and after re-sharpening.

Now let's turn the holder and the insert in re-sharpening position. Due to zero values of α_T and α_s in this position, the $\mathbf{M}_{im}$ matrix reduces to a translation matrix. Using $\mathbf{M}_{mi}$, the inverted matrix of $\mathbf{M}_{im}$, the equations of the rotated edge in $\mathbf{S}_m$ result as follows:

$$\begin{cases} x_m^{(e^*)}(u) = x_i^{(e)}(u) + R_0 \\ y_m^{(e^*)}(u) = y_i^{(e)}(u) \\ z_m^{(e^*)}(u) = z_i^{(e)}(u) \end{cases} . \tag{4}$$

According to *Fig. 3*, this corresponds to zero value of the rake face position angle λ. The generalized cutting edge equations, depend on the state of re-sharpening given by λ:

$$\begin{cases} x_m^{(e1)}(u,\lambda) = -x_m^{(e^*)}(u)\sin\lambda + z_m^{(e^*)}(u)\cos\lambda \\ y_m^{(e1)}(u,\lambda) = y_m^{(e^*)}(u) \\ z_m^{(e1)}(u,\lambda) = x_m^{(e^*)}(u)\cos\lambda + z_m^{(e^*)}(u)\sin\lambda \end{cases} . \tag{5}$$

This new edge must be turned now in the working position. For that, it is necessary to write its equations in the system of the insert, applying a translation along axis x_m. Using the coordinate functions (5), it results:

$$\mathbf{r}_i^{(e1)} = \begin{pmatrix} x_i^{(e1)} \\ y_i^{(e1)} \\ z_i^{(e1)} \\ 1 \end{pmatrix} = \begin{pmatrix} x_m^{(e1)} - R_0 \\ y_m^{(e1)} \\ z_m^{(e1)} \\ 1 \end{pmatrix}. \tag{6}$$

Now the cutting edge is turned back in working position. Let's denote with $\mathbf{r}_m^{(ge)}$ the vector of homogeneous coordinates of the re-sharpened cutting edge. Using again the transformation matrix from (3), it results:

$$\mathbf{r}_m^{(eg)} = \begin{pmatrix} x_m^{(ge)} \\ y_m^{(ge)} \\ z_m^{(ge)} \\ 1 \end{pmatrix} = \mathbf{M}_{mi}\mathbf{r}_i^{(e1)}. \tag{7}$$

Finally, the equations of the generated profile in the $\boldsymbol{S}_m$ system are given by the expressions:

$$\begin{cases} x_m^{(pr)} = \sqrt{\left[x_m^{(ge)}\right]^2 + \left[x_m^{(ge)}\right]^2} \\ y_m^{(pr)} = y_m^{(ge)} \\ z_m^{(pr)} = 0 \end{cases}. \tag{8}$$

4. The modeling of the profile error

The profile error can be calculated in many different ways. However, all models must correspond to the definition of the profile error [7] given by the corresponding standards [6]. The calculus is based on the hypotheses that profile error occurs, because the edge points change their position after re-sharpening. First calculus method tries to compute the average of the displacements. The comparison is made between the new generating profile and the translated theoretical workpiece profile. The translated theoretical workpiece profile coincides with the original one, but translation is realized in order to get the best approximant for the new generating profile.

As well shown in Fig. 4a, the original workpiece profile AB (generated by the new edge) is translated by parameters (a,b) to the position A^*B^*. The profile generated by the new edge is A_1B_1. Considering a set of N discrete points on the original profile defined by the certain values of parameter u, it

has to remarked that a given point M_i moves to M_i^*. With this, the local profile error is considered the distance $\overline{M_i M_i^*}$. The nominal value of the profile error is the maximum value encountered by the distance $\overline{M_i M_i^*}$ along the edge. The translation parameters (a,b) are calculated using the least squares method.

Fig.4b shows the definition of the profile error in the normal direction. The equations of the translated workpiece profile are:

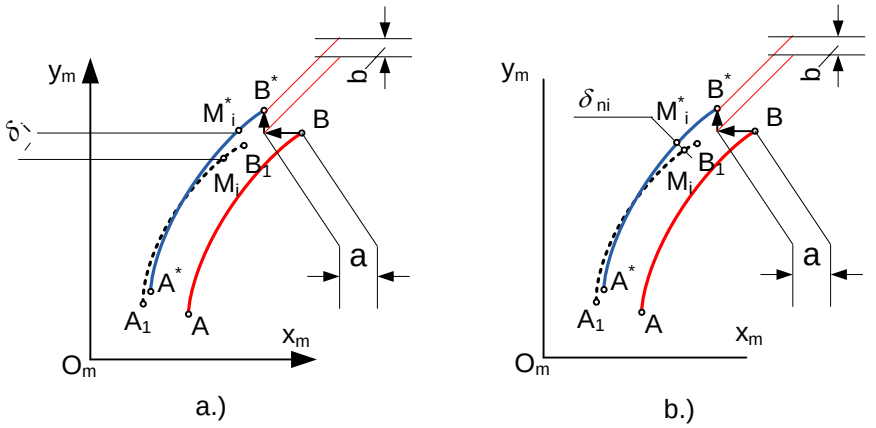

Figure 4: The modeling of the profile errors.

$$\begin{cases} x(u) = (\varphi(u) + R_0 + \Delta) + a \\ y(u) = \psi(u) + b \end{cases} . \tag{9}$$

The equation of the normal line started from the profile point $M_i^*(x_i^*, y_i^*)$ to the workpiece profile given by equations (9) is

$$(x_i^* - x(u))\dot{\varphi}(u) + (y_i^* - y(u))\psi(u) = 0 \tag{10}$$

and admits the root u_i. With this, the local normal error is defined through the distance $\overline{M_i M_i^*}$ on *Fig 4b*:

$$\delta_i^n = \sqrt{(x_i^* - x(u_i))^2 + (y_i^* - y(u_i))^2} \quad . \tag{11}$$

5. Numerical approach

In order to emphasize the evolution of the profile errors occurring by re-sharpening, let's consider a practical example. The workpiece profile is a parabola (*Fig. 5*) described by the equations

$$\begin{cases} x(u) \equiv \varphi(u) = u \\ y(u) = \psi(u) = -\dfrac{3}{20}u^2 + \dfrac{47}{20}u, \qquad u \in [0,5]. \end{cases} \tag{12}$$

The reference radius of the insert is set to $R_0 = 100\,\text{mm}$, and the approximate value of distance of the edge-top to the axis of the insert, along axis x is $\Delta = 5\,\text{mm}$.

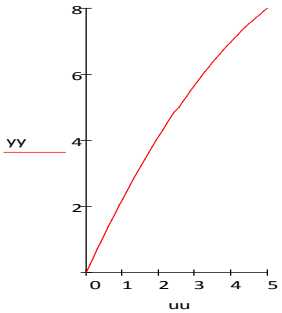

Figure 5: The workpiece profile.

The grinding allowance for the admissible wear of the relief face is considered $K_\alpha = 0{,}3\,mm$. After the re-sharpening, the new rake face rotates about axis z_m with $\Delta\lambda \approx K_\alpha / R_0 \approx 10'18{,}8''$ reported to its position before the grinding operation. Considering that the total grinding reserve of the insert is $A_\Sigma \approx 10\,mm$, it can be stated that the corresponding total rotation angle is $\lambda_\Sigma = A_\Sigma / R_0 \approx 5°43'46{,}5''$. According to this, the predicted number of re-sharpening becomes $N_{re} = [\lambda_\Sigma / \Delta\lambda] \approx 33$.

For studying the evolution of the profile errors according to the values of the angles γ_s, α_T and α_s, the proposed limits for their values are as follows:

$$\begin{aligned} 1° \le \alpha_T &\le 6° \\ 5° \le \alpha_s &\le 8° \\ 5° \le \gamma_s &\le 10° \end{aligned} \quad .$$

Angle γ_s is the conventional rake angle, that can be approximated by $\gamma_s \approx \gamma_0 - \alpha_s$. When the influence of one parameter is studied, the others are set to the middle of their interval: $\overline{\alpha}_T = 3°30'; \overline{\alpha}_s = 6°30'; \overline{\gamma}_s = 7°30'$. The simulation program calculates for each parameter combination and each state of re-sharpening, the evolution of the errors along the profile. Both types of errors mentioned in section 4 are calculated. The conclusion is that the shapes of error evolution diagrams are not significantly different. As follows, a consistent conclusion can be deduced studying only the normal errors.

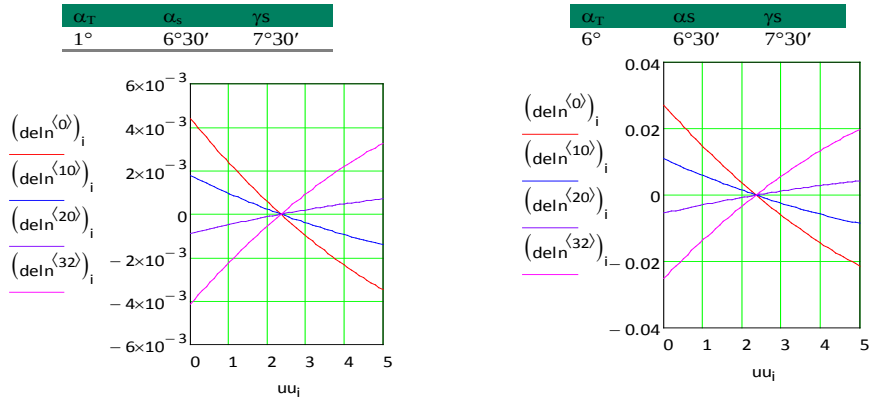

Figure 6: The evolution of the normal errors along the edge for different settings of α_T parameter and different states of re-sharpening.

Fig. 6 shows the evolution of the normal profile errors for the lowest and the highest value of the top relief angle α_T while α_s and γ_s are set to the median values. The horizontal axis contains the abscissa of discrete profile points ($N = 50$ points have been considered). The vertical axis contains the normal errors in millimeters, for different numbers of re-sharpening. The index $\langle 0 \rangle$ denotes the first, and the index $\langle 32 \rangle$ the last re-sharpening. It can be observed that the evolution of errors is the same for both cases. First, error is decreasing till the number of the re-sharpenings increases to approximately the half of its maximum. This error variation is obtained due to the fact, that the new cutting edge is turned away from its theoretical position with $-\lambda_\Sigma / 2$. The same technique of manufacturing is used to maintain the errors in the limits of tolerance by the gear cutting hobs [2, 3, 4, 5]. Due to the optimal positioning of the etalon curve, the errors encounter the maximum values at the endpoints of the edge. It is to remark that α_T has a severe influence on the profile error. The

right-side diagram shows approximately four times larger maximum error values when α_T increases to 6° representing the upper limit considered for this angle.

When studying the influence of the other two angular parameters α_s and γ_s it can be observed that variation of the maximum error values is theoretically zero. The error diagrams are presented in *Fig. 7*. The same evolution is encountered when the influence of γ_s is studied.

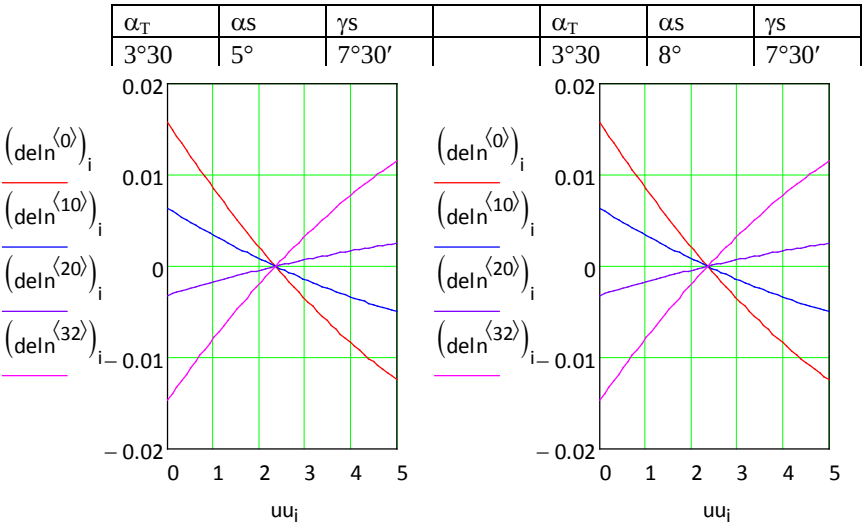

Figure 7: The influence of α_s parameter on the evolution of maximum value of profile error.

To ascertain the precision of the milling head it is necessary to calculate the maximum value of the errors. The computing routine is that used for outputting the drawings presented before. The results corresponding to the set values of the angular parameters α_T, α_s and γ_s are given in the table below.

Table 1: The evolution of the maximum error values.

α_T [°]	α_s [°]	γ_s [°]	γ_0 [°]	δ_{max} [mm]	δ^n_{max} [mm]
1	6,5	7,5	14	0,007934	0,007377
2	6,5	7,5	14	0,01613	0,01486
3	6,5	7,5	14	0,02433	0,02236
4	6,5	7,5	14	0,03254	0,02985
5	6,5	7,5	14	0,04075	0,03735
6	6,5	7,5	14	0,04897	0,04485
3,5	5	7,5	12,5	0,02857	0,02617
3,5	6	7,5	13,5	0,02848	0,02613
3,5	7	7,5	14,5	0,02838	0,02608
3,5	8	7,5	15,5	0,02826	0,02601
3,5	6,5	5	11,5	0,02851	0,02612
3,5	6,5	6	12,5	0,02848	0,02612
3,5	6,5	7	13,5	0,02845	0,02611
3,5	6,5	8	14,5	0,02842	0,0261

Considering just the shadowed part of the above table and represen-ting the last two columns versus the first it can be remarked that the variation of error is very close to linear (*Fig. 8*).

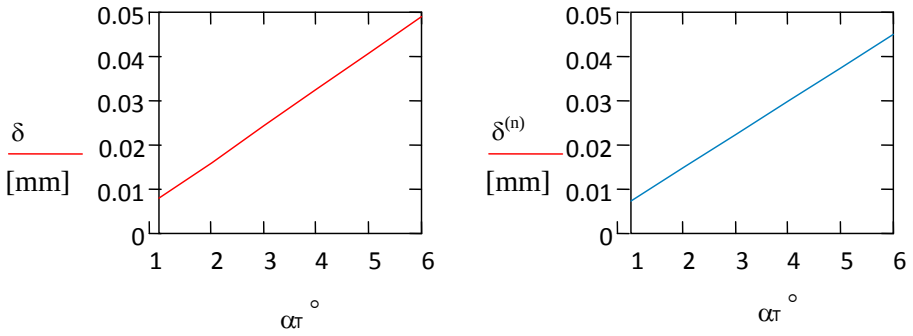

Figure 8: The linear dependence of the maximum profile error values on the top relief angle.

Performing a statistical analysis in order to establish the linear regression between the value of α_T and the corresponding value of the error, the following results were obtained:

$$\delta(\alpha_T) = -2.82666666667 \cdot 10^{-4}\,\alpha_T + 8.20714285714 \cdot 10^{-3} \qquad (13)$$

with a correlation coefficient of $c = 0.999999868303$ and a standard error $\sigma = 8.81 \cdot 10^{-6}$. Considering the normal error, the results are very slightly different:

$$\delta^{(n)}(\alpha_T) = -1.24666666667 \cdot 10^{-4} \alpha_T + 7.49500000000 \cdot 10^{-3} \qquad (14)$$

with a correlation coefficient of $c = 0.999999937271$ and a standard error $\sigma = 5.553 \cdot 10^{-6}$.

Conclusions

Analyzing the diagrams and the results presented before, the following conclusions can be established:

- the unique probable influence on the variation of the milling head profile precision due to the re-sharpening, is caused by the top relief angle α_T;
- the value of the top relief angle can be set smaller than 2°, that will lead to maximum profile errors less than 10μm;
- a profiled cutting tool construction with sufficient precision can be realized without applying the classical and pretty complicated relieving operation;
- relief faces are easily realizable through NC grinding, simultaneously for all inserts.

References

[1] Máté, M., and Hollanda, D., "A Possible Concept of Peripheral Edged Profile Mills for External Convex Profiles", in *Proc. of the IMC 2011-International Multidisciplinary Conference, 9-th Edition, Nyíregyháza*, May 19-21, 2011, pp. 173-178.

[2] Hollanda, D. , "Aşchiere şi scule", Universitatea din Braşov, 1983.

[3] Secară, Gh., "Proiectarea sculelor aşchietoare", Ed. Didactică şi Pedag. Bucureşti, 1979.

[4] Hollanda, D., Máté, M., "Aşchiere şi scule", Ed. Univ. „Petru Maior", Tîrgu-Mureş, 2003.

[5] Belous, V., "Sinteza sculelor aşchietoare", Editura Junimea, Iaşi, 1980.

[6] Y14.5.1M-1994 (R2004), "Mathematical Definition Of Dimensioning And Tolerancing Principles", ASME International Standards.

[7] Pasupathy, T. M. K., Wilhelm, R. G., Gregory, A. H., "Profile tolerance zones with control points", http://www.aspe.net/publications/, Annual_2000/PDF/ POSTERS/ METROL / FORM/.

[8] Maestre, J. M., Munoz de la Pena, D. and Camacho, E. F., "Distributed MPC: a supply chain case study", *IEEE Conference on Decision and Control, Shanghai, China*, December 16-18, 2009, pp. 7099 – 7104.

[9] Venkat, A. N., Hiskens, I. A., Rawlings, J. B. and Wright, S. J. "Distributed MPC Strategies With Application to Power System Automatic Generation Control", *IEEE Transactions on Control Systems Technology*, vol. 16, no. 6, pp. 1192-1206, November, 2008.

Acta Universitatis Sapientiae

The scientific journal of Sapientia University publishes original papers and surveys
in several areas of sciences written in English.
Information about each series can be found at
http://www.acta.sapientia.ro.

Acta Universitatis Sapientiae
Electrical and Mechanical Engineering

Sapientia University

Scientia Publishing House

ISSN 2065-5916
http://www.acta.sapientia.ro

Information for authors

Acta Universitatis Sapientiae, Electrical and Mechanical Engineering publishes only original papers and surveys in various fields of Electrical and Mechanical Engineering. All papers are peer-reviewed.

Papers published in current and previous volumes can be found in Portable Document Format (PDF) form at the address: `http://www.acta.sapientia.ro`.

The submitted papers must not be considered to be published by other journals. The corresponding author is responsible to obtain the permission for publication of co-authors and of the authorities of institutes, if needed. The Editorial Board is disclaiming any responsibility.

The paper must be submitted both in MSWord document and PDF format. The submitted PDF document is used as reference. The camera-ready journal is prepared in PDF format by the editors. In order to reduce subsequent changes of aspect to minimum, an accurate formatting is required. The paper should be prepared on A4 paper (210 $\times$ 297 mm) and it must contain an abstract of 200-250 words.

The language of the journal is English. The paper must be prepared in single-column format, not exceeding 12 pages including figures, tables and references.

The template file from http://www.acta.sapientia.ro/acta-emeng/emeng-main.htm may be used for details.

Submission must be made only by e-mail (`acta-emeng@acta.sapientia.ro`).

One issue is offered to each author free of charge. No reprints are available.

Contact address and subscription:
Acta Universitatis Sapientiae, Electrical and Mechanical Engineering
RO 400112 Cluj-Napoca
Str. Matei Corvin nr. 4.
E-mail: acta-emeng@acta.sapientia.ro

Printed by Digital Color Company